A Method for Robust Control of Systems with Parametric Uncertainty Motivated by a Benchmark Example

by

Carl S. Resnik

B.S., Aeronautics and Astronautics
Massachusetts Institute of Technology
(1986)

Submitted to the Department of Aeronautics and Astronautics
in partial fulfillment of the requirements for the degree of

Master of Science

at the

MASSACHUSETTS INSTITUTE OF TECHNOLOGY

June 1991

Signature of Author .....
Department of Aeronautics and Astronautics
March 27, 1991

Certified by .....
Lena Valavani
Associate Professor, Department of Aeronautics and Astronautics
Thesis Supervisor

Accepted by .....
Professor Harold Y. Wachman
Department, Graduate Committee

A Method for Robust Control of Systems with Parametric Uncertainty Motivated by a Benchmark Example

by

Carl S. Resnik

Submitted to the Department of Aeronautics and Astronautics
on March 27, 1991, in partial fulfillment of the
requirements for the degree of
Master of Science

Abstract

A multivariable compensator design methodology is constructed consisting of a model-matching, inner loop compensator and an H_∞ outer loop compensator to provide robust control of plants with real parametric uncertainty. The inner loop compensator desensitizes the plant to the parametric uncertainty. The inner loop compensator is constructed by minimizing the difference between a designer supplied desired closed loop system and the actual closed loop system in a least squares sense. The inner loop compensator design allows for arbitrary constraints on compensator order and structure. The H_∞ compensator provides the desired closed loop performance characteristics and robustness to unstructured uncertainty. Model reduction techniques are used to reduce the order of the H_∞ compensator.

The methodology is applied to a (SISO) benchmark problem for robust control, consisting of a mass-spring system with uncertainty in the value of the spring constant and it is shown to meet the problem stability and performance specifications. The design approach is then applied to a multivariable mass-spring-dashpot system with simultaneous uncertainty in the spring constants. Again, robust stability and performance to parametric uncertainty is achieved.

Thesis Supervisor: Lena Valavani
Title: Associate Professor, Department of Aeronautics and Astronautics

Acknowlegements

I would like to thank GE Aircraft Engines, especially my former boss, Mike Idelchik, and my current boss, Sheldon Carpenter for allowing me to pursue this degree (no matter how long it took). I would also like to thank my advisor, Prof. Lena Valavani, for her insight and advice, which have contributed greatly to this thesis. My coworkers lent both technical assistance and advice, while my friends kept listening as I continually claimed to be *almost* done. Most of all I'd like to thank my parents and family, especially my mother, for their love and support in this and (almost) everything I've done.

And now, hey dudes, let's party. Hopefully my real friends will buy the first round.

Contents

List of Figures

List of Tables

Chapter 1

Introduction

1.1 The Problem: Parametric Uncertainty and Robust Control

This thesis deals with an important problem in multivariable control system design, parametric uncertainty. In particular, practical methods of designing robust compensators in the face of such uncertainty are explored. A compensator design methodology is provided for systems which are modeled as finite dimensional, linear time invariant (FDLTI) and may be realized in terms of a set of state equations.

Uncertainty is inherent in all models of a given physical process. For FDLTI systems it has typically been modeled as unstructured uncertainty, dynamic structured uncertainty or real parametric uncertainty. Parametric uncertainty is a form of structured uncertainty; it is uncertainty in the real parameters used to construct the FDLTI model, the elements which make up the state-space equations. For example, in a mass-spring system the value of the mass or masses may only be known within a certain range, or some nominal value of the mass may be known but with some uncertainty.

Consider the FDLTI system expressed as a transfer function matrix $G(s)$.

Now $G(s)$ may be expressed as

$$G(s) = C(sI - A)^{-1}B + D$$

where A, B, C, D are the matrices defining the state-space equations which describe $G(s)$. Then $G(s)$ or G may be written conveniently as

$$G = (A, B, C, D).$$

Given a state-space system G with real parametric uncertainty, it may be expressed in terms of the system matrices:

$$G = (A + \Delta A,\ B + \Delta B,\ C + \Delta C,\ D + \Delta D)$$

where the parametric uncertainty is represented by the perturbations ΔA, etc. to the state-space matrices and the nominal system G_{nom} is

$$G_{nom} = (A, B, C, D).$$

The terms parametric uncertainty, parameter variation, etc. are used interchangeably throughout this document[1]. Efforts to incorporate parametric uncertainty into robustness specifications and analysis include the structured singular value (SSV) of Doyle [11, 10], Safonov's Multivariable Stability Margin (MSM) [23], and others such as the robustness margin presented in [24] by Sideris and Peña. Unfortunately, the most popular of these approaches, the SSV (μ), is conservative for multiple parameter uncertainty.

Most efforts in multi-input multi-output (MIMO) robust control of FDLTI systems have focused on producing control methodologies which provide ro-

[1]These are used only in the context of FDLTI systems; time-varying parameters are not treated here.

bust stability and nominal performance to (bounded) unstructured uncertainty, such as the H_2/H_∞ methodologies, see for example Doyle et al [12]. Unfortunately, such methodologies are not robust for parametric uncertainty, as shown by Craig [8]. Another alternative, the SSV based compensator design μ-synthesis technique is only approximate with no real guarantees. Some approaches to H_2/H_∞ which provide for real parameter variation have also recently been developed, such as [19] by Madiwale et al. However, these tend to yield conservative designs. The methodology introduced here does not explicitly account for parameter uncertainty but is shown to be insensitive to it. Given a measurement of the effects of the parametric uncertainty, it could be used to provide a non-conservative design by iterating on the inner loop compensator design until performance or stability was bounded by the uncertainty. The methodology provides the control system designer with a method which is easily implementable, practical, and robust, and operates within the frequency domain framework which many designers are used to working.

1.2 Motivation

The typical compensator synthesis techniques, H_2/H_∞, which are used to handle bounded unstructured uncertainty are not robust to parametric uncertainty. This stems from the fact that most compensators seek to invert the plant, i.e. cancel the plant dynamics, and substitute desirable dynamics specified by the designer. It is in the specifications of the desired dynamics, by limiting the closed loop bandwidth, for example, that the unstructured uncertainty is handled. However, parametric variation acts on the part of the methodology involved in the plant cancellation. If the plant contains lightly damped poles, whose locations may vary with parametric uncertainty, this may cause the closed loop system to be unstable in the presence of that uncertainty

[8].

However, since H_2/H_∞ techniques are very popular and are supported by several computer-aided design packages, it is desirable to investigate ways to improve their robustness to parametric uncertainty so as to be able to routinely use them to design multivariable control systems. These techniques also allow explicit loopshaping in the frequency domain, which is desirable from the viewpoint of the control system designer. A method is needed, however, which will desensitize the plant inversion techniques of H_2/H_∞ to parametric uncertainty. In [8] the use of (full-state) inner feedback loops was shown to accomplish this goal. Unfortunately, most control designs do not have the benefit of full-state feedback, so a method of output feedback dynamic compensation was needed to provide the same benefit. Such a method is developed here based on a model-matching feedback path compensator which is wrapped around the plant before an H_∞ compensator is constructed.

1.3 Thesis Contribution

This thesis contributes a design methodology for the synthesis of MIMO compensators which produce a closed loop system robust to bounded parametric and unstructured uncertainty. The approach used is the construction of an inner loop, feedback path, model-matching compensator which is insensitive to parametric uncertainty, and a unity feedback, forward path compensator which is insensitive to unstructured uncertainty and provides closed loop performance, disturbance rejection, command following, etc.

The approach presented *does not explicitly* account for parameter variation. The inner loop compensator is insensitive to parametric variation because it is a feedback compensator designed without attempting to cancel the plant dynamics. Other advantages of the inner loop design methodology allow for the

designer to set the compensator order and impose arbitrary constraints on the compensator structure. Inner loop performance is specified in the frequency domain. The outer loop is constructed using the H_∞ methodology which also allows for explicit frequency domain performance specifications and robustness to unstructured uncertainty.

It is the intention that this methodology be a systematic, easy to use approach to constructing compensators for problems with parametric uncertainty.

1.4 Thesis Organization

The thesis is organized into five chapters.

The first chapter has been the introduction. In Chapter 2 a comprehensive explanation of the compensator methodology, used to robustify the system to parametric uncertainty, is presented. Also discussed are frequency domain loopshaping and a robustness measure.

In Chapter 3 the methodology is applied to a benchmark problem for robust control [25]. Two separate designs are presented.

In Chapter 4 the methodology is applied to a MIMO mass-spring-damper system.

Last, in Chapter 5, the effectiveness of the methodology is assessed and recommendations for further research are given.

Chapter 2

The Approach: Inner Loop and H_∞

2.1 Overview

This chapter presents a methodology for designing a compensator structure which is robust in stability and performance to both the effects of parametric uncertainty and to normal additive or multiplicative unstructured uncertainty. The methodology involves first construction of an inner loop, feedback path, compensator using a model-matching design technique. This compensator reduces the effects of parametric uncertainty on the system. An H_∞ outer loop compensator is then designed to provide robust system performance. The reason for choosing this approach stems from needing to desensitize the H_∞ methodology to real parametric uncertainty since it provides a flexible, standardized architecture for designing multivariable compensators.

The methodology used here results in a closed loop system with both a feedback path, K_{inner}, and a forward path, K_∞, compensator as shown in Figure 2.1.

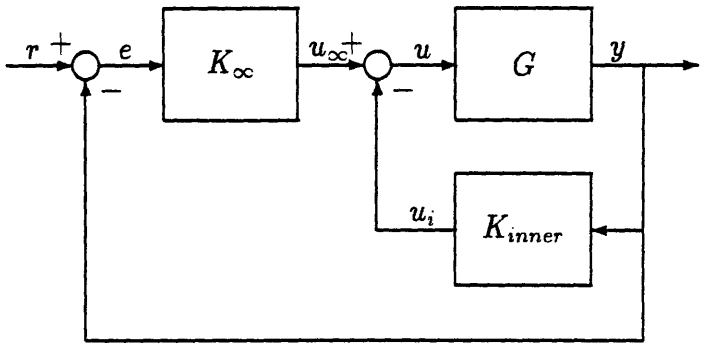

Figure 2.1: The Closed Loop System with Forward and Feedback Path Compensators

2.2 The Standard Feedback Configuration, Loopshaping, and Stability Robustness

The H_∞ methodology will be used to construct compensators for use in the standard feedback configuration. This configuration, shown in Figure 2.2, consists of a plant, G, unity gain feedback of the plant outputs, y, to constructing an error, e, by comparison with a set of reference inputs, r, and the controller, K, operating on that error in order to provide a set of plant control inputs, u.

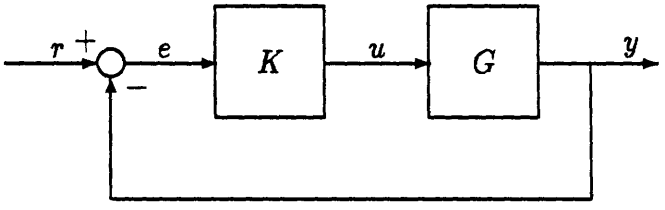

Figure 2.2: The Standard Feedback Configuration

For the standard feedback configuration, Figure 2.2, the common loopshapes which are examined are the open loop, sensitivity and complementary sensitivity transfer functions [2, 3, 9]. For the loop broken at the plant output,

the open loop transfer function is

$$L_s(s) = GK \tag{2.1}$$

where the s subscript signifies servo. For the loop broken at the plant input, the open loop transfer function is

$$L_r(s) = KG \tag{2.2}$$

where the r subscript signifies regulator. For SISO systems these are, of course, equivalent. The complementary sensitivity (or closed loop) transfer function, $T(s)$ is expressed as

$$T(s) = (I + GK)^{-1}GK. \tag{2.3}$$

While the sensitivity function calculated at the plant output, $S(s)$ is

$$S(s) = (I + GK)^{-1}. \tag{2.4}$$

The open loop transfer functions are indicative of performance at the plant input (regulator) versus the plant output (servo). The servo open loop transfer function provides information on command following, disturbance rejection to disturbances injected at the plant outputs, and insensitivity to sensor noise on the plant outputs. The regulator open loop transfer function provides information on disturbance rejection to disturbances injected at the plant inputs and actuator noise insensitivity at the plant inputs. The complementary sensitivity function provides indications of closed loop command following for a reference input, as well as stability robustness to unstructured uncertainty, if such specifications have been developed [2, 3]. The sensitivity function provides the transfer function from error to output or the attenuation of disturbances injected at the plant output.

The sensitivity transfer function is also used to provide the MIMO gain and phase margin of the system, [16]. This is a conservative measure of plant stability robustness at the plant output. It can also be used to measure robustness at the plant input if the input sensitivity transfer function is used, i.e.

$$S_i(s) = (I + KG)^{-1}. \tag{2.5}$$

This technique is based on the multivariable Nyquist criterion and may be computed as follows. For robustness at the plant output let α be

$$\alpha = \|S(s)\|_\infty. \tag{2.6}$$

Then the gain/phase margins are computed as

$$\uparrow GM \leq \frac{\alpha}{\alpha - 1} \tag{2.7}$$

$$\downarrow GM \geq \frac{\alpha}{\alpha + 1} \tag{2.8}$$

$$PM = \geq 2\, sin^{-1}\left(\frac{1}{2\alpha}\right) \tag{2.9}$$

where these are independent and simultaneous margins in all of the channels of the closed loop system. The arrows indicate upward or downward gain margin. For robustness at the plant input, $S_i(s)$ is used instead.

2.3 Loopshaping with Both Forward and Feedback Path Compensators

For the compensator configuration used here, Figure 2.1, the equivalent formulas for the transfer functions are derived as follows. The servo open loop transfer function is obtained by breaking the loop in Figure 2.1 at the plant

output, y. The transfer function from y to y is then

$$L_s(s) = G(K_\infty + K_{inner}). \tag{2.10}$$

Similarly, breaking the loop at the plant input u yields

$$L_r(s) = (K_\infty + K_{inner})G \tag{2.11}$$

the open loop regulator transfer function.

The closed loop, or complementary sensitivity, is obtained by computing the transfer function from r to y in Figure 2.1 and is

$$T(s) = [I + G(K_\infty + K_{inner})]^{-1}GK_\infty. \tag{2.12}$$

Finally, the sensitivity transfer function is computed from a fictional disturbance, d, which is thought to be injected at the plant output in Figure 2.1, to y and yields

$$S(s) = [I + G(K_\infty + K_{inner})]^{-1}. \tag{2.13}$$

Notice however, that if the transfer function from the reference input r to the tracking error e is computed from Figure 2.1, (an alternate definition of the sensitivity) it will be

$$S_e(s) = [I + G(K_\infty + K_{inner})]^{-1}(I + GK_{inner}) \tag{2.14}$$

Since specifying the tracking error specifies the command following ability of the closed loop system this means that, unlike in the standard feedback configuration, Figure 2.2, that specifications on disturbance rejection and com-

mand following are no longer equivalent. That is now

$$T(s) + S(s) \neq 1 \tag{2.15}$$

but,

$$T(s) + S_e(s) = 1 \tag{2.16}$$

which may be seen by simply adding the appropriate equations given above. So, specifiying an $S(s)$ does not specify a $T(s)$.

2.4 Inner Loop Compensator Synthesis with a Model-Matching Design Methodology

2.4.1 Introduction to the Inner Loop Model-Matching Methodology

The inner loop compensator, K_{inner}, is designed so the closed loop system shown in Figure 2.3 is relatively invariant to the parametric variation. Inoue [14] showed that a robust H_∞ design requires a "smooth" singular value plot, which this compensator provides. Specifically, it is the transfer function from u_∞ to y which is of interest. This is the transfer function which will be "seen" by the outer loop compensator and is expressed as:

$$T_{inner} = (I + GK_{inner})^{-1}G \tag{2.17}$$

The approach used to design the inner loop compensator for plants with output feedback is based on a model-matching methodology, specifically that developed in the GE based ISICLE system [20, 21]. The approach in ISICLE was in turn based on Edmunds' algorithm, an explanation of which is contained

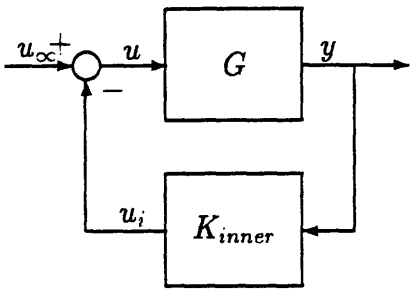

Figure 2.3: The Closed Loop System, T_{inner}: Plant with Inner Loop Compensator

in [18]. The reasons for choosing this methodology are primarily its flexibility. The methodology is amenable to dealing with square plants, i.e. those with the same number of inputs and outputs. It allows the introduction of designer imposed constraints on compensator structure and *order*. As an intermediate step, the methodology indicates the frequency response of the compensator needed to exactly obtain the desired closed loop performance, regardless of whether this compensator is causal. The compensator generating algorithm is itself iterative. Because the design method is easy to use, it allows the designer to try several alternative designs to obtain one which best meets the requirements.

The model-matching design methodology starts with the designer choosing a desired closed loop transfer function H_d. For a multivariable system, the designer chooses every desired closed loop transfer function element of the closed loop transfer function matrix H_d. To do this one examines the individual *nominal plant* transfer function matrix elements and then replaces each one with a similar element which has the effects of the uncertainty removed. For example, if the uncertainty is manifested in an element of the plant transfer runction matrix as the location of lightly damped poles, one simply defines a transfer function matrix element with those poles damped. The methodology then pro-

vides a compensator which minimizes the difference between the desired closed loop transfer function, H_d, and the actual closed loop transfer function, H, in a least squares sense over some specified frequency range. The minimization process is subject to a number of designer imposed constraints. These include selecting the compensator denominator transfer function matrix, selecting the numerator transfer function matrix order and structure, and the frequency range over which the minimization is to proceed. The designer can also weight the compensator channels relative to each other.

An analysis and discussion of the methodology is provided in the following sections. It is important to realize that this is a frequency domain methodology, i.e. by this it is meant that it is *implemented* as point-by-point calculations in the frequency domain. The importance of this will become apparent in the realizations computed and the lack of guarantees provided by the methodology, though it does have a theoretical underpinnings based on the Youla parametrization [18]. The following is based on a similar explanation for unity feedback compensators by Minto in [20].

2.4.2 The Model-Matching Problem

The motivation for the methodology is visualized in Figure 2.4, which shows the inner loop transfer function T_{inner}, referred to here as H, in parallel with some *desired* representation of the plant dynamics, H_d.

It is desired that for an input u a compensator K be constructed so the actual output y is equal to the desired output y_d. The objective of the methodology is to minimize the error, ϵ in a least squares sense by choosing an appropriate K, or, mathematically,

$$\min_K \|H_d - H\|_2 \tag{2.18}$$

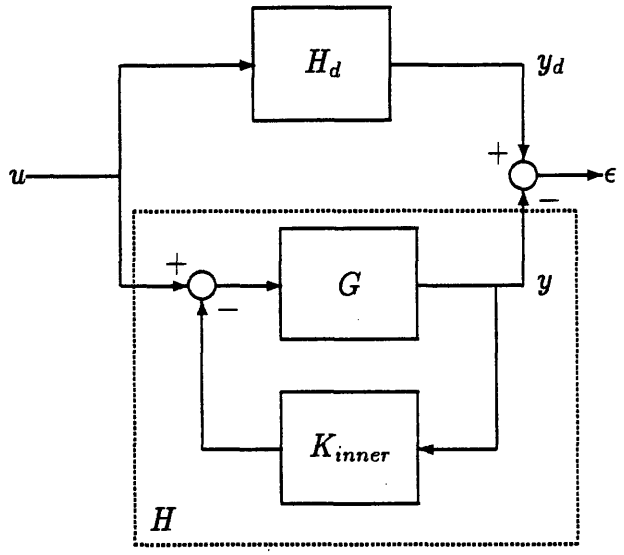

Figure 2.4: Model-Matching Design Objective

2.4.3 Compensator Parametrization

In this section the theoretical underpinnings which led to the use of the model-matching algorithm are explored. It is also shown why placing the compensator in the feedback path desensitizes the closed loop system T_{inner} to parametric variation.

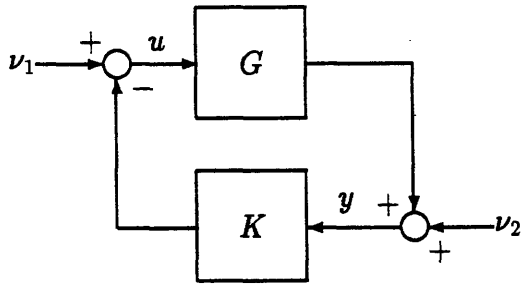

Figure 2.5: General Feedback System

The Youla parametrization [13, 18] states, given the general feedback system shown in Figure 2.5, for a stable plant G, the set of *all* controllers K that

stabilize G may be parameterized as

$$K = Q(I - GQ)^{-1} \tag{2.19}$$

where Q is *any* stable transfer function matrix. This result is a special case as the Youla parametrization allows for an unstable plant G [13, 18]. The Youla parametrization for an unstable plant could be used here, but would only cloud the presentation. This result means that, if K stabilizes G, it must be of the form given in equation 2.19 for some Q equal to

$$Q = K(I + GK)^{-1}. \tag{2.20}$$

Also, given *any* stable Q, a compensator K may be obtained from equation 2.19. Notice that Figure 2.5 applies to compensators in either the forward or feedback path.

A closed loop system H with a feedback path compensator K may be expressed as

$$H = (I + GK)^{-1}G \tag{2.21}$$

from equation 2.17. Substituting equation 2.19 for K yields

$$H = G - GQG. \tag{2.22}$$

This implies that all achievable closed loop transfer functions are also parametrized by Q. Furthermore, the desired closed loop response H_d may be decoupled from the plant G by choosing

$$Q = G^{-1} - G^{-1}H_d G^{-1} \tag{2.23}$$

if G is square, invertible, and minimum phase. If this is substituted into

equation 2.22, it yields

$$H = H_d$$

indicating this desired transfer function is achievable. If G and H_d are square, invertible, and minimum phase, Q is chosen as in equation 2.23, and the result is substituted into equation 2.19, then K is shown to be

$$K = {H_d}^{-1} - G^{-1} \tag{2.24}$$

which *does not necessarily have the poles of G present in the compensator K.* This result is important in avoiding the effects of plant inversion because even though G appears inverted in the compensator, it is present not as a product but as a sum.

To demonstrate this consider a simple SISO example with lightly damped poles. Let,

$$G = \frac{(s+2)(s+2)}{(s+1+0.1j)(s+1-0.1j)}$$

and

$$H_d = \frac{(s+2)(s+2)}{(s+1.005)(s+1.005)}$$

where H_d and G are identical except the lightly damped poles of G have been moved to the real axis. Then from equation 2.24 the solution for the compensator necessary to obtain this closed loop transfer function is

$$\begin{aligned} K &= \frac{(s+1.005)(s+1.005) - (s+1+0.1j)(s+1-0.1j)}{(s+2)(s+2)} \\ &= \frac{(s^2+2.01s+1.01) - (s^2+2s+1.01)}{(s+2)(s+2)} \\ &= \frac{0.01s}{(s+2)(s+2)} \end{aligned}$$

which has none of the poles of G present in its transfer function. Now H equals H_d as that is the definition of equation 2.24. This provides added robustness

to the feedback path compensator for parameter variation. This can be seen by extending the example, if there was some parameter uncertainty in G and it actually had the transfer function

$$G = \frac{(s+2)(s+2)}{(s+2+0.1j)(s+2-0.1j)}$$

then using equation 2.21, H would be

$$\begin{aligned} H &= \frac{(s+2)(s+2)(s+2)(s+2)}{(s+2)(s+2)[.01s+(s+2+0.1j)(s+2-0.1j)]} \\ &= \frac{(s+2)(s+2)}{s^2+4.01s+4.01} \\ &= \frac{(s+2)(s+2)}{(s+2.1051)(s+1.9049)} \end{aligned}$$

which shows that the actual closed loop system also has its poles on the real axis. The lightly damped poles of G do not appear here. This example clearly demonstrates the robustness of the feedback path compensators designed to parameter uncertainty.

However, if a a unity feedback compensator were to be designed using the same method, Figure 2.2, the equivalent results are as follows [20]. Since

$$H = (I+GK)^{-1}GK$$

substituting equation 2.19 into it yields the parametrization of all closed loop systems

$$H = GQ. \tag{2.25}$$

Again if G is square, invertible and minimum phase then given an H_d Q may be expressed as

$$Q = G^{-1}H_d. \tag{2.26}$$

This can be substituted back into equation 2.19 to yield a compensator of the

form

$$K = G^{-1}H_d(I - H_d)^{-1}. \tag{2.27}$$

Notice this compensator will always have the poles of G present in it because it is a product of the inverse of G and the desired closed loop dynamics.

2.4.4 The Ideal Compensator

As stated in equation 2.21, the transfer function H may be expressed as:

$$H = (I + GK)^{-1}G.$$

Now, if we assume that some *ideal* compensator is available — even if it can't actually be realized as G does not meet the conditions given in Section 2.4.3 — to attain the desired plant H_d, the latter may be expressed as

$$H_d = (I + GK_{ideal})^{-1}G. \tag{2.28}$$

This may then be rearranged to yield

$$K_{ideal} = {H_d}^{-1} - G^{-1}. \tag{2.29}$$

Notice this is the form given in equation 2.24; an explicit state-space form for K_{ideal} is realizable only if both H_d and G are invertible. Often the ideal compensator K_{ideal} will not be realizable. However, the frequency response of both G and H_d can be computed over some finite frequency vector ω made up

of p discrete frequency points or

$$\omega = \begin{bmatrix} \omega_1 \\ \omega_2 \\ \vdots \\ \omega_p \end{bmatrix}.$$

Then if G has m inputs and outputs, the frequency responses of G and H_d are available as $mp \times m$ matrices expressed as

$$G_{fr} = \begin{bmatrix} G(j\omega_1) \\ G(j\omega_2) \\ \vdots \\ G(j\omega_p) \end{bmatrix}$$

$$H_{dfr} = \begin{bmatrix} H_d(j\omega_1) \\ H_d(j\omega_2) \\ \vdots \\ H_d(j\omega_p) \end{bmatrix}.$$

These frequency responses can then be inverted at each frequency point, ω_p, to obtain H_{dfr}^{-1} and G_{fr}^{-1}. Therefore, K_{ideal} may always be expressed as a frequency response and may be thought of as the subtraction of two bode plots or

$$K_{idealfr} = H_{dfr}^{-1} - G_{fr}^{-1}.$$

In fact, it is not necessary to have a state-space realization of K_{ideal}; besides it is often not desirable as it would be of unnecessarily high order. This ideal compensator frequency response is generally used as a guide to selecting the order and structure of the actual compensator.

Because the ideal compensator is calculated as a frequency response, each

channel of this response can be plotted as a bode plot. Then its structure, whether *non-causal or causal*, will be apparent to the designer. For example, if rate feedback is needed to achieve the desired plant, the ideal compensator will indicate this. Regardless of the form of the ideal compensator, information is available to guide the designer in choosing the compensator structure or in assessing the choice of H_d.

2.4.5 Formulating the Minimization Problem

The error in outputs between the ideal y_d and the actual outptut y is defined to be

$$\epsilon \triangleq H_d - H. \tag{2.30}$$

This may also be expressed as

$$\epsilon = H_d - (I + GK)^{-1}G.$$

After some manipulation (see Appendix A) this results in

$$\epsilon = H(G^{-1}H_d - I) + HKH_d \tag{2.31}$$

Where G^{-1} is available since all of the above transfer function matrices are given in terms of frequency responses.

Since K can be expressed as a transfer function matrix

$$K = \begin{bmatrix} \frac{n_{11}}{d_{11}} & \frac{n_{12}}{d_{12}} & \cdots & \frac{n_{1m}}{d_{1m}} \\ \frac{n_{21}}{d_{21}} & \frac{n_{22}}{d_{22}} & & \vdots \\ \vdots & & \ddots & \\ \frac{n_{m1}}{d_{m1}} & \cdots & & \frac{n_{mm}}{d_{mm}} \end{bmatrix}$$

then, if the denominator transfer function matrix, D_k is fixed as

$$D_k = \begin{bmatrix} \frac{1}{d_{11}} & \frac{1}{d_{12}} & \cdots & \frac{1}{d_{1m}} \\ \frac{1}{d_{21}} & \frac{1}{d_{22}} & & \vdots \\ \vdots & & \ddots & \\ \frac{1}{d_{m1}} & \cdots & & \frac{1}{d_{mm}} \end{bmatrix}$$

equation 2.31 may be transformed into a linear least squares problem for the numerator transfer function matrix N_k. We note N_k may be expressed as

$$N_k = \begin{bmatrix} n_{11} & n_{12} & \cdots & n_{1m} \\ n_{21} & n_{22} & & \vdots \\ \vdots & & \ddots & \\ n_{m1} & \cdots & & n_{mm} \end{bmatrix}.$$

The designer chooses the structure and order of N_k guaranteeing the causality of the compensator K.

This minimization problem may then be solved on a point-by-point basis in the frequency domain. The minimization problem shown in equation 2.31 can be more generally expressed (dropping the fr subscript)

$$\min_K \|Y - AKB\|_2 \tag{2.32}$$

where

$$Y = H(G^{-1}H_d - I)$$

$$A = -H$$

$$B = D_k H_d$$

and all have been evaluated point-by-point in the frequency domain. This

problem may then be converted to the form

$$\min_{\Theta} \|Y - X\Theta\|_2 \tag{2.33}$$

by using the *vec* operator on equation 2.32 [18].

The *vec* operator is defined as the following. Given a matrix

$$Z = \begin{bmatrix} z_1 & z_2 & z_3 \end{bmatrix}$$

where z_1, z_2, z_3 are the column vectors of Z, the operation $vec\, Z$ is defined as

$$vec\, Z = \begin{bmatrix} z_1 \\ z_2 \\ z_3 \end{bmatrix}.$$

Also, given the matrices, X, Y, Z, the quantity $vec\,(XYZ)$ is

$$vec\,(XYZ) = (Z^T \otimes X) vec\, Y$$

where $\otimes$ signifies a kronecker delta multiplication.

Therefore, if the frequency responses for the system are arranged as an $mm \times p$ matrix, then for example,

$$Y_{fr} = \begin{bmatrix} y_1(j\omega_1) & \cdots & y_m(j\omega_1) \\ y_1(j\omega_2) & \cdots & y_m(j\omega_2) \\ \vdots & \ddots & \vdots \\ y_1(j\omega_p) & \cdots & y_m(j\omega_p) \end{bmatrix}$$

where each $y_m(j\omega_p)$ is an $1 \times m$ matrix of the form

$$y_m(j\omega_p) = \begin{bmatrix} y_{1m}(j\omega_p) & \cdots & y_{mm}(j\omega_p) \end{bmatrix}$$

Notice that N_k is still in coefficient form. Therefore, for a compensator of order l, N_k takes the form:

$$N_k = \begin{bmatrix} n_{11}^l(j\omega^l) & n_{11}^{l-1}(j\omega^{l-1}) & \cdots & n_{11}^0(j\omega^0) \\ n_{21}^l(j\omega^l) & n_{21}^{l-1}(j\omega^{l-1}) & \cdots & n_{21}^0(j\omega^0) \\ \vdots & \vdots & \ddots & \vdots \\ n_{mm}^l(j\omega^l) & n_{mm}^{l-1}(j\omega^{l-1}) & \cdots & n_{mm}^0(j\omega^0) \end{bmatrix}$$

Since any element n_{mm}^l may be zero, the numerators are not all constrained to be of the same order. So applying the *vec* operator to equation 2.32 the classic least squares form is obtained or

$$Y - X\Theta = 0. \tag{2.34}$$

where

$$Y = vec\, Y$$

$$X = B^T \otimes A\Sigma$$

$$\Theta = vec\, N_k.$$

The matrix Y is now $mml \times 1$ of the form

$$Y = \begin{bmatrix} y_{11}(j\omega_1) \\ \vdots \\ y_{mm}(j\omega_1) \\ \vdots \\ y_{mm}(j\omega_p) \end{bmatrix}$$

and the matrix $B^T \otimes A$ is $mm \times mm$. Then Σ results from factoring $vec\, N_k$

into the $mm(l+1) \times 1$ vector

$$\Theta = \begin{bmatrix} n_{11}^{l} \\ n_{11}^{l-1} \\ \vdots \\ n_{11}^{0} \\ \vdots \\ n_{mm}^{l} \\ n_{mm}^{l-1} \\ \vdots \\ n_{mm}^{0} \end{bmatrix}$$

made up of the constant elements of the numerator transfer function matrix and the $mm \times mm(l+1)$ matrix Σ containing the dynamics, where

$$\Sigma = \begin{bmatrix} (j\omega)^l & (j\omega)^{l-1} & \cdots & 1 & & & & & & \mathbf{0} \\ & & & & (j\omega)^l & (j\omega)^{l-1} & \cdots & 1 & & \\ & & & & & & & & \ddots & \\ \mathbf{0} & & & & & & & & (j\omega)^l & (j\omega)^{l-1} \quad \cdots \quad 1 \end{bmatrix}.$$

Finally, since it is desired that the solution to the least squares problem be real, the problem may be restated as

$$\begin{bmatrix} Y_{Re} \\ Y_{Im} \end{bmatrix} = \begin{bmatrix} X_{Re} \\ X_{Im} \end{bmatrix} \Theta \tag{2.35}$$

where $Y = Y_{Re} + jY_{Im}$, $X = X_{Re} + jX_{Im}$. This can then be solved for a real solution Θ using the numerically stable QR algorithm [18].

Therefore, returning to equation 2.31 the procedure to obtain N_k is as follows:

1. Choose an H_d, D_k and ω.

2. Let $H = H_d$, $\epsilon = 0$.

3. Compute the appropriate frequency responses and find a least squares solution to equation 2.31.

4. Compute H and ϵ.

5. If ϵ is less than some tolerance, quit, else return to step 3.

The algorithm may also be stopped after some specified number of iterations. Note that the algorithm is not convex and is not guaranteed to converge. Extensive experience shows, however, that for reasonable choices of H_d, the algorithm will converge quickly. Generally, a few iterations will suffice. It is recommended that the designer observe the error after each iteration and stop the iterations when deemed appropriate.

2.4.6 Constraints

One of the advantages of this methodology is that the order of each individual transfer function in the compensator transfer function matrix may be constrained. Therefore, the order of each transfer function element may be set appropriately, usually using the ideal compensator as a guide. This is achieved within the minimization by setting higher order terms to zero and not letting the minimization routine act on them. Similarly, the values of any of the individual transfer function elements and even just the individual values of a specific numerator may be fixed and the minimization allowed to proceed. The constraints are achieved within the minimization by moving the constrained elements to the left side of equation 2.34.

2.4.7 Weights

Another aspect of the methodology is that it is possible to weigh individual channels of the actual transfer function H within the minimization problem. This may be expressed as

$$\min_{K} \|W. * (H_d - H)\|_2 \tag{2.36}$$

Where the .* operation signifies an element-by-element multiplication. Note that all elements of the weight matrix W must be greater than zero.

2.4.8 Methodology Summary

After several iterations of choosing ideal plants and manipulating the denominators, channel weights, etc., the designer should be able to derive an inner loop compensator which will provide the necessary damping over the full range of parameter variation.

To summarize, the steps for constructing an inner loop compensator are as follows.

1. A desired closed loop transfer function, H_d, in terms of channel-by-channel desired transfer functions is obtained; H_d reflects the system shown in Figure 2.3. The most important decisions in using the methodology are choosing the desired closed loop shape, H_d, the compensator pole locations, and the numerator order. Remember the methodology provides no guarantees, therefore it helps to choose H_d "intelligently" with roughly the same magnitude and bandwidth of the plant. While the methodology can provide compensators which improve the closed loop performance, here the H_∞ compensator will provide performance, the inner loop is used to desensitize the plant to parameter uncertainty.

2. A frequency domain channel-by-channel representation of the ideal compensator, K_{ideal}, is obtained. It is suggested that a fairly large frequency range be used in this step to fully obtain the ideal compensator characteristics.

3. Using this ideal compensator and the constraints of the problem, the denominators for the individual channel transfer functions are chosen (fixing the order of the compensator). Generally, the denominators are chosen using the ideal compensator as a guide. The shape of the ideal compensator will also provide guidance on choosing the order of the denominator. An advantage of this methodology is that it allows the compensator order to be less than that of the plant. Some iteration may be necessary to place the denominator poles correctly.

4. Any remaining constraints on the numerators are expressed; these include fixing the order of each of the elements of N_k and also constraining any of the elements of N_k as desired, i.e. setting a particular element of N_k to a predetermined numerator polynomial (including 0). Here one also reflects the relative weighting of the individual channels.

5. The compensator is then optimized to reduce the least squares error between the desired plant, H_d, and the actual plant, H, point-by-point along a given frequency vector. The frequency range chosen is a design variable. It is recommended that the range be limited to some interval about crossover. If the compensator or desired plant has low or high frequency characteristics that the designer wishes to maintain, the frequency range may be extended. The number of frequency points must also be chosen so as to seek a balance between fully reflecting the plant characteristics and achieving desirable numerical iteration speed.

6. The resulting system, T_{inner}, is checked to determine if it meets the

requirements.

This process is repeated as necessary until a satisfactory compensator is obtained.

This methodology is useful and effective for the following reasons:

- The compensator structure chosen is inherently resistant to parametric uncertainty, especially that affecting the plant open loop pole location. See Section 2.4.3.

- The methodology lets the designer choose the order of the compensator and this allows the minimization of compensator complexity (see Section 2.4.5.

- The methdology allows the designer to work in the frequency domain, choosing the desired closed loop system (T_{inner}) frequency response. Based on this response the methodology indicates the structure of the necessary compensator, K_{inner}(see Sections 2.4.2 and 2.4.4).

- The methodology is amenable to various compensator constraints (see Section 2.4.6).

After completing the design of the inner loop compensator, one would be ready to proceed with the outer loop design using the H_∞ methodology.

2.5 Design of the H_∞ Compensator

The H_∞ methodology was chosen for the outer loop compensator because it is a popular MIMO technique which derives closed loop system performance through explicit frequency domain loopshaping. H_∞ designs tend to be robust to *unstructured uncertainty* for *well behaved* plants. The H_∞ design procedure is well documented, see for example [9, 13] for the theory and [5, 8] for actual

design examples, and, therefore, it will be explained only briefly here. Though in this application it is desired that the H_∞ methodology construct a compensator of the standard feedback design, the methodology is very general. Given a FDLTI system of the form shown in Figure 2.6, where

u_1 = exogenous inputs (references, disturbances, etc.)

u_2 = control (actuator) inputs

y_1 = controlled outputs

y_2 = measured outputs.

The objective of the H_∞ methodology is: for a transfer function matrix, $P'(s)$, construct a stabilizing compensator, $K_\infty(s)$, to minimize the closed loop transfer function from u_1 to y_1, T_{y1u1} such that

$$\min_{K_\infty} \|T_{y1u1}\|_\infty = \gamma_{optimal} \tag{2.37}$$

Practically, one iterates on the value of γ until it is aribrarily close to (but not necessarily equal to) $\gamma_{optimal}$.

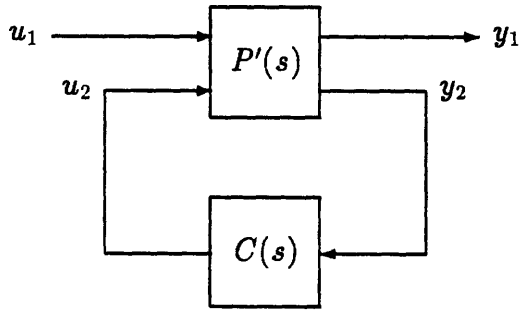

Figure 2.6: The H_∞ Problem

The transfer function $P'(s)$ represents the plant (in this thesis with the inner loop compensator) augmented by some weighting functions. To solve the problem, the H_∞ methodology expresses this augmented plant, P' in state-space form as

$$P'(s) = \left[\begin{array}{c|cc} A & B_1 & B_2 \\ \hline C_1 & D_{11} & D_{12} \\ C_2 & D_{21} & D_{22} \end{array}\right]$$

The H_∞ compensator is then obtained by solving two Ricatti equations, see [12].

To design a controller for the standard feedback configuration, the H_∞ methodology generally uses the following approach. The plant, P (here the original plant G with the inner loop compensator, K_{inner}), is augmented with weighting functions $W_1(s), W_2(s)$, and $W_3(s)$ as shown in Figure 2.7 to yield an augmented plant, P'.

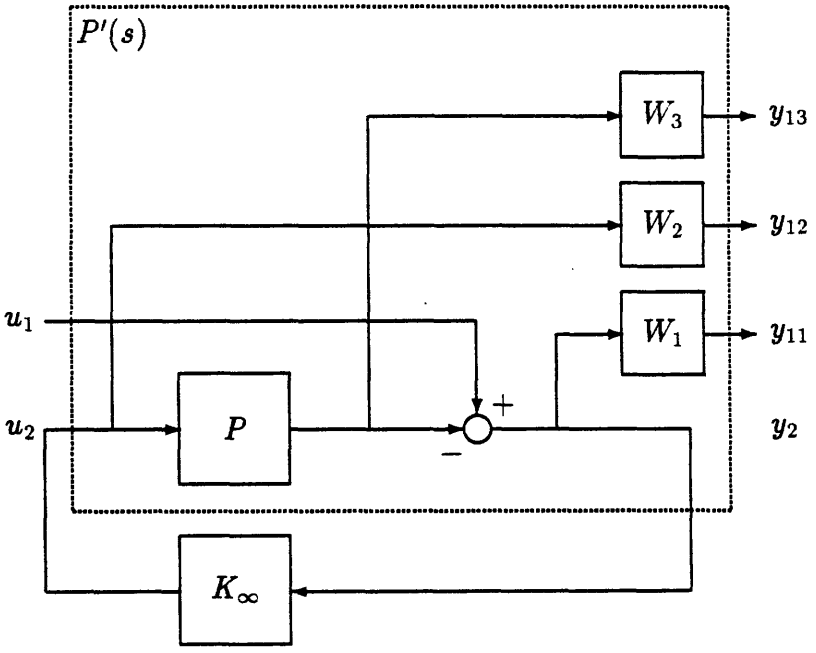

Figure 2.7: The H_∞ Standard Feedback Configuration with Weights

The weighting functions are used for loopshaping, where $W_1(s)$ provides performance and is generally the inverse of the desired sensitivity function. $W_3(s)$ is used to provide robustness to unstructured uncertainty and is generally the inverse of the desired closed loop (complementary sensitivity) transfer function. $W_2(s)$ provides any desired weighting on the controller. The transfer function which is being reflected by W_2 will be called R. It is the transfer function from r to u, and is expressed as

$$R = K(I + GK)^{-1}$$

in terms of the standard feedback configuration as shown in Figure 2.2.

The combination of weights W_1 and W_3 is known as the mixed sensitivity problem. The designer attempts to find a balance between disturbance rejection, as reflected by W_1, and the closed loop bandwidth which will specify robustness to unstructured uncertainty and command following performance, reflected by W_3. One of the many issues that arise in this type of problem is whether to allow peaking in the sensitivity and complementary sensitivity transfer functions. To allow more freedom in the design, W_1 is often weighted by a scalar ρ; this allows it to be adjusted independently of W_3. If so, this system of plant and weights may be represented as the following transfer function matrix.

$$\begin{bmatrix} y_{11} \\ y_{12} \\ y_{13} \\ y_2 \end{bmatrix} = \begin{bmatrix} \rho W_1(s) & -\rho W_1(s)P(s) \\ 0 & W_2(s) \\ 0 & W_3(s)P(s) \\ I & -P(s) \end{bmatrix} \begin{bmatrix} u_1 \\ u_2 \end{bmatrix}$$

The actual solution to the H_∞ problem now may be expressed as

$$\left\| \begin{array}{c} \rho W_1 S \\ W_2 R \\ W_3 T \end{array} \right\|_\infty = \gamma \tag{2.38}$$

where

$$\gamma \geq \gamma_{optimal}.$$

The weight, $W_1(s)$ used to express the constraint on the sensitivity transfer function (the actual constraint is enforced by W_1^{-1}) is subject to a special condition in this design. Given the system shown in Figure 2.2, the system to which the H_∞ design process is being applied, is the standard feedback configuration with G equal to T_{inner}, with the sensitivity function given as

$$S'(s) = (I + T_{inner} K_\infty)^{-1}. \tag{2.39}$$

Substituting for T_{inner} and rearranging,

$$S'(s) = [I + G(K_{inner} + K_\infty)]^{-1}(I + GK_{inner}) \tag{2.40}$$

which is equal to to $S_e(s)$ as given in equation 2.14, the transfer function from reference r to error e. Since the sensitivity of the closed loop system with both compensators to an output disturbance was given in equation 2.13 as

$$S(s) = [I + G(K_\infty + K_{inner})]^{-1}$$

this indicates that the inverse of the actual constraint placed on the sensitivity by $W_1(s)$ is

$$W_1'(s) = (I + GK_{inner})W_1. \tag{2.41}$$

Care must be used in choosing W_1 so as to restrict the disturbance sensitivity function, $S(s)$ as well as the command following properties of $S_e(s)$. If a W_1' is chosen then the weight W_1 to be used in the H_∞ design is

$$W_1 = (I + GK_{inner})^{-1} W_1'. \tag{2.42}$$

Therefore, the designer can determine the desired sensitivity function relating to an output disturbance, $S(s)$, and check the error sensitivity function, $S_e(s)$, or vice-versa.

Software to facilitate the standard feedback problem is commercially available as is software which solves the general H_∞ problem, for example, the PRO-MATLAB Robust Control Toolbox. Since the H_∞ approach is general, any feedback configuration, with any fictitious inputs or outputs desired, could be used as long as the problem can be put in the form of Figure 2.6. If so it is relatively easy to write the accompanying state-space description which will allow this to be used with commercially available H_∞ software packages.

Generally, $P(s)$ will be in state-space form while the weights are expressed as multivariable transfer function matrices. Several methods exist to allow for improper $W_3(s)$. $W_2(s)$ is often chosen to be of the form ϵI, where ϵ is some small number, to ensure that D_{12} is of full rank [5].

Explanations of how the H_∞ methodology is applied are contained in the design examples. For further explanation the references cited above, [5, 8] are useful.

When the H_∞ design is finished, the complete compensation network will have been designed. This compensation network should then provide stability and performance which is robust to the range of parametric uncertainty expected. Moreover, this design should be robust to standard design uncertainties such as unmodelled dynamics, plant disturbances, etc. if a reasonable bandwidth was selected for W_3.

2.6 H_∞ Compensator Order Reduction

One disadvantage of the H_∞ methodology is that it leads to compensators of high order, as an H_∞ compensator will always have at least the order of the augmented plant, $P'(s)$, used to create it. High order and complexity makes the compensator more difficult to implement. Therefore, it is desirable to reduce the compensator order when possible. Fortunately, some amount of compensator order reduction is usually possible. However, though the H_∞ methodology guarantees some amount of robust stability, all such gurantees are lost when the compensator order is reduced. Therefore, it is very important to check that the system with the reduced order compensator meets the same specifications which the original system achieved.

The steps used here to reduce the order of the H_∞ compensator are as follows.

1. From the bode or singular value plots of the n^{th} order H_∞ compensator, estimate the number of states (k) the compensator can be reduced to. This may be done by observing the changes in slope in the plot and estimating the number of poles necessary to achieve those changes in slope. The algorithms used, see (2) below, also allow the examination of the Hankel singular values of the full order compensator which may provide information on the number of states which can be eliminated.

2. Compute a reduced order realization of the compensator. The techniques used herein are Schur model reduction, as implemented by the PRO-MATLAB Robust Control Toolbox function *schmr* [5], and balanced least squares model reduction, as implemented by the PRO-MATLAB Robust Control Toolbox function *balmr* [5].

3. Compare the reduced order compensator to the original compensator. This can be done in several ways. A quantitative measure of the dif-

ference in the compensators is contained in the algorithms used. Both algorithms compute a k^{th} order reduced compensator according to the criterion

$$\|K_\infty - K_\infty^{ro}\|_\infty \leq 2 \sum_{i=k+1}^{n} k_\infty(i) \tag{2.43}$$

and return the value of $2\sum_{i=k+1}^{n} k_\infty(i)$. It is also useful to compare the Bode or singular value plots of the compensators and compute the error as a function of frequency. If these measures are small it is likely that the reduced order compensator will achieve the design objectives. It is advisable to iterate between steps 2 and 3 until the compensator has been reduced as much as possible while maintaining its frequency response characteristics. The H_∞ methodology guarantees that the nominal system is closed loop stable; reducing the order of the compensator removes this guarantee. However, one is usually able to reduce the compensator order by some amount while maintaining all of the stability and performance results of the nominal H_∞ compensator.

4. Generate the compensated system with the reduced order compensator and *check* the system stability, frequency response, and time domain response as for the original H_∞ compensator. If the reduced order compensator does not meet the performance of the original H_∞ compensator, obviously a higher order compensator should be used. If the system response with the reduced order compensator meets the requirements, then the design is finished.

2.7 Analyzing the Closed Loop System

This compensation network should provide stability and performance which is robust to the range of parametric uncertainty expected. Moreover, this design should be robust to standard design uncertainties such as unmodelled

dynamics, plant disturbances, etc. The following loopshapes will be examined in an attempt to determine the success of a design: open loop (both servo and regulator), closed loop, and the sensitivity. The MIMO or SISO gain and phase margins will be calculated to determine robustness to unstructured uncertainty.

It is also important to determine the effect of the inner loop on the plant without the presence of the outer loop because it is unlikely that the full compensation network will have desirable properties if T_{inner} does not desensitize the plant to parameter uncertainty. In fact, this should be determined before design of the outer loop begins. Therefore, one should examine the open and closed loop shapes to determine robustness to both the parametric variation and unstrucured uncertainty. It also important to know the characteristics of the T_{inner} loop shape the H_∞ methodology will use.

For all of the above loop shapes the fact that this is a plant with some amount of parametric variation must be accounted for. Therefore, it is important to examine the loop shapes not only in terms of some nominal parameter values for which the compensator has been designed, but also the ranges of parameter variation to be considered. Therefore, in this thesis the following cases are examined:

- The nominal case (also the design case).
- The minimum value of the parameter variation.
- The maximum value of the parameter variation.

The assumption of the nominal case as the design case implies that it is desired that the system performance be optimized for this case, with the system robustness extending that performance over the range of parametric uncertainty. The approach listed above will lead to a large number of singular value plots.

Notice that for cases of multiple parametric uncertainty one may not be able to calculate the minimum and maximum cases of parametric variation as these may be hard to determine. The cases examined in this thesis allow for such a determination and were chosen as such for illustration purposes. In a case where this information is not available, the options include use of a multivariable margin which accounts for real parametric uncertainty, see Section 1.1, through Monte Carlo simulation, or placing an upper (or lower) bound on each element of the state-space matrices and assuming this reflects the worst case.

One of the primary results of the parameter variation in the examples considered in this thesis is that the positions of lightly damped poles will vary with the uncertainty. Since the primary function of the inner loop will be to damp these poles, it will also be instructive to consider the locations and damping ratios of these poles over the range of parameter variation with the inclusion of the inner loop compensator. This will be expressed in terms of root locus plots and tabular listings of poles, frequencies, and damping ratios.

Time domain responses of the compensated systems are also important to understanding the system and determining if they meet the time domain design specifications. Several types of time response simulations will be considered. These include:

- Injection of an impulse disturbance to determine disturbance rejection characterisitics.
- Injection of a constant frequency sinusoidal disturbance to determine disturbance rejection characteristics.
- Reference step commands to determine the command following characteristics of the closed loop system.
- The inclusion of random Gaussian measurement noise in certain simula-

tions to determine the system noise rejection characteristics.

For each of these simulations the items of interest are the output position and the control efforts of the model-matching and H_∞ compensators as functions of time.

2.8 Summary of the Methodology

The approach taken here towards constructing compensators which provide robust stability and performance to systems with parametric uncertainty may be summarized in the following steps.

1. Obtain/construct a model of the plant. Ascertain the range of parameter uncertainty or variation present in this model. Construct/apply design specifications both for the nominal plant and the range of parameter variation, i.e. nominal performance or performance over a specified range of parametric variation.

2. Construct an inner loop compensator using the model-matching methodology presented herein. Attempt to minimize the effects of the parametric uncertainty.

3. Construct an H_∞ compensator using the standard H_∞ methodology. Use weighting functions which reflect the design specifications and/or robustness bounds.

4. Analyze the entire system, plant, inner loop compensator, and H_∞ compensator with regard to the design specifications. If the nominal system does not meet the performance specifications return to step 3. If the parametric uncertainty degrades the performance significantly return to step 2. Iterate until a satisfactory system has been obtained.

5. If compensator complexity is an issue, apply a model reduction algorithm to the H_∞ compensator. Check the stability robustness and performance of the reduced order compensator with regard to the design specifications.

Chapter 3

A Benchmark Problem for Robust Control Design

The following problem was proposed by Wie and Bernstein [25] as a benchmark for testing different robust control methodologies. A 1990 American Control Conference (ACC) session was devoted to controllers which "solved" the problem [4, 6, 7, 17, 22]. Here the methodology of a model matching inner loop and an H_∞ outer loop is used to construct two different designs. Both designs meet most of the performance goals of the problem while producing designs of high order. The results are compared to those from the ACC session and are shown to outperform the majority of the ACC designs.

3.1 The Plant

The benchmark problem is shown in Figure 3.1 and is a two mass, one spring system with non-colocated sensor and actuator.

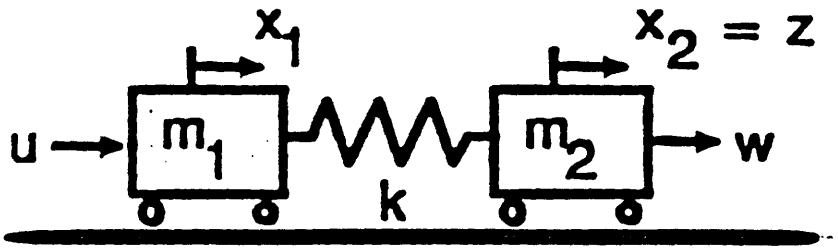

Figure 3.1: The Mass-Spring System with Noncolocated Sensor and Actuator

The system may be expressed in state-space form as:

$$\begin{bmatrix} \dot{x}_1 \\ \dot{x}_2 \\ \dot{x}_3 \\ \dot{x}_4 \end{bmatrix} = \begin{bmatrix} 0 & 0 & 1 & 0 \\ 0 & 0 & 0 & 1 \\ \frac{-k}{m_1} & \frac{k}{m_1} & 0 & 0 \\ \frac{k}{m_2} & \frac{-k}{m_2} & 0 & 0 \end{bmatrix} \begin{bmatrix} x_1 \\ x_2 \\ x_3 \\ x_4 \end{bmatrix} + \begin{bmatrix} 0 \\ 0 \\ \frac{1}{m_1} \\ 0 \end{bmatrix} u + \begin{bmatrix} 0 \\ 0 \\ 0 \\ \frac{1}{m_2} \end{bmatrix} w$$

$$y = x_2 + v$$

$$z = x_2$$

where

x_1 = position of body 1

x_2 = position of body 2

x_3 = velocity of body 1

x_4 = velocity of body 2

u = control input

w = plant disturbance

y = sensor measurement

v = sensor noise

z = performance variable (output to be controlled).

The problem may also be expressed in transfer function form [6] as

$$\frac{z(s)}{u(s)} = \frac{k}{m_1 s^2[m_1 s^2 + k(1 + \frac{m_2}{m_1})]} \tag{3.1}$$

3.2 Design Specifications

The design specifications are presented as three sub-problems. All three specify that $m_1 = m_2 = 1$, in the nominal system $k = 1$, and that the compensator be a constant gain, linear feedback design expressible in state-space form. The three specifications are then:

Design 1

(i) The closed loop system is stable for $0.5 < k < 2.0$.

(ii) For $w(t)$ = unit impulse at $t = 0$, z has a settling time of 15 seconds for the nominal system.

(iii) The measurement noise is to be characterized by each designer.

(iv) Achieve reasonable performance and stability robustness.

(v) Minimize controller effort.

(vi) Minimize controller complexity.

Design 2

Replace (ii) above with

> $w(t)$ is a sinusoidal disturbance of frequency 0.5 rad/sec but unknown amplitude and phase. Achieve asymptotic rejection of the disturbance in z with a 20 second settling time for $0.5 < k < 2.0$.

Design 3

Replace (i) with

maximize a stability performance measure with respect to the three uncertain parameters, m_1, m_2, k, whose nominal values are 1.0.

The concept of parametric uncertainty is represented here as a known parametric variation which is easily measured. The effort shall be to design a compensator system which attempts to meet the requirements of the first two designs simultaneously. The criteria for **Design 3** are not addressed.

3.3 Analysis of the Plant

To help understand the problem, Figure 3.2 shows the bode plots of the nominal system, as well as the system with $k = 0.5$ and $k = 2.0$. It can be seen that the natural frequency of the undamped poles migrates from 1 rad/sec to 2 rad/sec as k varies from 0.5 to 2.0, with a value of 1.414 ($\sqrt{2}$) when $k = 1.0$. Both pole location and plant gain are changing as k varies.

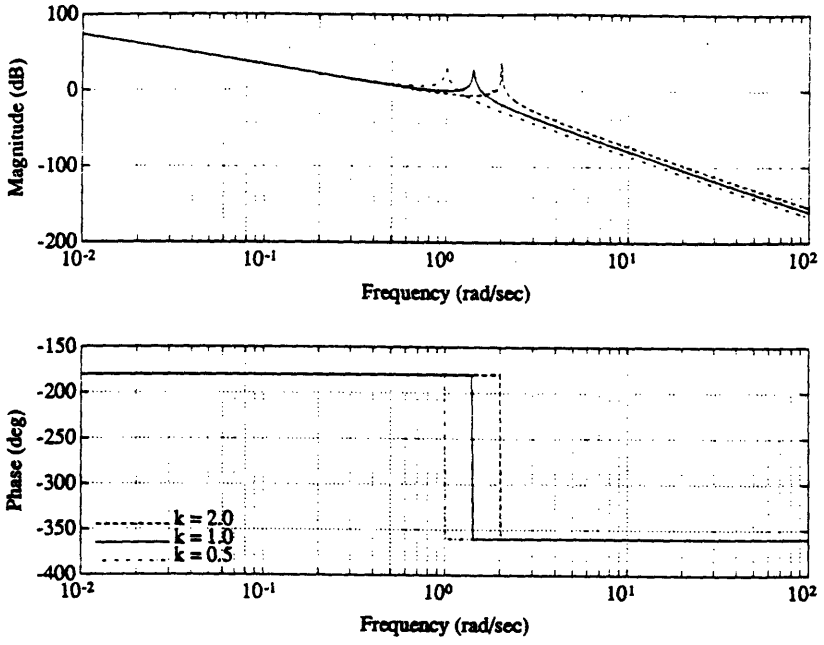

Figure 3.2: Bode Plot of the Benchmark Problem with $k = 0.5,\ 1.0,\ 2.0$

3.4 Compensator Design A

It was stated above that the designs in this section would be developed in two stages. The first stage is where the inner closed loop transfer function T_{inner} is designed to have two free integrators, as does the nominal plant. The reason for this approach is to have the integrators available for closed loop performance (Type 2 system) and to attempt to replicate the original plant as closely as possible with the effects of the uncertainty removed. The second stage, Design B, won't have any free integrators in the inner closed loop transfer function.

The closed loop system with both compensators and all of the signals of interest is shown in Figure 3.3. This closed loop system is used to analyze all of the designs in this thesis.

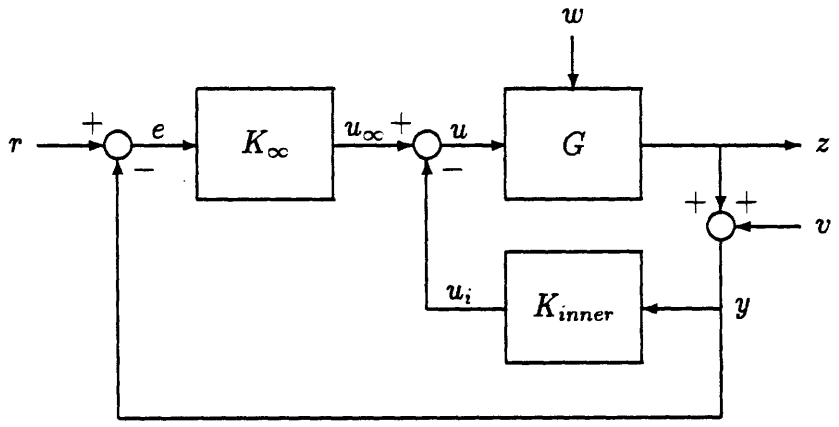

Figure 3.3: The Closed Loop System with Feedforward and Feedback Path Compensators, Showing All Inputs and Outputs

The variables shown in Figure 3.3 are:

G = the plant

K_∞ = the compensator generated using the H_∞ methodology

K_{inner} = the inner loop compensator generated using the model-matching methodology

r = an external reference

e = the error signal

y = the measured output

z = the performance output (the controlled variable)

w = an external disturbance

v = measurement noise

u = the plant input $(u_\infty - u_i)$

u_∞ = the H_∞ compensator output (control signal)

u_i = the inner loop compensator output (control signal)

3.4.1 Constructing the Inner Loop Compensator: Design A

The first step in constructing the inner loop compensator is construction of a desired plant, H_d. Here an obvious choice for such a plant is the same system as that given in the problem, but with the undamped poles placed on the real axis. Such a desired plant would have the transfer function

$$\frac{z(s)}{u(s)} = \frac{1}{\frac{s^2}{1.414^2} + \frac{2(1)s}{(1.414)} + 1}$$

for the nominal case ($k = 1$) and the bode plot shown in Figure 3.4. Constructing a frequency vector from 0.01 to 100 rad/sec and computing the frequency responses of G^{-1} and ${H_d}^{-1}$ yields the frequency domain realization of the ideal compensator as shown in Figure 3.5. The ideal compensator is obviously non-causal and appears to consist of two zeros at the origin and two lead networks.

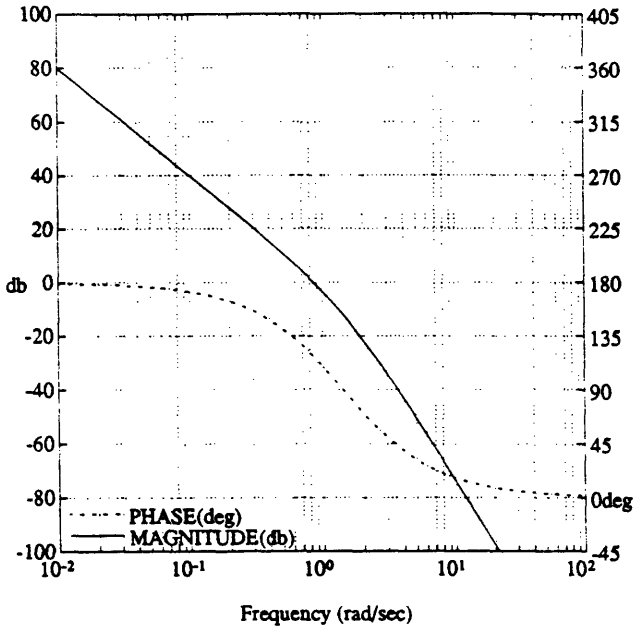

Figure 3.4: Bode Plot of the Ideal Plant, H_d

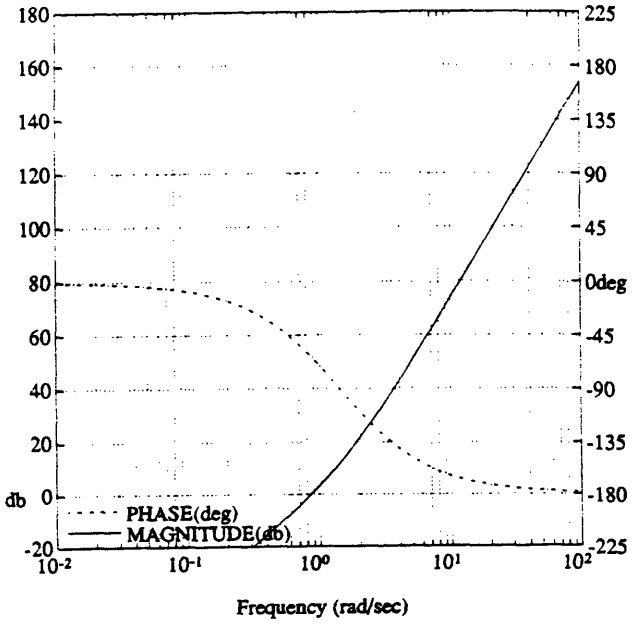

Figure 3.5: Bode Plot of the Ideal Compensator, K_{ideal}

Using this information, we then construct a fourth order compensator to match the ideal compensator; choosing its form to be

$$K_{inner}(s) = \frac{s^2(\alpha_2 s^2 + \alpha_1 s + \alpha_0)}{(.01s+1)^4}.$$

The two free zeros in the numerator are necessary to guarantee that there will be two free integrators in the denominator of the closed loop system, T_{inner}. Therefore, the zeros at the origin are *constrained* to be present in the compensator (see Section 2.4.6) and the model matching method has the freedom to iterate on the values of $\alpha_0, \alpha_1, \alpha_2$. The ability to arbitrarily constrain the compensator in this way is one of the key advantages of this methodology. The denominator is chosen to have four poles at 100 rad/sec. Since the ideal compensator indicates that a pure lead network is desired, the poles are moved out past the frequency range of interest to allow a realizable system. The frequency vector over which to match the desired plant is chosen from 0.1 to 100 rad/sec with fifty frequency points. Experience has shown that fifty frequency points represent accurately the desired and actual closed loop dynamics. Therefore, this number of frequency points is used for all of the designs in this thesis.

The method then yields the compensator

$$K_{inner}(s) = \frac{(0.5174s-1)(0.8577s-1)s^2}{(0.01s+1)^4}$$

which has the bode plot as shown in Figure 3.6. The model-matching algorithm yielded this compensator in two iterations, guaranteeing a least-squares norm (2-norm) of the error ϵ (see equation 2.30) equal to 0.0267. The difference between this error and the least-squares error after the first iteration was -4.335×10^{-8}. This illustrates that, for well chosen plants, the algorithm converges rapidly. In fact, two iterations were used for all of the inner loop compensators generated in this thesis because good convergence was observed

after this number of iterations.

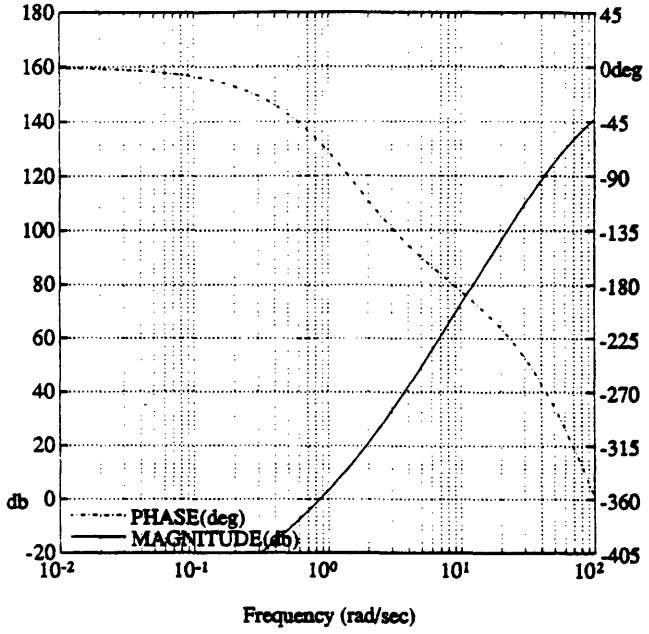

Figure 3.6: Bode Plot of the Initial Inner Loop Compensator

Combining this compensator with not only the nominal plant but also the plants with the values $k = 0.5$ and $k = 2.0$, yields the results shown in Table 3.1 and Figure 3.7. Table 3.1 shows the poles with associated frequencies and damping ratios and Figure 3.7 is a root locus of the closed loop system for $0.5 \leq k \leq 2.0$.

These indicate that, while the compensator does a reasonably good job on the nominal plant by moving the undamped poles to the real axis, it does not perform well in reducing the effect of the parametric variation. Therefore, we have to investigate using an inner loop compensator of the form

$$K_{inner}(s) = \frac{s^2(\alpha_1 s + \alpha_0)}{(.01s + 1)^3}.$$

Here the compensator will iterate on the value of α_1 and α_0. The reduced order of this compensator is chosen based on a desire to reduce complexity.

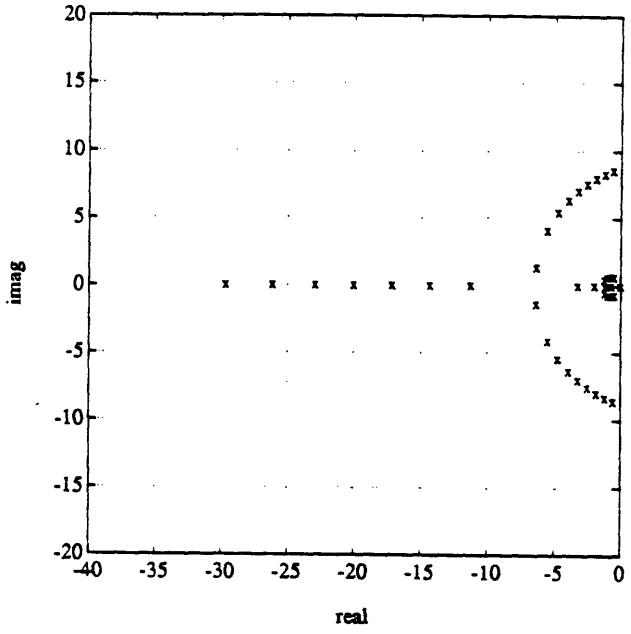

Figure 3.7: Root Locus of the Closed loop System, T_{inner}, for $0.5 \leq k \leq 2.0$

$k = 0.5$			$k = 1.0$			$k = 2.0$		
Poles	ω	ζ	Poles	ω	ζ	Poles	ω	ζ
0	0	NaN	0	0	NaN	0	0	NaN
0	0	NaN	0	0	NaN	0	0	NaN
-.473-0.6716j	0.8214	0.5758	-1.163	1.163	1	-0.702	0.702	1
-.473+0.6716j	0.8214	0.5758	-1.971	1.971	1	-.5616-8.569j	8.587	6.540e-02
-29.62	29.62	1	-14.29	14.29	1	-.5616+8.569j	8.587	6.540e-02
-100.2-68.99j	121.7	0.8238	-100.3-82j	129.6	0.7742	-100.4-97.45j	139.9	0.7175
-100.2+68.99j	121.7	0.8238	-100.3+82j	129.6	0.7742	-100.4+97.45j	139.9	0.7175
-168.9	168.9	1	-182	182	1	-197.4	197.4	1

Table 3.1: Poles of the Closed Loop System, T_{inner}, for $k = 0.5,\ 1.0,\ 2.0$

Also, from a classical viewpoint, the compensator needs to supply at least 180 degrees of phase to stabilize the system. The first design matched H_d well, but did not desensitize the system to parametric variation. Therefore, a compensator of lower order may be less "optimized" for the nominal plant and so provide greater robustness to parametric variation.

The compensator obtained is

$$K_{inner}(s) = \frac{0.9922(1.396s - 1)s^2}{(.01s + 1)^3}$$

and has the bode plot shown in Figure 3.8 below.

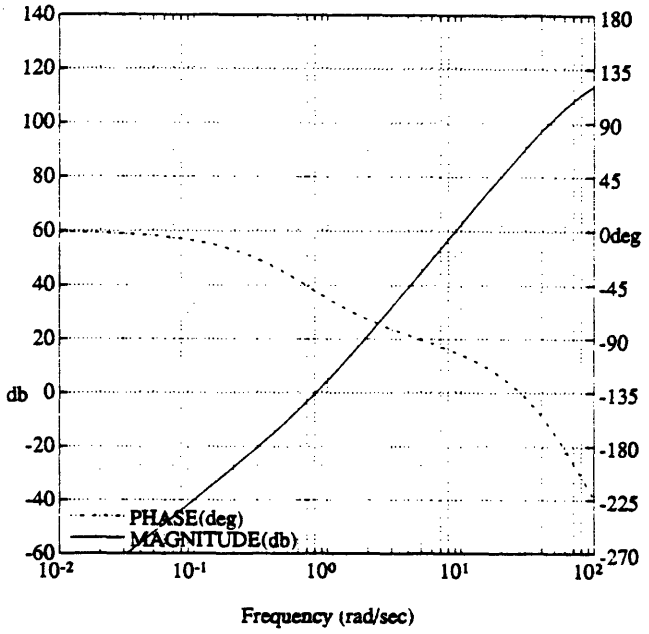

Figure 3.8: Bode Plot of the Third Order Inner Loop Compensator: Design A

Again the closed loop systems are formed and the results presented in Table 3.2 show the poles with their frequencies and damping ratios. Figure 3.9 shows the root locus as k varies over the range of parametric uncertainty. Here the poles start complex and move towards the real axis as k increases from 0.5 to 2.0.

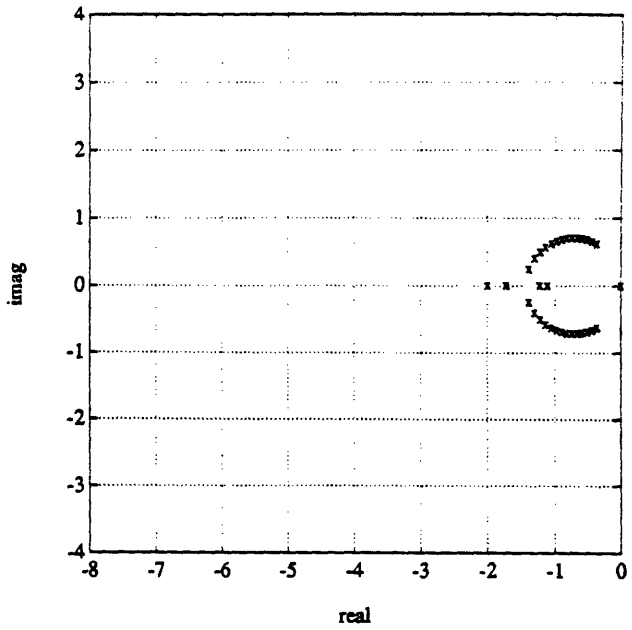

Figure 3.9: Root Locus of the Closed loop System, T_{inner}, for $0.5 \leq k \leq 2.0$

$k = 0.5$			$k = 1.0$			$k = 2.0$		
Poles	ω	ζ	Poles	ω	ζ	Poles	ω	ζ
0	0	NaN	0	0	NaN	0	0	NaN
0	0	NaN	0	0	NaN	0	0	NaN
-0.3613-0.62j	0.7176	0.5035	-0.739-0.7123j	1.026	0.72	-1.111	1.111	1
-0.3613+0.62j	0.7176	0.5035	-0.739+0.7123j	1.026	0.72	-1.993	1.993	1
-79.35	79.35	1	-73.28	73.28	1	-64.94	64.94	1
-110-15.52j	111.1	0.9902	-112.6-19.25j	114.3	0.9857	-116-23.79j	118.4	0.9796
-110+15.52j	111.1	0.9902	-112.6+19.25j	114.3	0.9857	-116+23.79j	118.4	0.9796

Table 3.2: Poles of the Closed Loop System, T_{inner}, for $k = 0.5,\ 1.0,\ 2.0$

The bode plot of the closed loop transfer function, $T_{inner}(s)$, is shown in Figure 3.10 for $k = 0.5,\ 1.0,\ 2.0$. All three magnitude plots have about the same crossover frequency, so the inner loop compensator has significantly reduced the variation due to the parameter uncertainty. This example shows that while the nominal case does not fully match the desired plant, as T_{inner} has complex poles while H_d has real poles, they are well-damped and the compensator does robustify the system to the parametric variation. Though when k is equal to 0.5 there is a pair of slightly underdamped poles near the origin. It is important to realize that robustness to parameter variation is the goal when choosing the compensator structure.

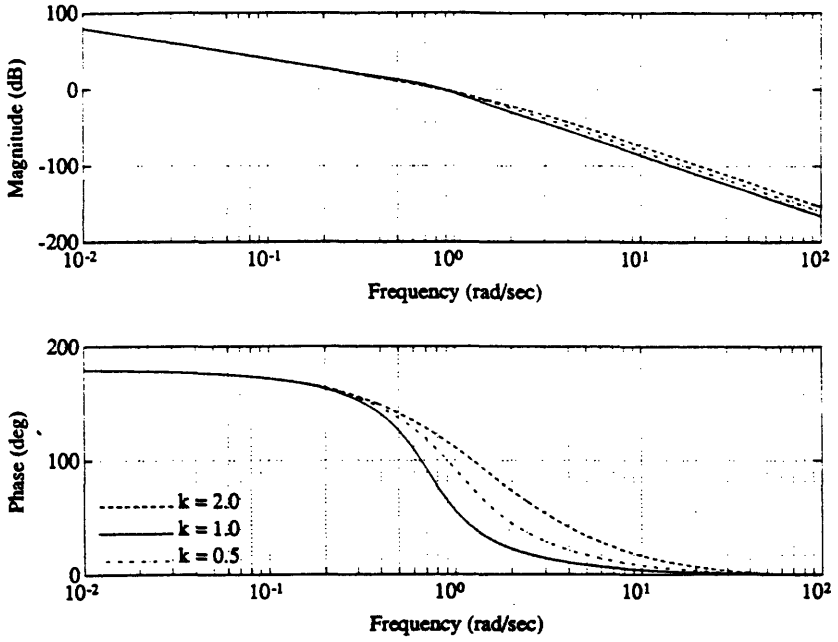

Figure 3.10: Bode Plot of The Closed Loop System, T_{inner}, for $k = 0.5,\ 1.0,\ 2.0$

Notice also that, although the compensator is nonminimum phase, the closed loop system is minimum phase. This is because, for an inner loop compensator, the closed loop transfer function has the form

$$T_{inner}(s) = (I + GK)^{-1}G$$

or, for a SISO system, specifically, the closed loop transfer function can be written explicitly in terms of compensator and plant numerators and denominators, respectively:

$$T_{inner}(s) = \frac{n_G d_K}{n_G n_K + d_G d_K}.$$

Notice that the zeros of the compensator n_K are not present in the zeros of the closed loop transfer function $n_G d_K$. A nonminimum phase compensator does not necessarily result in a nonminimum phase overall closed loop system. The normal performance limitations induced by nonminimum phase zeros are not necessarily induced by a nonminimum phase feedback path compensator; however, it does complicate implementation issues, such as sampling, initialization, etc.

Before proceeding on to the H_∞ design we compare the desired plant with the actual plant. Figure 3.11 combines the two transfer functions bode plots. It

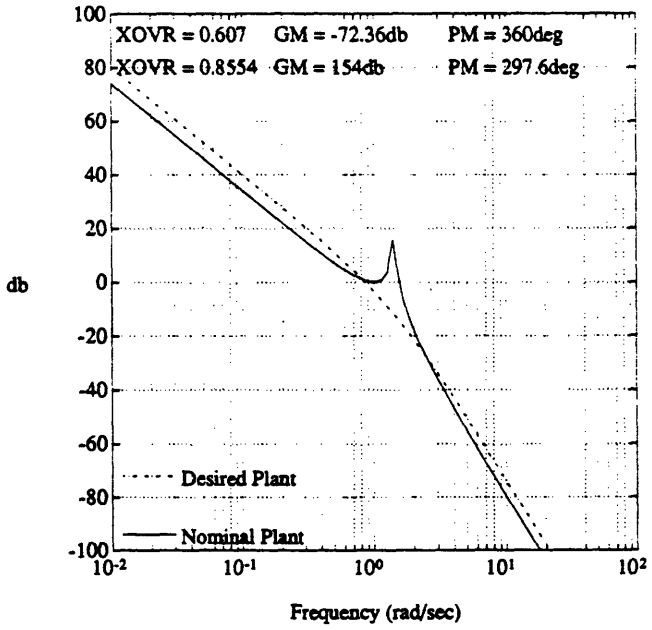

Figure 3.11: Bode Plot Comparing the Desired and Actual Plants

shows that while the desired plant has about the same gain crossover frequency

as the actual plant it does not have quite the same magnitude characteristic above the crossover frequency. Perhaps a better design can be achieved by lowering the gain of the desired plant.

If H_d takes the form

$$\frac{z(s)}{u(s)} = \frac{0.25}{\frac{s^2}{(1.414)^2} + \frac{2(.7071)s}{(1.414)} + 1}$$

then the following third order compensator can be achieved

$$K_{inner}(s) = \frac{1.973(2.967s + 1)}{(.02s + 1)^2(.03s + 1)^2}.$$

The fourth order design is also worse in this case in terms of minimizing the effects of the parametric uncertainty, as measured by the damping ratios of the closed loop poles. The compensator poles have been moved to lower frequencies to bound the compensator gain at high frequencies so as to achieve better measurement noise rejection properties. The compensator bode plot is shown in Figure 3.12.

The effects of parametric variation on this system are illustrated in Table 3.3, showing the closed loop poles and their damping ratio and natural frequency. Also, Figure 3.13 shows the root locus of the closed loop system for $0.5 \leq k \leq 2.0$. For this compensator design the poles in the frequency range of interest remain on the real axis regardless of the value of k.

The reason for the high degree of robustness to the parametric variation appears to be that the second H_d was easier to achieve, since not as much compensator "effort" was necessary to push down the high frequency magnitude. Therefore, the compensator produced was able to also achieve similar results over the full range of parametric uncertainty.

Examining the open loop bode plot for the given range of parameter variation, Figure 3.14 indicates that the system has good gain and phase margins,

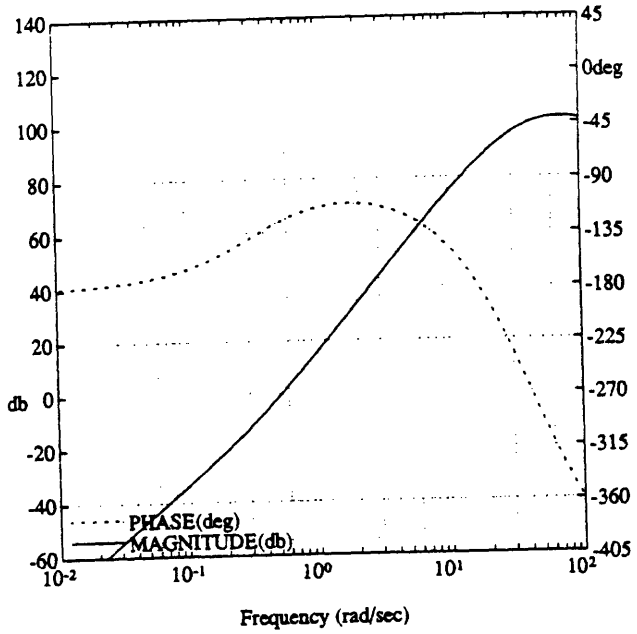

Figure 3.12: Bode Plot of the Model-Matching Design Inner Loop Compensator

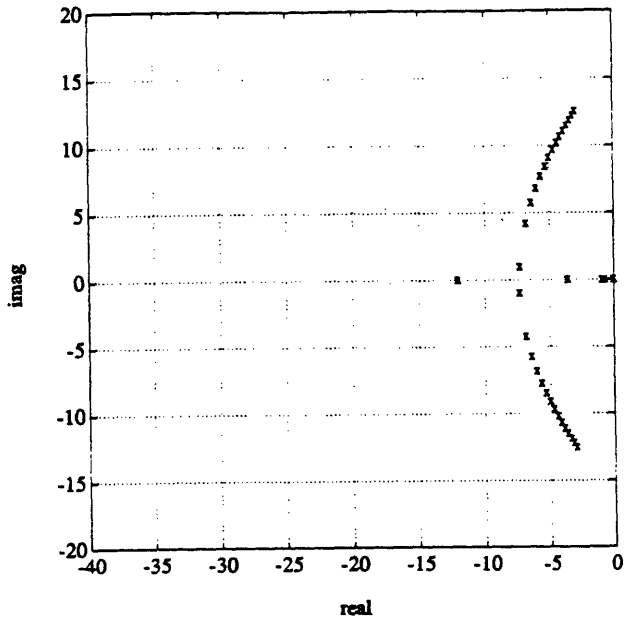

Figure 3.13: Root Locus of the Closed loop System, T_{inner}, for $0.5 \leq k \leq 2.0$

which are tabulated in Table 3.4.

The closed loop bode plot (Figure 3.15) reveals that the inner loop compensator:

- Provided a well behaved nominal system for use in the H_∞ design.
- Significantly reduced the effect of the parameter uncertainty in the frequency range of interest.
- Achieved these results at the expense of the closed loop crossover frequency.

Next, the H_∞ methodology will be used to extend this as needed.

3.4.2 Lessons of the Inner Loop Design

The examples of inner loop compensator design have shown that the methodology presented can achieve an inner loop design that is more amenable to the H_∞ design methodology by removing the effects of parameter uncertainty. It has also demonstrated some useful lessons in using the methodology.

- Choice of the desired plant, H_d will dictate the results of the compensator design and resulting closed loop system. That is, one wants to define a desired plant that differs as little as possible from the nominal plant, while removing the effects of the parametric uncertainty, here the peaking caused by the lightly damped poles. This is no different from any other frequency design technique; intelligent specifications (here on H_d) lead to achievable systems.
- Therefore, choosing a desired plant with a magnitude characteristic (over all frequencies) which is less than or equal to that of the actual plant facilitates a good design. While this may cause a loss in closed loop

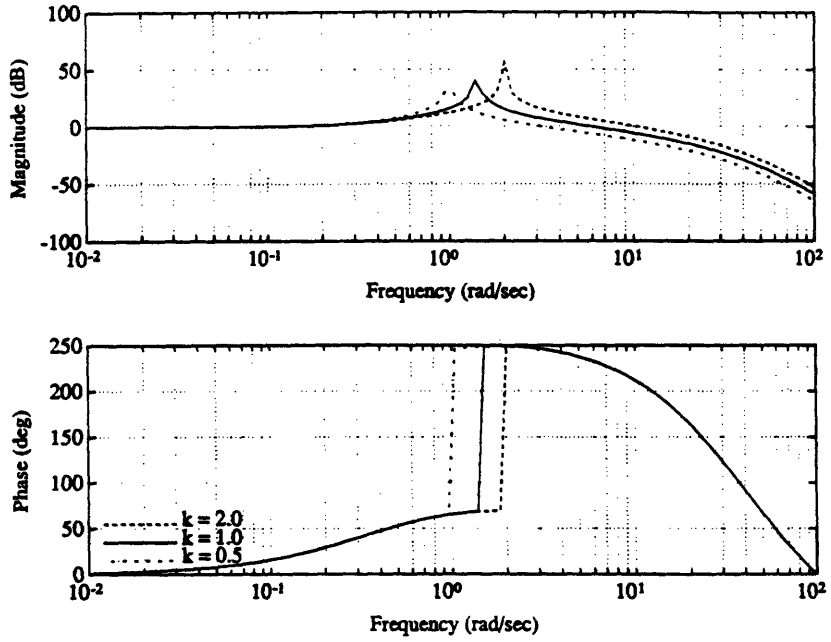

Figure 3.14: Bode Plot of The Open Loop System, GK_{inner}, for k = 0.5, 1.0, 2.0

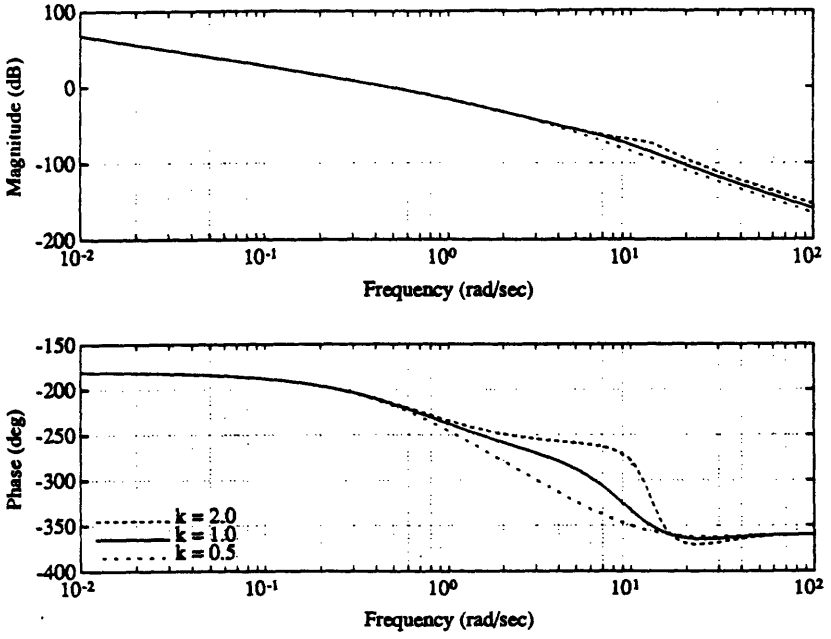

Figure 3.15: Bode Plot of The Closed Loop System, T_{inner}, for k = 0.5, 1.0, 2.0

system bandwidth versus the nominal plant, the H_∞ design can be used to extend the bandwidth as necessary.

- The ideal compensator is a useful indicator in choosing the order and placement of the poles of the inner loop compensator. However, it is just an indicator; the algorithm which constructs the compensator attempts to minimize the difference between the actual and desired closed loop transfer function matrices at selected frequency points without any explicit information from the ideal compensator directly.

- Since the parametric uncertainty is not explicitly accounted for, the designer must exercise judgement in applying the methodology. This means choosing a desired plant which is attainable over the range of parametric variation and choosing the compensator poles so they do not interfere with the compensator effort over the range of parametric variation. For example, in the above design, keeping the compensator poles at a high enough frequency so they do not interfere with the lead network when k is equal to 2.0.

3.4.3 Constructing the H_∞ Compensator: Design A

Both the H_∞ methodology in designing the outer loop compensator and the model matching methodology in designing the inner loop compensator make use of frequency domain choices of the desired closed loop system response. The difference, however, lies in that in the H_∞ methodology, the frequency domain specifications are expressed as limits on the maximum singular values of various closed loop transfer function matrices, while in the model-matching inner loop the specifications are expressed in terms of the transfer functions of each element of the desired closed loop transfer function matrix. In the H_∞ methodology these choices are expressed as frequency dependent weights

on various transfer functions. In the standard feedback configuration used here the weights express the desired sensitivity and complementary sensitivity transfer functions. A constant weight on the control output is also used to meet certain technical aspects of the methodology.

The weight $W_1(s)$ is subject to the following conditions in this design; first, $W_1(s)$ must be designed to reflect desired disturbance rejection characteristics as reflected in $S(s)$ and command following characteristics as reflected in $S_e(s)$ (Section 2.5). Second, because the design plant, the plant augmented by the inner loop compensator, G', has two free integrators $W_1(s)$ must also have two free integrators to guarantee the stability of the closed loop system (with the H_∞ compensator) [15]. For W_3, the closed loop transfer function using the standard feedback configuration with T_{inner} substituted for G, remains identical to that given in equation 2.12 for the closed loop system, T.

After several iterations the following weights were used to obtain a compensator which meets the requirements for the problem set forth above.

$$W_1(s) = \frac{1}{\gamma}\frac{20\rho}{s^2(100s+1)}$$

$$W_2(s) = \frac{1}{\gamma}0.02$$

$$W_3(s) = \frac{1}{\gamma}\frac{(0.5s+1)^2}{1}$$

Where equation 2.38 has been converted to the form

$$\left\| \begin{array}{c} \frac{1}{\gamma}W_1 S \\ \frac{1}{\gamma}W_2 R \\ \frac{1}{\gamma}W_3 T \end{array} \right\|_\infty = 1. \tag{3.2}$$

It should be noted, as was already mentioned in Section 2.5, that this is a case of an improper W_3 and a constant W_2. If the plant $P(s)$ (T_{inner}) is strictly

proper, the improper W_3 can be incorporated into the plant. This results in y_2 being the output of the original plant C_p matrix and y_{13} (see Figure 2.7) being the output of a new matrix, C_{pw_3}. If the plant is augmented in this way then the following state-space formulation of the problem may be obtained.

$$P'(s) = \left[\begin{array}{cc|cc} A_p & 0 & 0 & B_p \\ -B_{w_1}C_p & A_{w_1} & B_{w_1} & 0 \\ \hline -D_{w_1} & C_{w_1} & D_{w_1} & 0 \\ 0 & 0 & 0 & W_2 \\ C_{pw_3} & 0 & 0 & C_{pw_3} \\ -C_p & 0 & I & 0 \end{array}\right]$$

This is a general multivariable realization where all of the elements represent matrices and all of the inputs and outputs are vectors. It is used not only for this design, but all others found in this thesis. Note that ρ is generally incorporated into W_1 before this realization is constructed.

The design parameters for the near optimal H_∞ compensator obtained were

$$\rho = 1,$$

$$\gamma = 2.1.$$

The magnitudes of the inverses of the weights are shown in Figure 3.16 as functions of frequency. The inverse of the sensitivity specification

$$W_1'^{-1}(s) = W_1(s)^{-1}(I + GK_{inner})^{-1},$$

is also illustrated in the same plot.

The compensator obtained is shown in Figure 3.17 with a state-space realization given in Appendix B.1.1. It acts as a low frequency lag followed by a

$k = 0.5$			$k = 1.0$			$k = 2.0$		
Poles	ω	ζ	Poles	ω	ζ	Poles	ω	ζ
0	0	NaN	0	0	NaN	0	0	NaN
0	0	NaN	0	0	NaN	0	0	NaN
-0.9033	0.9033	1	-0.7411	0.7411	1	-0.6939	0.6939	1
-3.584	3.584	1	-5.65-7.73j	9.575	0.59	-2.94-12.55j	12.89	0.2281
-12.07	12.07	1	-5.65+7.73j	9.575	0.59	-2.94+12.55j	12.89	0.2281
-43.86-18.42j	47.57	0.922	-44.58-22.22j	49.81	0.895	-45.49-26.5j	52.64	0.8641
-43.86+18.42j	47.57	0.922	-44.58+22.22j	49.81	0.895	-45.49+26.5j	52.64	0.8641
-62.39	62.39	1	-65.47	65.47	1	-69.12	69.12	1

Table 3.3: Poles of the Closed Loop System, T_{inner}, for $k = 0.5,\ 1.0,\ 2.0$

	$k = 0.5$	$k = 1.0$	$k = 2.0$
Gain Margin	7.70	3.83	1.90
Phase Margin (deg)	65.64	53.0	29.1

Table 3.4: Gain and Phase Margin of the Open Loop System, GK_{inner}: Design A

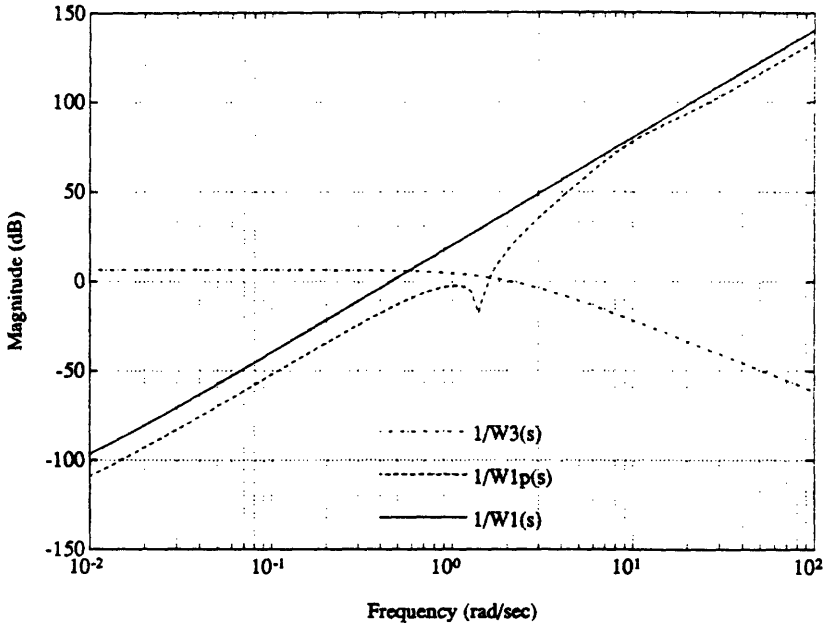

Figure 3.16: H_∞ Design Weights and Actual Sensitivity Specification

lead-lag network, with a high gain at low frequencies for disturbance rejection and lead around 1 rad/sec to boost the bandwidth of the closed loop system.

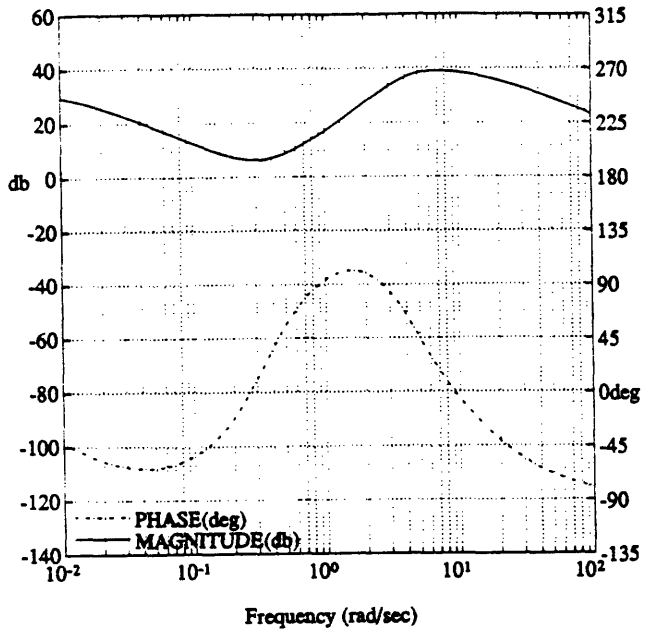

Figure 3.17: Bode Plot of the H_∞ Compensator

The compensator provides a stable closed loop system not only for the nominal plant, but also for the full range of k. The range of parametric variation for which the closed loop system is stable is

$$0.24 < k < 3.78$$

which clearly exceeds the design requirements and demonstrates the ability of the methodology to construct robust compensators. The behavior of the closed loop poles as k is varied is shown by the root locus in Figure 3.18. One can detect one pair of poles moving towards the imaginary axis as k increases. Another pair of poles, with a small natural frequency, moves towards the imaginary axis as k decreases. The movement of these pole pairs bound the range of stable closed loop systems for varying k.

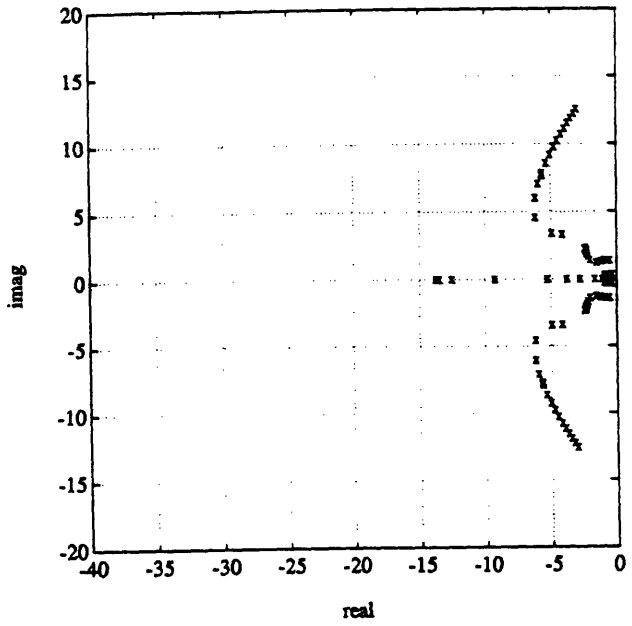

Figure 3.18: Root Locus of the Plant with Inner and H_∞ Compensators for $0.5 \leq k \leq 2.0$

3.4.4 Frequency Response of the Compensated System: Design A

The loop transfer bode plot of the system is shown in Figure 3.19 and shows how the H_∞ compensator causes the nominal system to crossover at -20 dB/decade for good closed loop performance. It can also be noticed that, for k equal to 0.5, the magnitude plot crosses closer to a higher slope and so the closed loop performance can be expected to be slightly degraded for this case.

The gain and phase margins of the open loop system are shown in Table 3.5. These margins are almost identical to those given for the plant and inner loop, Table 3.4, though the H_∞ compensator appears to have degraded the margins slightly for $k = 0.5$. The nominal system has excellent robustness margins. However, stability robustness is degraded as k increases due to the increase in crossover frequency. Still, even at $k = 2.0$, reasonable margins are obtained.

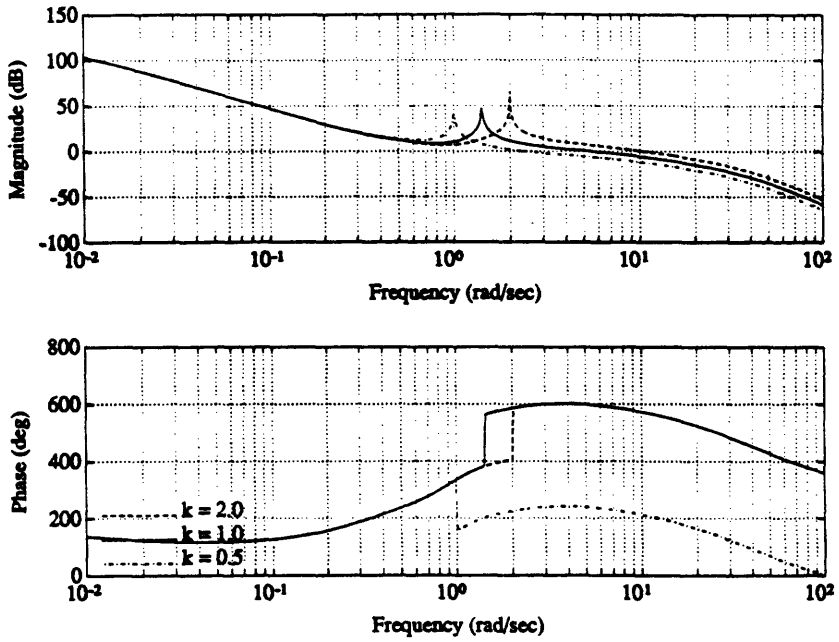

Figure 3.19: Bode Plot of the Open Loop System $G(K_{inner} + K_\infty)$ for $k = 0.5, 1.0, 2.0$

	$k = 0.5$	$k = 1.0$	$k = 2.0$
Gain Margin	7.74	3.85	1.91
Phase Margin (deg)	52.8	56.9	30.1

Table 3.5: Gain and Phase Margin of the Open Loop System, $G(K_{inner} + K_\infty)$: Design A

The loss in closed loop performance for k equal to 0.5 is shown in Figure 3.20, the closed loop system bode plot, which shows exhibits peaking in $T(s)$ for k equal to 0.5 versus k equal to 1.0 or 2.0. However, none of the three cases exhibits excessive peaking, which should lead to good stability robustness.

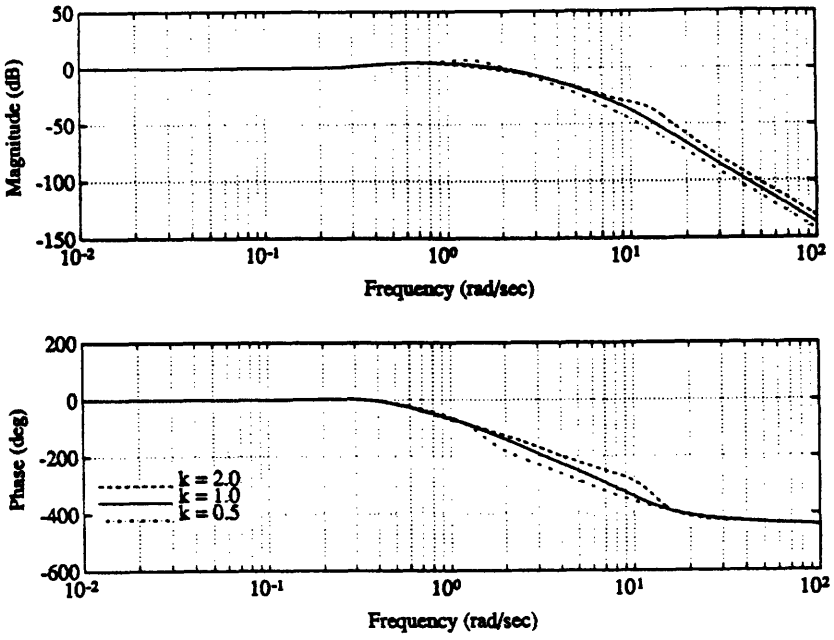

Figure 3.20: Bode Plot of the Closed Loop System $T(s)$ for $k = 0.5,\ 1.0,\ 2.0$

In this problem the design specifications set an emphasis on disturbance rejection and so it is the sensitivity transfer function S(s) which is of the greatest importance. Its bode plot is shown in Figure 3.21 which shows good disturbance attenuation up to 2 rad/sec for the nominal case.

These frequency response plots seem to indicate that a good design has been achieved. The design specifications concentrate on attenuating the specific transfer function from the actual disturbance w to the performance variable z as the design goal. The bode plot of this transfer function is shown in Figure 3.22 and suggests that this objective has largely been achieved as the disturbance is attenuated for all frequencies.

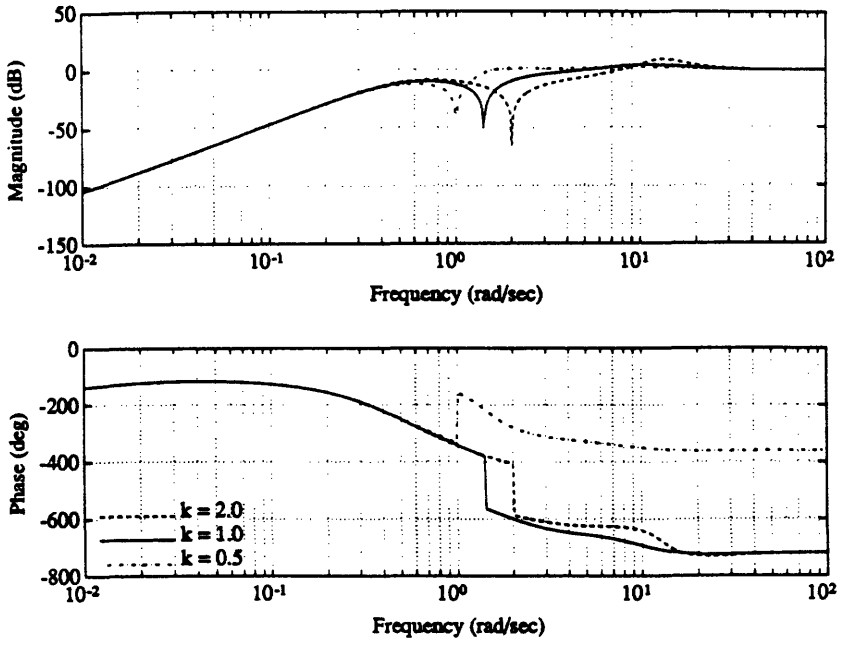

Figure 3.21: Bode Plot of the Sensitivity Transfer Function $S(s)$ for k = 0.5, 1.0, 2.0

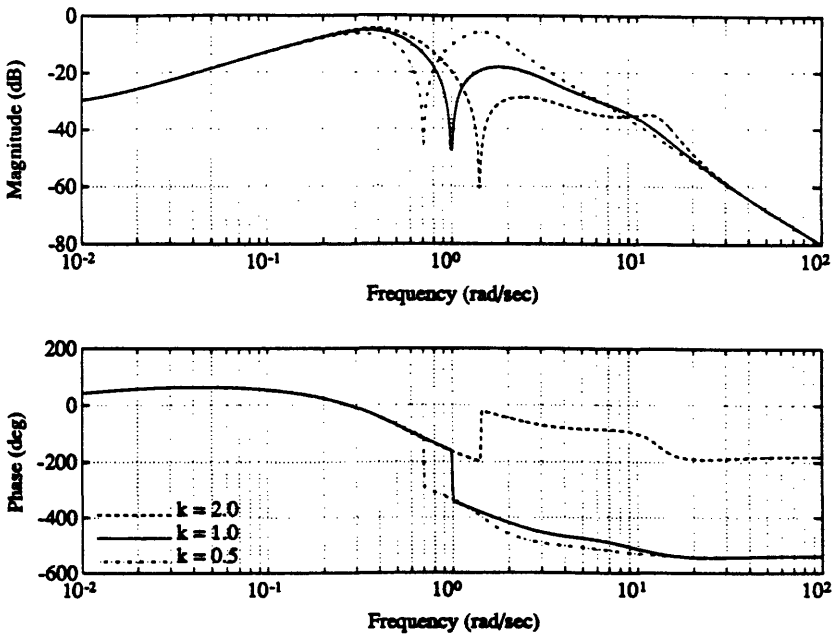

Figure 3.22: Bode Plot of the Transfer Function from w to z for k = 0.5, 1.0, 2.0

3.4.5 Time Response of the Compensated System: Design A

The time response of the compensated system, to the unit impulse disturbance at time zero specified in **Design 1** of the Design Specifications, is shown in Figure 3.23. The various plots show, for the cases where k is equal to 0.5, 1.0, and 2.0, the response of the closed loop system. The first plot shows the performance variable, z, the position of mass 2. The next plot shows the output of the inner loop compensator. The last plot shows the output of the H_∞ compensator. The plots show that the disturbance is well attenuated in z, which also meets the requirement of a 15 second settling time. The disturbance is attenuated by the large initial response of the inner loop compensator. A compensator effort this large could cause problems and fails to meets one of the given specifications. The effort of the H_∞ compensator is of a reasonable magnitude. This example does not have any measurement noise present in the output y.

Consider the time response of the impulse disturbance with measurement noise v; the measurement noise was characterized as Gaussian white noise with a variance of 0.0001. This is a common, general noise model with a standard deviation equal to 1% of the disturbance magnitude. Obviously, with the high lead inner loop compensator constructed, it can be expected that the control signal will have a large noise content. This is expected to hamper noise attenuation in the closed loop system. Before examining the time response of the system we calculate the transfer function from the measurement noise, v, to the controlled variable, z,

$$N(s) = [I + G(K_\infty + K_{inner})]^{-1} G(K_\infty + K_{inner}) \tag{3.3}$$

from Figure 3.3. Because of the presence of the high lead inner loop compen-

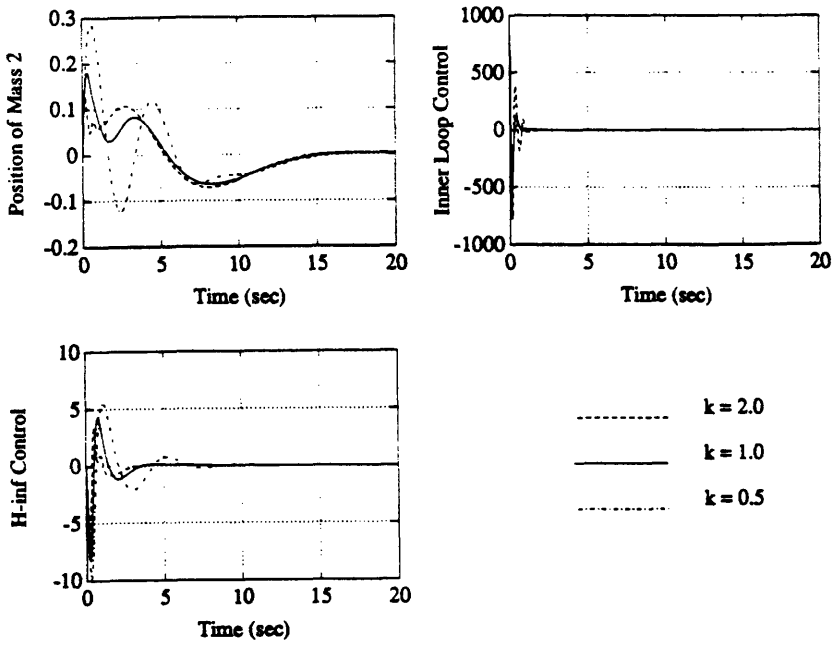

Figure 3.23: Closed Loop System Response to a Unit Impulse Disturbance

sator in the numerator of the transfer function, it can be expected that the above assumption is true. Figure 3.24, showing the Bode plot of $N(s)$, indicates that measurement noise is not attenuated in the output until a frequency of 10 rad/sec (and peaking occurs here for $k = 2.0$).

This behavior is harder to detect in the time response, as shown in Figure 3.25, except for the output of the inner loop compensator which shows large noise amplification. However, the noise content in the system output, z is small for all of the cases considered and does not otherwise disturb the system. If this system were actually implemented, software limits could be placed upon the output of the inner loop actuator. Therefore, the actual effect of noise on the system would likely be small.

The design specifications in **Design 2** require the system to attenuate a sinusoidal disturbance of frequency 0.5 rad/sec with unknown phase and

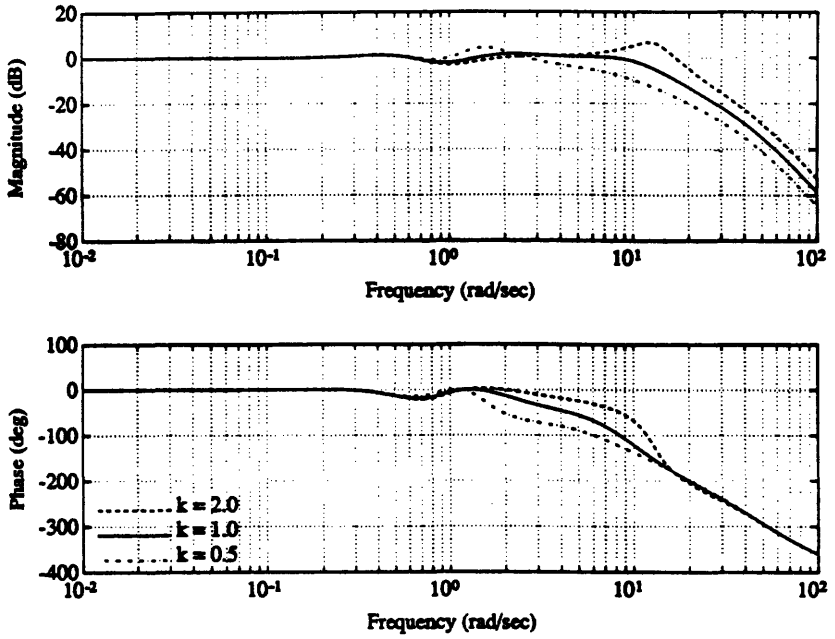

Figure 3.24: Bode Plot of the Transfer Function, $N(s)$, for $k = 0.5,\ 1.0,\ 2.0$

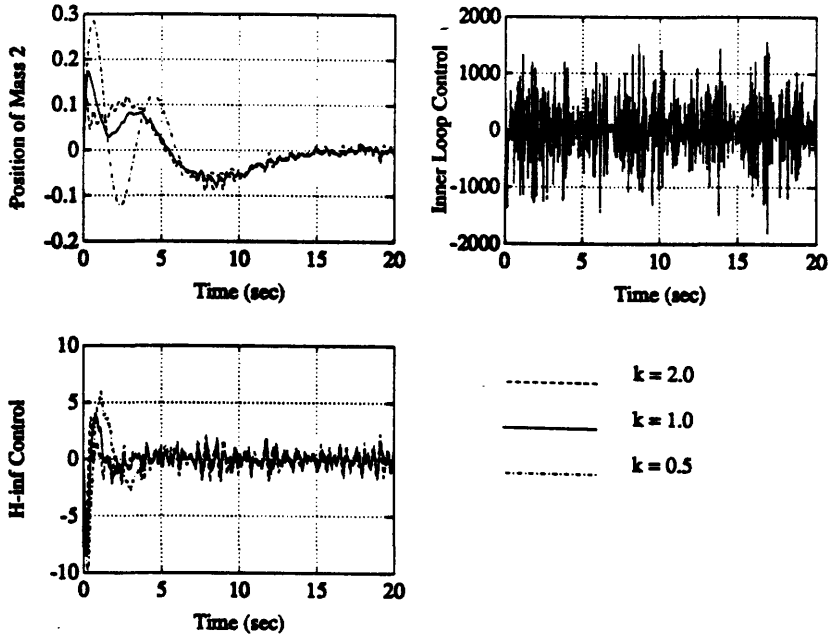

Figure 3.25: Closed Loop System Response with Measurement Noise to a Unit Impulse Disturbance

amplitude. The disturbance is modeled as

$$w(t) = 1.0\, sin(0.5t).$$

The response of the system to this disturbance is shown in Figure 3.26. The compensated system attenuates the disturbance by approximately a factor of one half over the full range of parameter uncertainty. The asymptotic settling time of the system to the disturbance is less than 20 seconds for the full range of parameter uncertainty, thus meeting the **Design 2** specification.

The effects of measurement noise in this case are much the same as for the impulse disturbance considered above. Therefore, the case of the sinusoidal disturbance with measurement noise will not be considered here.

While not explicitly called for in the design specifications, the command following performance of the control system is of interest. It is explored here through the use of a unit step change in the reference. The response is shown in Figure 3.27. Response is characterized by a very large overshoot of approximately 50%. This is due to the peaking found in the closed loop response bode plot. The control efforts of both compensators are also large. This indicates the nominal design does not have good command folowing performance. Interestingly, Figure 3.27 indicates that the system is robust in terms of command following performance. Therefore, though it was not done, constructing a new H_∞ compensator could possibly improve command following over the range of parametric uncertainty.

3.4.6 H_∞ Compensator Order Reduction: Design A

The approach to the H_∞ compensator reduction outlined in Section 2.6 was used to reduce the H_∞ compensator from 9 states to 4 states using the Schur model reduction technique. The bode plot of the reduced order H_∞ compen-

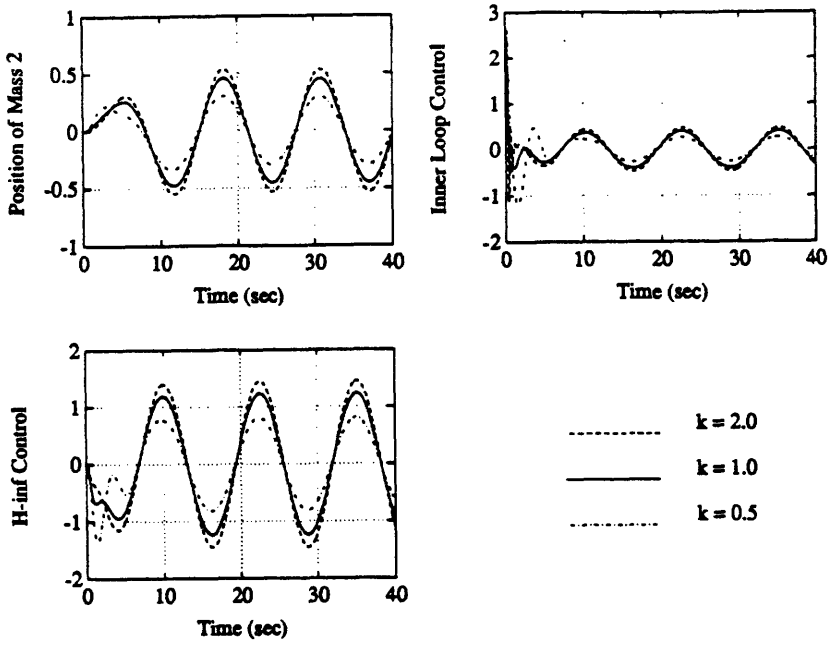

Figure 3.26: Closed Loop System Response to a Sinusoidal Disturbance

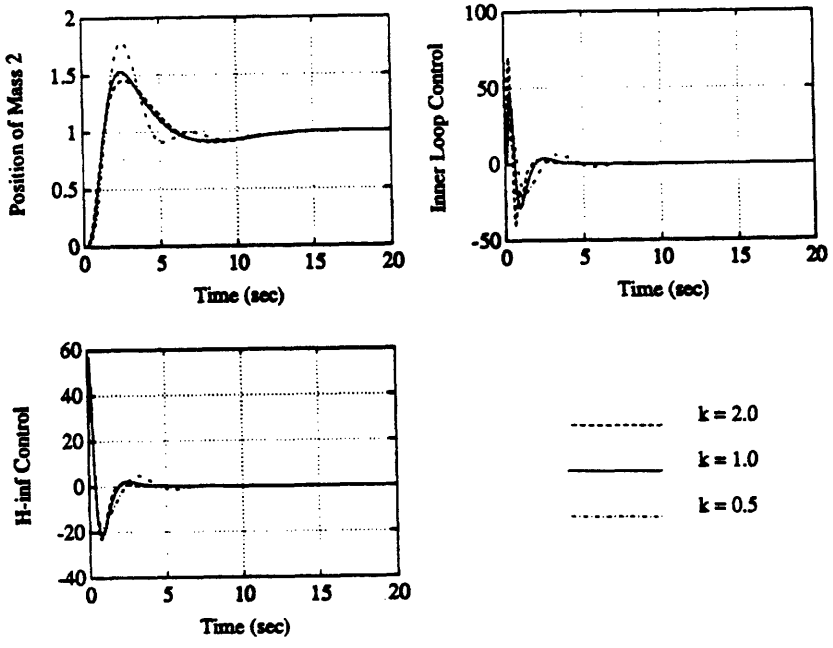

Figure 3.27: Closed Loop System Response to a Unit Step in the Reference

sator, K_∞^{ro} is indistinguishable from the original H_∞ compensator. The infinity norm of the difference between the compensators (equation 2.43) is equal to 0.096. The state-space realization of the reduced order compensator is given in Appendix B.1.2.

The root locus plots of the closed loop system as k varies is shown in Figures 3.28 and 3.29. These indicate that the robustness of the system with the reduced order compensator is identical to that of the full order compensator; in fact, the reduced order compensator stabilizes the plant over the same range of k as the full order compensator. The set of frequency response, and time domain response plots for the system with the reduced order compensator are identical to those of the original compensator indicating performance and robustness have been maintained. The entire set of plots and tables presented above may be found for the reduced order compensator in Appendix C.

3.4.7 Summary of Design A

The system of compensators consisting of an inner loop and reduced order H_∞ compensator were used to provide a "solution" for the benchmark problem. The compensators met the following design objectives:

- The closed loop system is stable over more than the full range of parameter variation, for $0.24 < k < 3.78$.
- For a disturbance consisting of a unit impulse at time zero, the position of mass 2 (the performance variable) has a settling time of less than 15 seconds *for the full range of parameter variation.*
- For $0.5 \leq k \leq 2.0$ the system has phase and gain margins of

$$30.08 \leq PM \leq 56.88$$

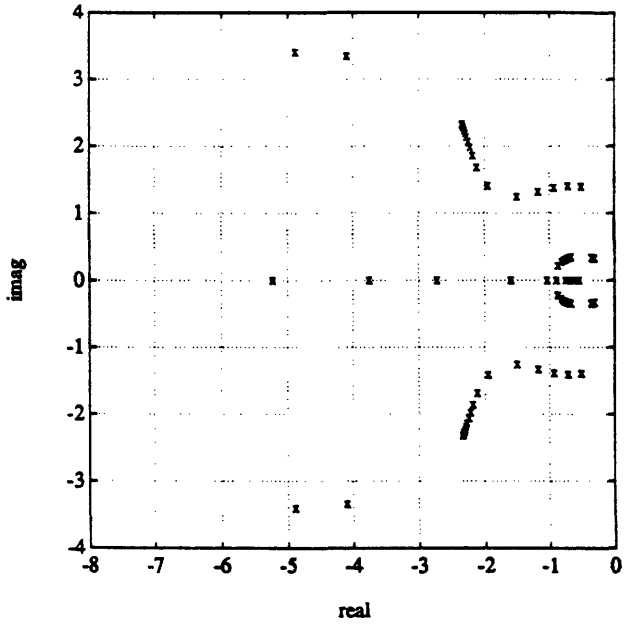

Figure 3.28: Root Locus of the Design A Closed Loop System with the Reduced Order H_∞ Compensator for $0.5 \leq k \leq 2.0$ — Poles Near the Origin

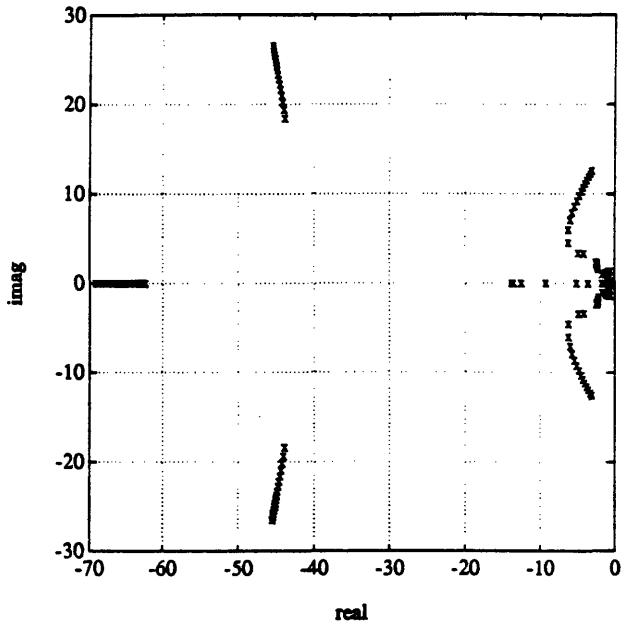

Figure 3.29: Root Locus of the Design A Closed Loop System with the Reduced Order H_∞ Compensator for $0.5 \leq k \leq 2.0$

$$1.91 \leq GM \leq 7.74$$

- For a sinusoidal disturbance with a frequency of 0.5 rad/sec the compensated system will attenuate the disturbance by a minimum of nearly 50% regardless of the parametric variation. Again, regardless of the parameter variation the disturbance will be asymptotically rejected in less than 20 seconds.

The following design objectives were not fully met.

- The controller effort was large in response to the impulse disturbance and measurement noise. However, the impulse response effort would not present a problem as the large control effort was of very short duration; in an actual system it probably would not saturate the actuator. The results of measurement noise are slightly more problematic. Because of the large phase loss in the plant, lead compensation, which leads to measurement noise amplification, is required.

- Measurement noise was not attenuated until almost a decade past the closed loop bandwidth of the system. This is due to the large lead in the inner loop compensator.

- The compensator system (K_∞ and K_{inner}) is an 8-state system, twice the order of the plant. It is a complex compensator and this is an inherent property of the methodology. The methodology trades off compensator complexity for performance.

The compensated system met most of the design requirements and overall the methodology was successful. Of the requirements not met the compensator complexity is an inherent drawback of the methodology, one that is traded for compensator performance and relative ease of design. The high lead compensator that resulted is a product of the plant dynamics. Noise might cause an

actuator to "bounce" between its positive and negative limits. It is recommended that, in an actual implementation limits be placed upon the inner loop control magnitude to limit the large actuator commands.

The use of such limits on the inner loop actuator was investigated for a unit impulse disturbance. A nonlinear simulation of the plant, inner loop compensator, and reduced order H_∞ compensator was constructed for k equal to 1.0. The effects of the impulse disturbance were evaluated for the nominal system and for the system with limits of ± 100 on the inner loop compensator signal u_i. A comparison of the two simulations is shown in Figure 3.30. The figure shows that the inner loop limits cause a dramatic reduction in the

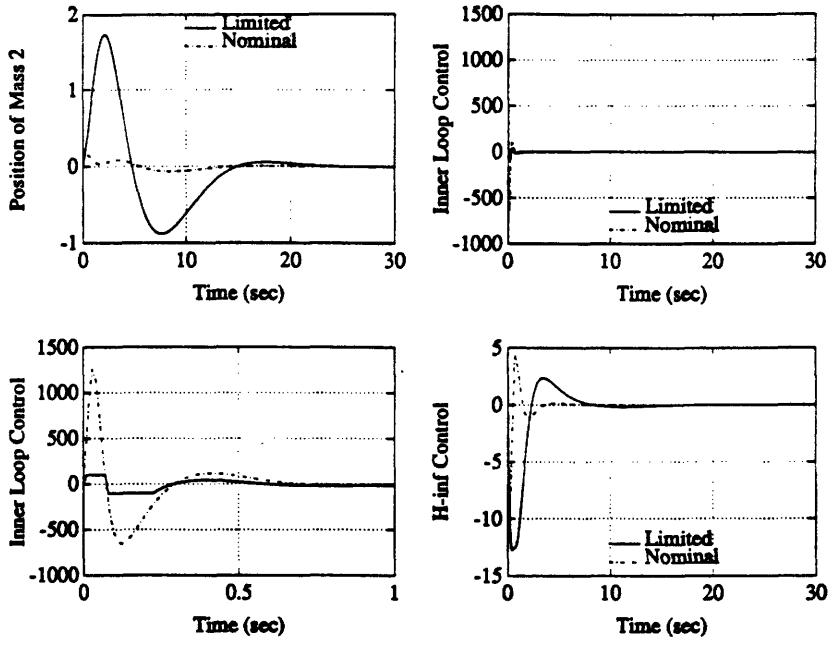

Figure 3.30: Comparison of the Nominal System and the Limited Inner Loop Control System to a Unit Impulse Disturbance

disturbance attenuation. While the settling time of the system still remains within 15 seconds. An examination of the inner loop compensator effort for both the sinusoidal disturbance and reference step simulations shows that the inner loop compensator effort does not exceed ± 100, so these would not be

affected by the limits. Therefore, the effects of large control efforts by the inner loop could be handled with nonlinear design techniques such as the limits used here. More sophisticated approaches could also be used such as limiting the output of each lead-lag in the inner loop compensator independently. However, the design of such nonlinear "fixes" and their use under a variety of inputs is beyond the scope of this study. The example given here is intended to show that the high gain compensator resulting from the methodology can indeed be implemented.

3.5 Compensator Design B

In this case an inner loop compensator was designed to remove the parametric uncertainty without specifically attempting to retain the double integrator characterisic of the plant. Since the benchmark problem has no requirements on command following, only disturbance rejection at low frequency, this should not pose a problem. However, the H_∞ design will include an integrator to facilitate command following and ensure that the DC gain of the closed loop system $T(s)$ is equal to one regardless of the value of k.

3.5.1 Constructing the Inner Loop Compensator: Design B

Following on the guidelines given in Section 3.4.2, that is not allowing the magnitude of the desired plant to exceed that of the actual plant, the desired plant chosen here has the transfer function

$$H_d(s) = \frac{(1.414)^2(0.6)^2}{(s+1.414)^2(s+0.6)^2}.$$

This has the bode plot shown below in Figure 3.31, which also shows the actual plant. Note the magnitude of the desired plant is always less than that of the actual plant.

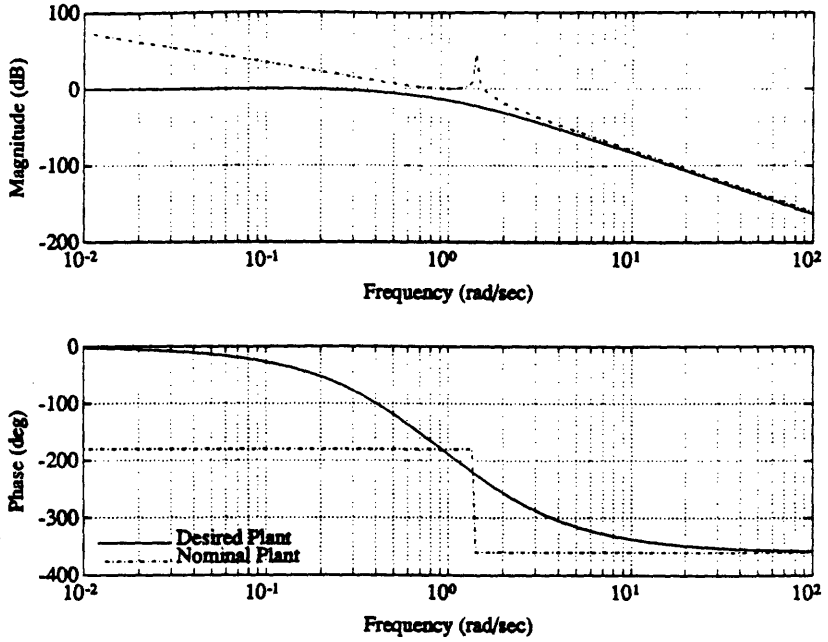

Figure 3.31: Bode Plots of the Desired Plant, $H_d(s)$, and the actual plant $G(s)$

This yields an ideal compensator which is shown as a function of frequency in Figure 3.32. The ideal compensator appears to be a lead network requiring three or four lead components. After trying several compensators of different order, a third order numerator design was settled on. While the design objectives were achievable with both third or fourth order numerators, a third order numerator was chosen in an attempt to reduce the compensator magnitude at high frequency and limit noise amplification. The poles of the compensator were iterated upon several times. The intention was to place them at a high enough frequency so that they do not interfere with the compensator function in the frequency range of interest; yet roll off the compensator to the extent possible. This is the reason why the denominator has a higher order than the numerator. A key advantage of using this methodology is demonstrated here,

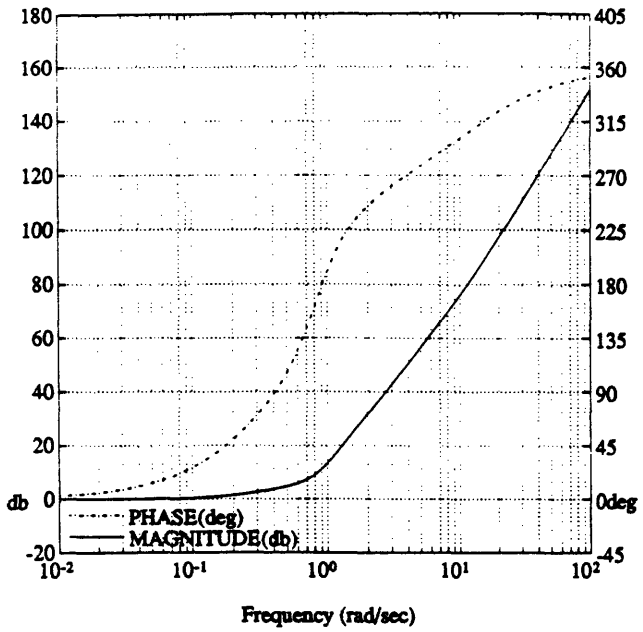

Figure 3.32: Bode Plot of the Ideal Compensator, $K_{ideal}(s)$

i.e. the ability to choose the compensator structure, order and complexity to obtain the design goals. The structure of the selected compensator was fixed to be

$$K_{inner}(s) = \frac{(\alpha_3 s^3 + \cdots + \alpha_0)}{(.02s+1)^2(.03s+1)^2}.$$

The methodology has built-in flexibility to minimize the difference between the closed loop transfer function, T_{inner} and the desired closed loop transfer function H based on a least squares fit of $\alpha_0, \alpha_1, \alpha_2, \alpha_3$. Thus, using a frequency vector from 0.1 to 10 rad/sec, yields a compensator of the form

$$K_{inner}(s) = \frac{0.9883(3.687s+1)(1.692s^2+1.215s+1)}{(.02s+1)^2(.03s+1)^2}.$$

Examining the closed loop poles and their damping ratios and frequencies, in Table 3.6, shows that the damping has been increased substantially from the uncompensated plant. Notice as k increases from 0.5 to 2.0 a set of poles migrates from the real axis towards the imaginary axis. At k equal to 2.0 these

poles have a damping ratio of only 0.1925 at 12.8 rad/sec. The decision has been made to trade off this damping and gain margin for reduced magnitude of the compensator at high frequencies.

$k = 0.5$			$k = 1.0$			$k = 2.0$		
Poles	ω	ζ	Poles	ω	ζ	Poles	ω	ζ
-0.3879	.3879	1	-0.3703	.3703	1	-0.3637	.3637	1
-.7622-.5303j	.9285	0.8209	-.539-.4908j	0.729	0.7394	-.4919-.4818j	.6886	0.7144
-.7622+.5303j	.9285	0.8209	-.539+.4908j	0.729	0.7394	-.4919+.4818j	.6886	0.7144
-2.394	2.394	1	-5.179-7.641j	9.231	0.5611	-2.47-12.59j	12.83	0.1925
-12.07	12.07	1	-5.179+7.641j	9.231	0.5611	-2.47+12.59j	12.83	0.1925
-43.87-18.63j	47.66	0.9204	-44.59-22.46j	49.93	0.8931	-45.51-26.78j	52.8	0.8619
-43.87+18.63j	47.66	0.9204	-44.59+22.46j	49.93	0.8931	-45.51+26.78j	52.8	0.8619
-62.56	62.56	1	-65.67	65.67	1	-69.36	69.36	1

Table 3.6: Closed Loop Poles of T_{inner}: Design B

Examining the root locus of T_{inner}, Figure 3.33, shows that a pole pair begins real for k equal to 0.5 and moves towards the imaginary axis as k increases. This is the pole pair referred to above.

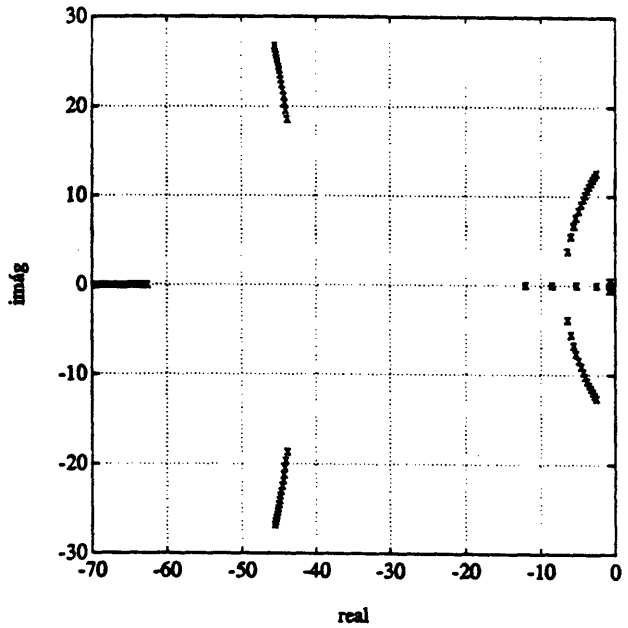

Figure 3.33: Root Locus of the Closed Loop System, $T_{inner}(s)$ for $0.5 \leq k \leq 2.0$

The open loop bode plot, shown in Figure 3.34 reveals that the systems have a wide range of crossover frequencies for varying k. The closed loop bode

	$k = 0.5$	$k = 1.0$	$k = 2.0$
Gain Margin	6.97	3.47	1.72
Phase Margin (deg)	53.5	45.8	23.7

Table 3.7: Gain and Phase Margin of the Open Loop System, GK_{inner}: Design B

plot in Figure 3.35 indicates that the inner loop compensator has performed its main function of removing a large part of the effects of the parameter uncertainty in the frequency range of interest. The reduced damping at 12.8 rad/sec for k equal to 2.0 is rolled off enough so it should not impact the subsequent H_∞ design.

Gain and phase margins of the inner loop compensator are slightly worse than that of design A (see Table 3.4 vs. Table 3.7). However, nominally, they are reasonable relative to classical controller design theory. Note the declining gain margin as the pole pair discussed above moves towards the imaginary axis.

3.5.2 Constructing the H_∞ Compensator: Design B

For this H_∞ design the standard feedback configuration will also be used as explained in Sections 2.5 and 3.4.3. The weight $W_1(s)$ used here is also subject to some conditions. First it must be designed to provide a constraint on the disturbance sensitivity. Secondly, instead of "obscuring" the free integrators of the plant, a free integrator must be added to assure a zero DC gain. Since the H_∞ methodology does not accept free integrators, a very slow pole will be used to approximate the integrator and prevent numerical computation difficulties.

After several iterations the following weights and scalings are found to provide a compensator which meets the design requirements.

$$W_1(s) = \frac{1}{\gamma} \frac{0.02\rho}{(s + 1 \times 10^{-6})}$$

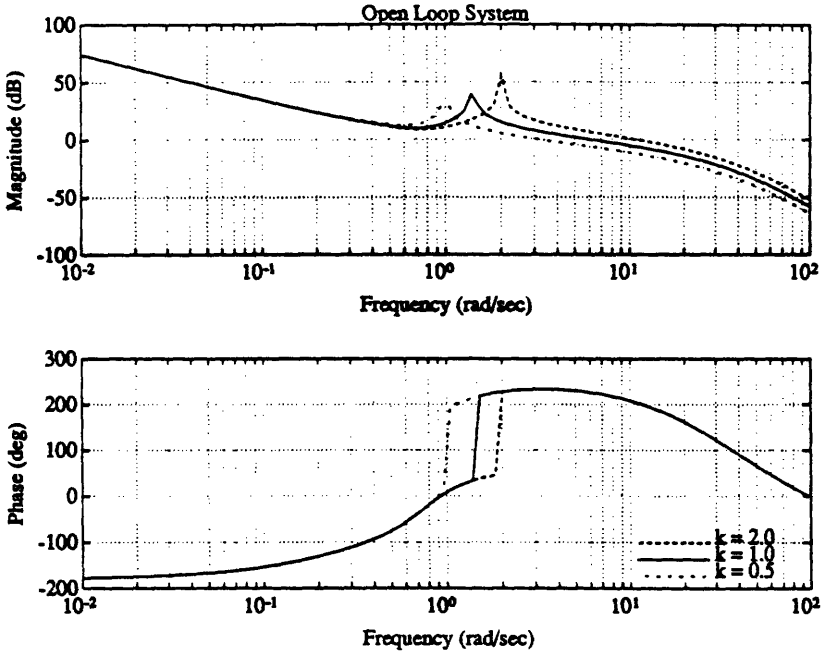

Figure 3.34: Bode Plot of the Open Loop System, GK_{inner}

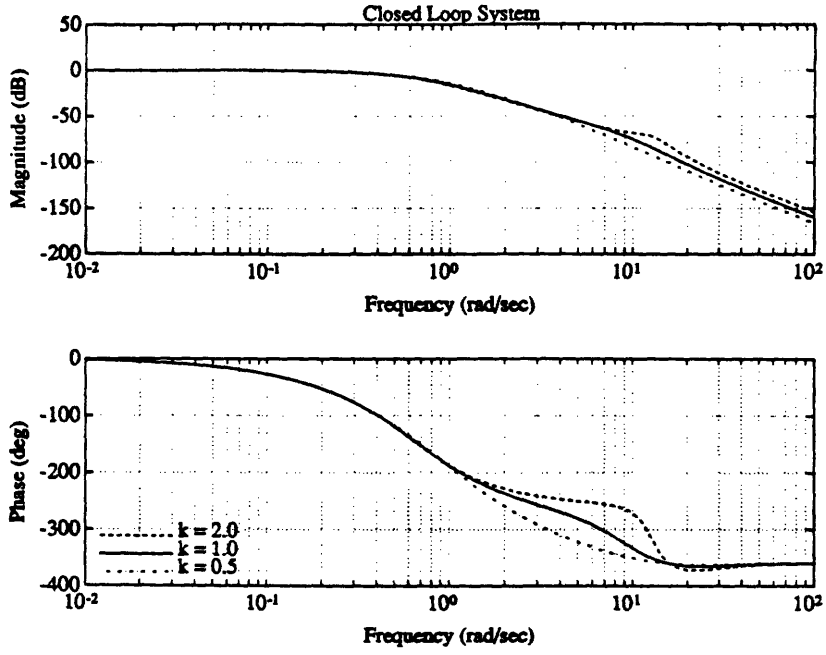

Figure 3.35: Bode Plot of the Closed Loop System, T_{inner}

$$W_2(s) = \frac{1}{\gamma}0.02$$

$$W_3(s) = \frac{1}{\gamma}s^2$$

The near optimal H_∞ compensator found had scaling values of

$$\rho = 28,$$

$$\gamma = 1.$$

The bode magnitude plots of the inverses of the weights and the sensitivity specification, $W_1'(s)$ are shown in Figure 3.36.

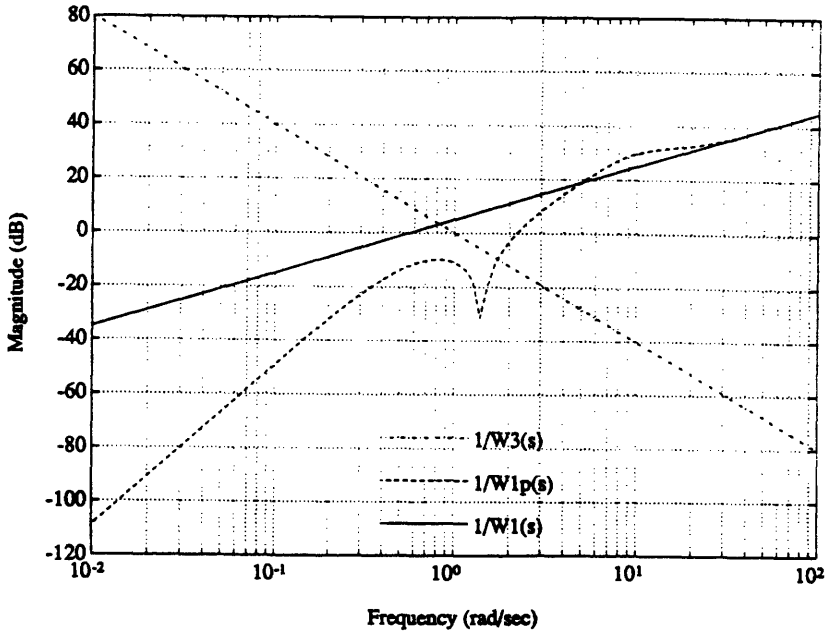

Figure 3.36: H_∞ Design Weights and Actual Sensitivity Specification

The compensator obtained is shown in Figure 3.37; it is very similar to the compensator obtained in design A with the addition of the low frequency pole approximating an integrator. The state-space realization of the compensator is given in Appendix B.2.1.

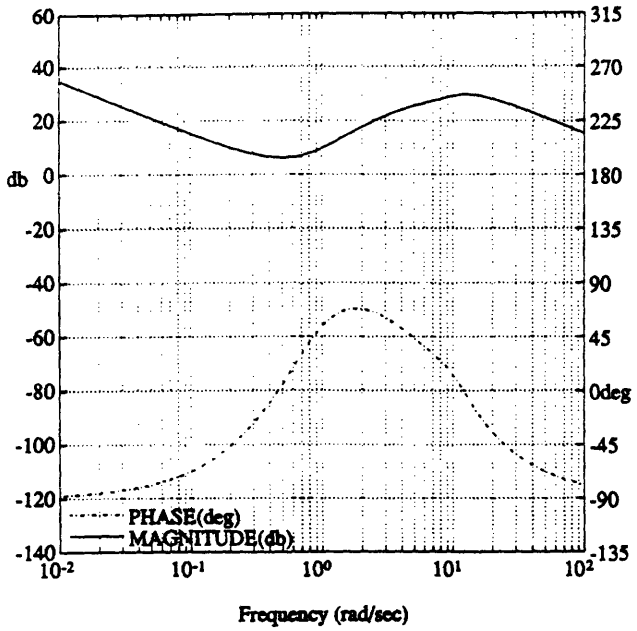

Figure 3.37: Bode Plot of the H_∞ Compensator

The compensator provides a stable closed loop system over the full range of parameter variation. The range of k for which the closed loop system is stable is

$$0.21 < k < 3.42.$$

The closed loop poles are reasonably well damped in the frequency range of interest for the full range of k. This is illustrated by the root locus in Figure 3.38; note one pair of the complex poles has decreased damping as k goes from 1 to 0.5.

3.5.3 Frequency Response of the Compensated System: Design B

The bode plot of the open loop system, $G(K_\infty + K_{inner})$, is given in Figure 3.39. As expected, it is very similar to Figure 3.19 for Design A. Interestingly the magnitude plot crosses over at less than -20 dB/decade.

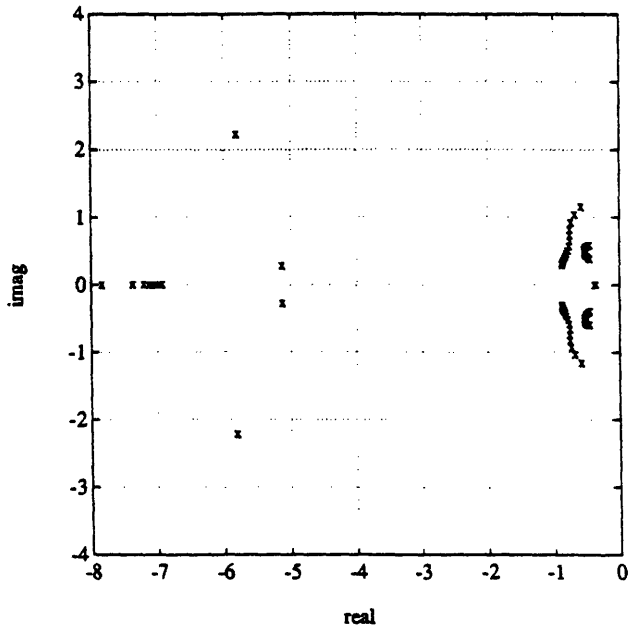

Figure 3.38: Root Locus of the Plant with Inner and H_∞ Compensators for $0.5 \leq k \leq 2.0$

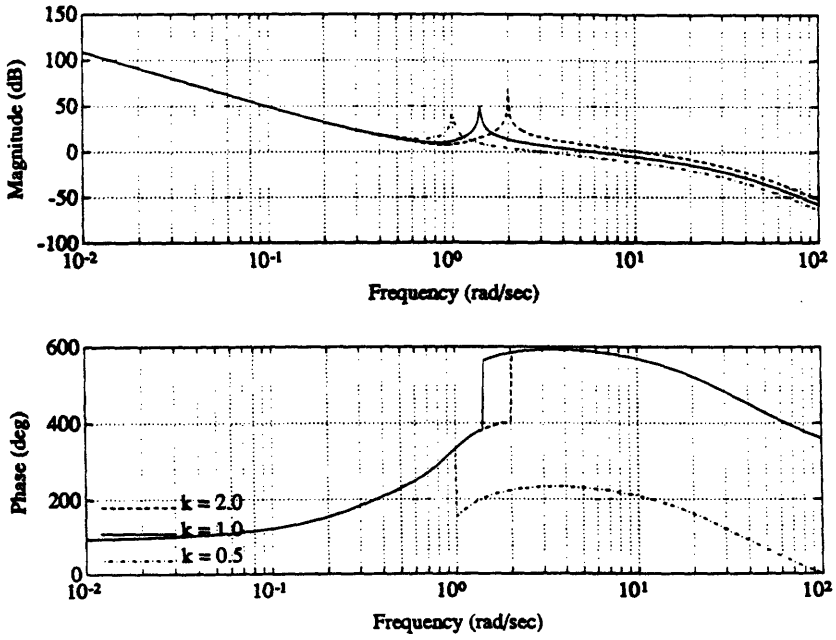

Figure 3.39: Bode Plot of the Open Loop System $G(K_{inner} + K_\infty)$ for $k =$ 0.5, 1.0, 2.0

The gain and phase margins of the open loop system are shown in Table 3.8. The margins are slightly degraded from Design A but provide reasonable stability robustness. The same trends as in Design A are present, though in this design phase margin continues to increase as k decreases.

	$k = 0.5$	$k = 1.0$	$k = 2.0$
Gain Margin	6.99	3.48	1.73
Phase Margin (deg)	52.9	46.3	23.9

Table 3.8: Gain and Phase Margin of the Open Loop System, $G(K_{inner} + K_\infty)$: Design B

The closed loop bode plot is shown in Figure 3.40 and varies from that in design A. It has slightly less bandwidth, 0.9 rad/sec versus 2.4 rad/sec, but does not have the peaking of Design A which contributes to this increased bandwidth. The closed loop shape for design B is better from a command following viewpoint.

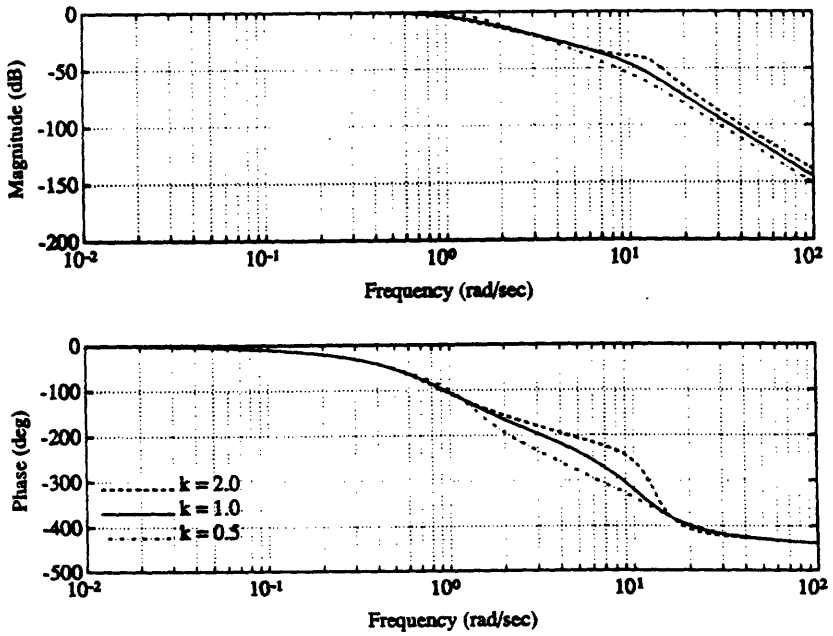

Figure 3.40: Bode Plot of the Closed Loop System $T(s)$ for $k = 0.5,\ 1.0,\ 2.0$

Again the sensitivity transfer function is of great importance and its bode plot is shown in Figure 3.41. Disturbances are attenuated past 2 rad/sec for the nominal case (as for Design A) and past 1 rad/sec regardless of the value of k.

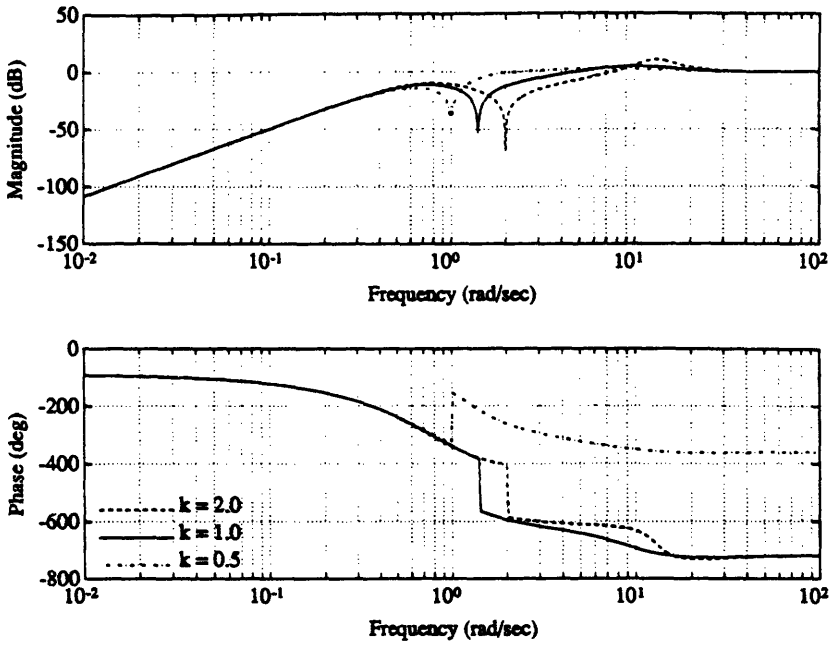

Figure 3.41: Bode Plot of the Sensitivity Transfer Function $S(s)$ for k = 0.5, 1.0, 2.0

The transfer function from the design disturbance w to z is shown in Figure 3.42. It appears that Design B should also do a good job in rejecting w, as w is attenuated over all frequencies.

Finally, it is of interest to check the noise transfer function, $N(s)$. It is shown in Figure 3.43 and is very similar to that of Design A. This design will also have poor noise attenuation.

Based on frequency response analysis it appears that the combination of inner loop and H_∞ has yielded a compensated system which will successfully meet most of the design requirements.

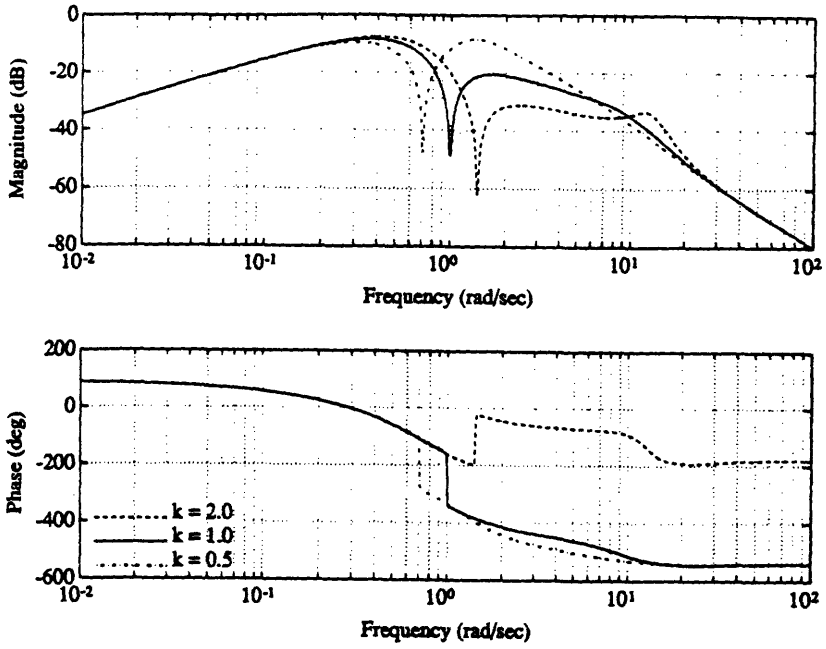

Figure 3.42: Bode Plot of the Transfer Function from w to z for k = 0.5, 1.0, 2.0

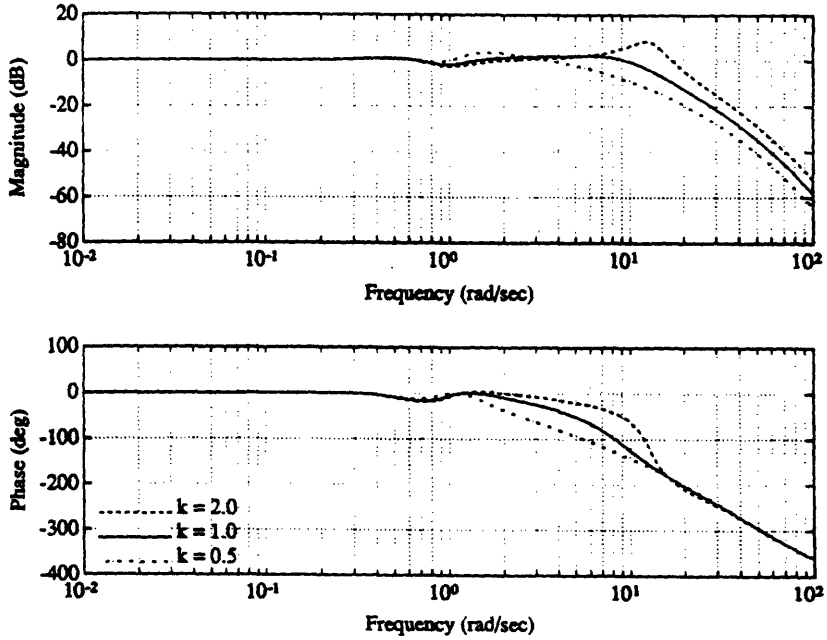

Figure 3.43: Bode Plot of the Transfer Function, $N(s)$, for $k = 0.5, 1.0, 2.0$

3.5.4 Time Response of the Compensated System: Design B

The time response of this system to a unit impulse disturbance w is shown in Figure 3.44. Again both the performance variable z and the controls are presented. The response is very comparable to design A (no surprise based on the comparative frequency responses). The performance variable z has a very similar trajectory, meeting the specified requirements for the entire range of parameter variation. The inner loop control again has a very large initial response to the disturbance.

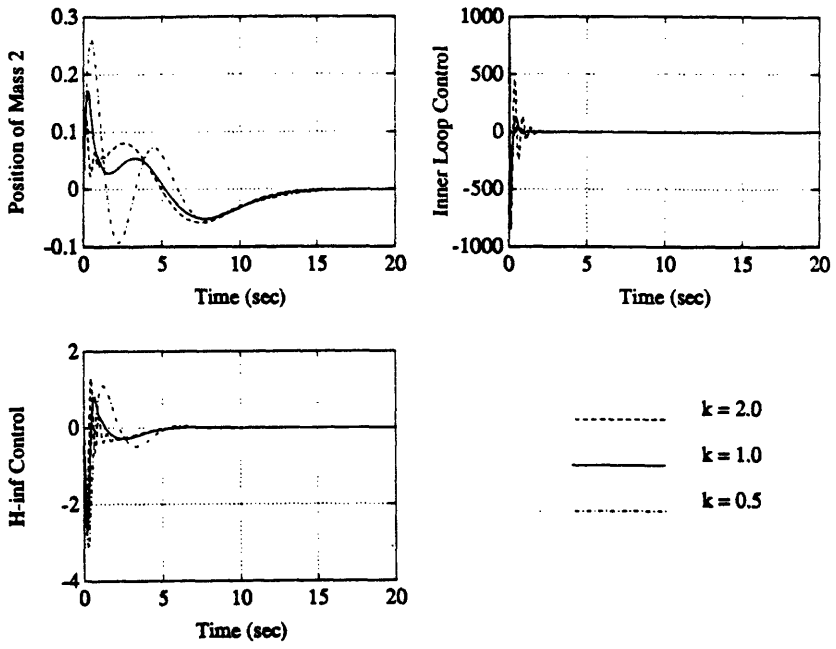

Figure 3.44: Closed Loop System Response to a Unit Impulse Disturbance

In general, the time response of Design B is very similar to Design A, except for the step response. The step response shown in Figure 3.45 has very little overshoot and rise times of less than four seconds regardless of the value of k. The command following performance of the system is robust to the parameter variation.

As stated above, the remainder of the time response is very similar to Design A and so it is presented without comment in Figures 3.46 and 3.47.

Overall, the time response of the compensated system meets the requirements of Section 3.2 and provides excellent command following performance, over the entire range of parameter variation.

3.5.5 H_∞ Compensator Order Reduction: Design B

Again the technique of Schur model reduction was applied to the H_∞ compensator. The resulting reduced order compensator has six states (versus nine) and its state-space realization is given in Appendix B.2.2. The bode plot of the reduced order compensator is indistinguishable from that of the full order compensator. The infinity norm of the difference between the compensators is equal to 0.023.

The root locus plots of the closed loop with the reduced order compensator are shown in Figures 3.48 and 3.49. Stability over the full range of parametric uncertainty is unchanged with the reduced order compensator. Performance with the reduced order compensator is indistinguishable from that of the full order compensator. The figures containing the system performance with the reduced order compensator are shown in Appendix D.

3.5.6 Summary of Design B

The compensator system designed provides excellent performance and stability robustness to the full range of parameter variation. The compensator system provides Type 1 system response for the closed loop system and met the following design objectives.

- The closed loop system is stable over the entire range of parameter variation. The range of k for which the system is stable is $0.21 < k < 3.42$.

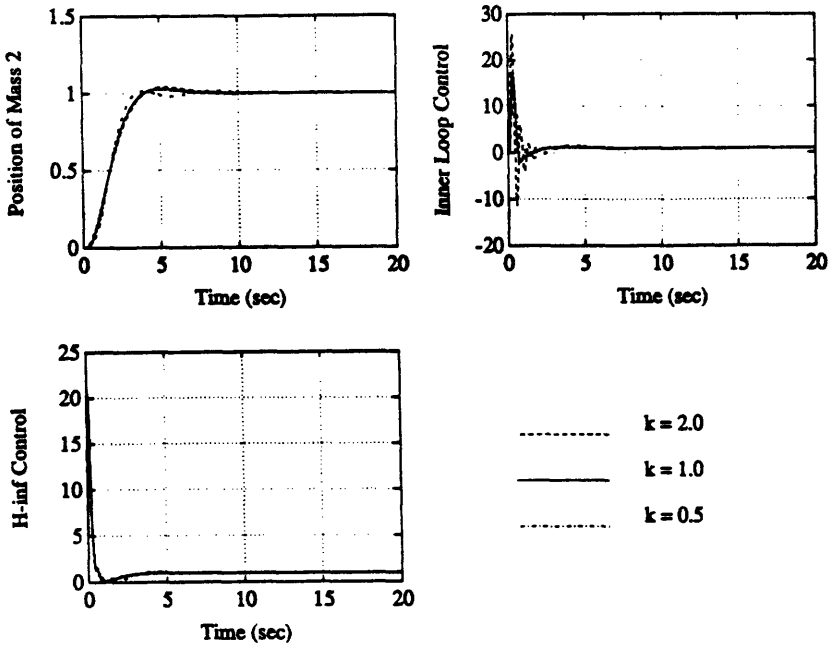

Figure 3.45: Closed Loop System Response to a Unit Step in the Reference

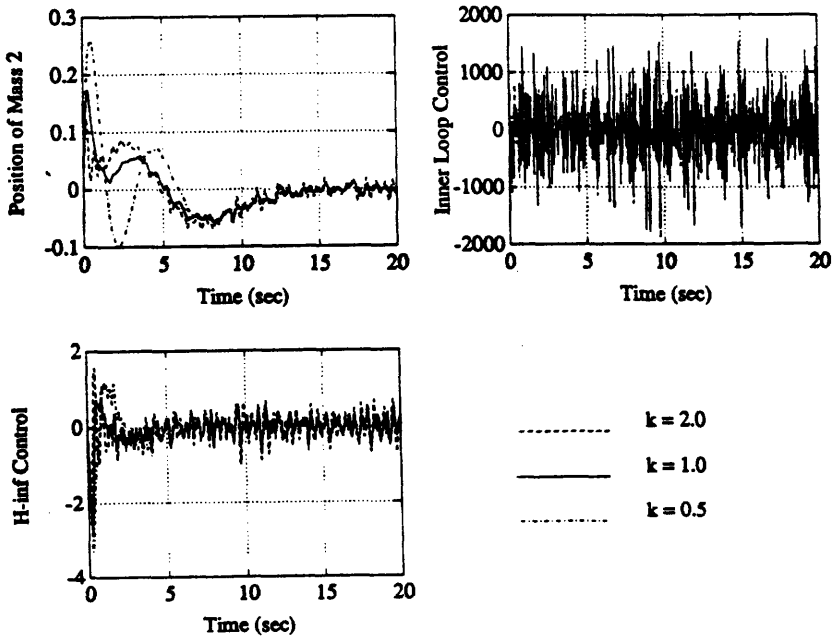

Figure 3.46: Closed Loop System Response with Measurement Noise to a Unit Impulse Disturbance

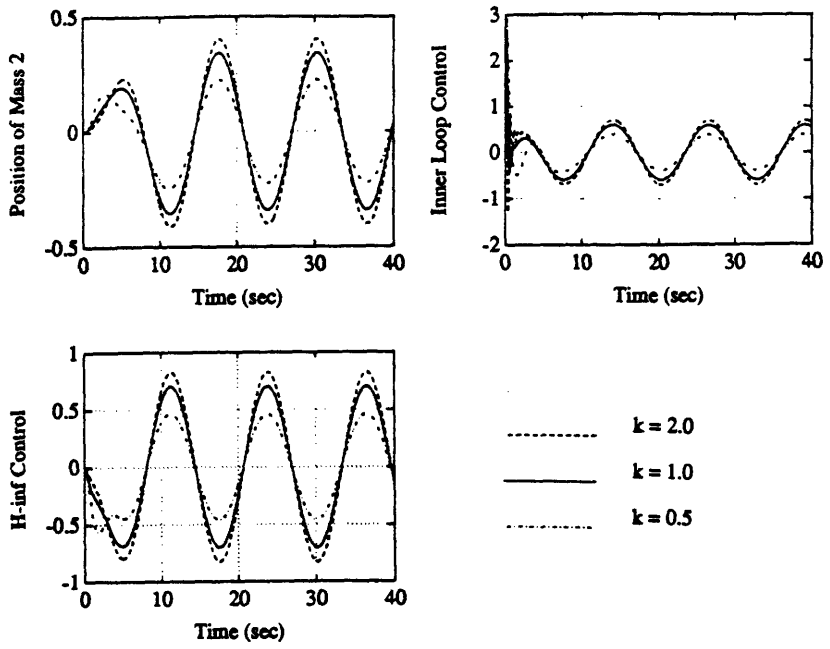

Figure 3.47: Closed Loop System Response to a Sinusoidal Disturbance

- The system attenuates a unit impulse disturbance to at least 25% of the input magnitude. The system has a settling time of less than 15 seconds. This is regardless of the value of k.

- The sinusoidal disturbance is attenuated by more than 50% and is asymptotically rejected in less than 20 seconds regardless of the parameter variation.

- The performance variable response to a step change in the reference has characteristics of a 4 second rise time and almost no overshoot, regardless of the parameter variation.

- The system has phase and gain margins of

$$23.92 \leq PM \leq 52.85$$

$$1.73 \leq GM \leq 6.99$$

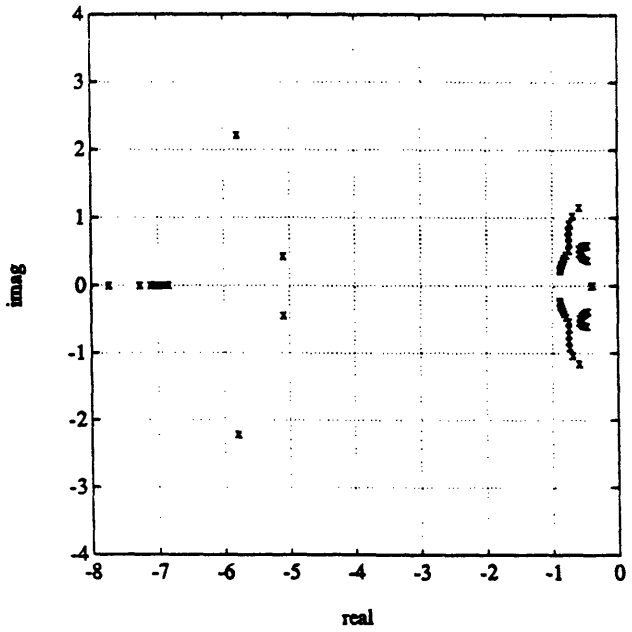

Figure 3.48: Root Locus of the Design B Closed Loop System with the Reduced Order H_∞ Compensator for $0.5 \leq k \leq 2.0$ – Poles Near the Origin

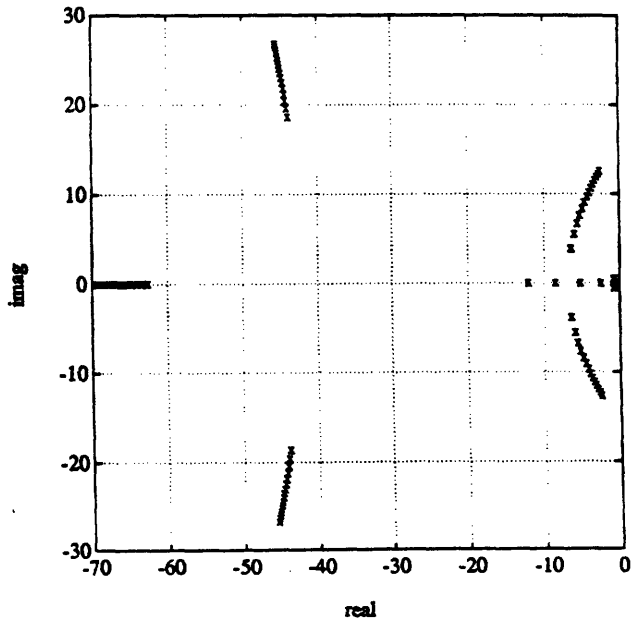

Figure 3.49: Root Locus of the Design B Closed Loop System with the Reduced Order H_∞ Compensator for $0.5 \leq k \leq 2.0$

for $0.5 \leq k \leq 2.0$.

The following objectives were not fully met.

- The controller effort was large in response to the impulse disturbance and measurement noise (re: discussion in Sections 3.4.5 and 3.4.7).
- The compensator system is complex, consisting of a four state inner loop compensator and a six state H_∞ compensator, a total of ten states.
- Measurement noise is not attenuated till almost a decade past the closed loop system bandwidth.

The compensated design met the performance objectives of the problem using a complex, high bandwidth compensator system. The advantages and disadvantages are discussed in Section 3.4.7.

3.6 Comparison to Published Results for a Benchmark Problem for Robust Control

Five papers presented at the 1990 ACC [4, 6, 7, 17, 22] proposed compensators to meet the requirements of this problem. A comparison with those papers of the designs presented in this thesis elicits the following conclusions.

All of the papers stabilized the closed loop system over the range of parametric variation, $0.5 < k < 2.0$, except [4] which was stable for $0.55 < k < 2.0$.

The impulse disturbance time response of the designs presented here is superior to all of the ACC designs except that by Chiang and Safonov [6]. The impulse disturbance response specifications are met by only [6, 7] for the nominal case and only [6] over the entire range of parameter uncertainty. No impulse response was presented for [22].

The only papers which investigated the sinusoidal disturbance were [6, 22], with the design of Rhee and Speyer [22] designed specifically designed to reject a sinusoidal disturbance at 0.5 rad/sec. Both designs met the requirements with [22] completely attenuating the sinusoidal disturbance. Both designs presented here also meet this requirement and effectively attenuate a sinusoidal disturbance at any frequency.

The compensator designs presented here are of greater order than any of the other designs with the exception of [22] which is an 8 state compensator.

Control magnitudes given in this thesis are greater than the control magnitudes of the ACC compensators except for that of Chiang and Safonov [6] which is a lead network with a high frequency gain of greater than 100 dB. The problems that apply to the inner loop compensator due to its high gain, will also apply to Chiang and Safonov's compensator.

The effects of measurement noise are only investigated by [22]. The noise model used is Γv where Γ is 0.033 and ν has unit covariance. This noise does not appear to show up in the system output and has no significant impact on the control effort.

The designs presented here have higher gain and phase margins than the designs which tabulate their margins. All of the compensators except [6] were nonminimum phase. Both compensators presented here are minimum phase. This is important for implementation.

Overall the designs presented here compare favorably to the designs presented at the ACC. Both designs give better performance and stability margins than most of the designs from the ACC. The designs presented here trade increased complexity, controller effort, and noise rejection for the performance gained.

Chapter 4

A MIMO Mass-Spring-Dashpot Problem

4.1 Introduction

In this chapter the design methodology outlined in Chapter 2 and sucessfully applied to Wie and Bernstein's SISO problem (Chapter 3) is applied to a multi-input multi-output (MIMO) problem with parametric uncertainty. Again the problem considered is a mass-spring problem, though in this case the problem contains dashpots and so it is lightly damped. Here there are two inputs and two outputs, with one set of sensors and actuators colocated and the other non-colocated. The basic framework of the problem is set up as in Wie and Berstein's and similar requirements will be applied.

4.2 The Plant: A MIMO Mass-Spring-Dashpot (MSD) System

A schematic diagram of the plant can be seen in Figure 4.1 below. Here the actuators of the plant (the inputs) are forces acting on m_1 and m_2 while the

plant sensors (the outputs) measure the positions of m_1 and m_3.

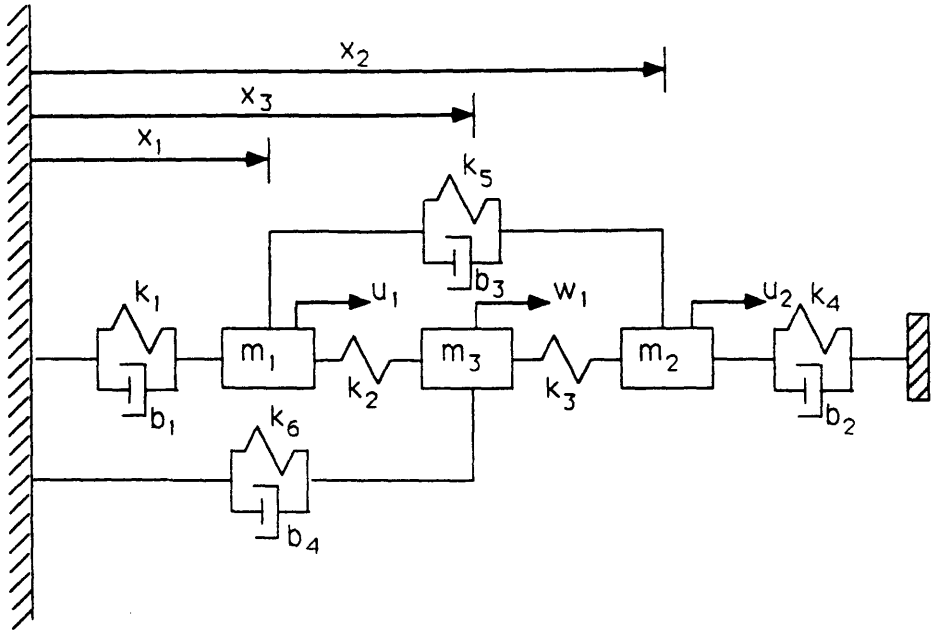

Figure 4.1: Schematic Diagram of the MIMO Mass-Spring-Dashpot Plant

The state equations of this system may be expressed as

$$\begin{bmatrix} \dot{x}_1 \\ \dot{x}_2 \\ \dot{x}_3 \\ \dot{x}_4 \\ \dot{x}_5 \\ \dot{x}_6 \end{bmatrix} = \begin{bmatrix} 0 & 0 & 0 & 1 & 0 & 0 \\ 0 & 0 & 0 & 0 & 1 & 0 \\ 0 & 0 & 0 & 0 & 0 & 1 \\ \frac{-(k_1+k_2+k_5)}{m_1} & \frac{k_5}{m_1} & \frac{k_2}{m_1} & \frac{-(b_1+b_3)}{m_1} & \frac{b_3}{m_1} & 0 \\ \frac{k_5}{m_2} & \frac{-(k_3+k_4+k_5)}{m_2} & \frac{k_3}{m_2} & \frac{b_3}{m_2} & \frac{-(b_2+b_3)}{m_2} & 0 \\ \frac{k_2}{m_3} & \frac{k_3}{m_3} & \frac{-(k_2+k_3+k_6)}{m_3} & 0 & 0 & \frac{-b_4}{m_3} \end{bmatrix} \begin{bmatrix} x_1 \\ x_2 \\ x_3 \\ x_4 \\ x_5 \\ x_6 \end{bmatrix}$$

$$+ \begin{bmatrix} 0 & 0 \\ 0 & 0 \\ 0 & 0 \\ \frac{1}{m_1} & 0 \\ 0 & \frac{1}{m_2} \\ 0 & 0 \end{bmatrix} \begin{bmatrix} u_1 \\ u_2 \end{bmatrix} + \begin{bmatrix} 0 \\ 0 \\ 0 \\ 0 \\ 0 \\ \frac{1}{m_3} \end{bmatrix} w_1$$

$$\begin{aligned} z_1 &= x_1 \\ z_2 &= x_3 \\ y_1 &= x_1 + v \\ y_2 &= x_3 + v \end{aligned}$$

Where the variables are defined as:

m_i = mass of body i

k_i = spring constant of spring i

b_i = damping factor of dashpot i

x_1 = position of body 1

x_2 = position of body 2

x_3 = position of body 3

x_4 = velocity of body 1

x_5 = velocity of body 2

x_6 = velocity of body 3

u_1 = control input (force) acting on body 1

u_2 = control input (force) acting on body 2

w = plant disturbance (force) acting on body 3

y_1 = measured position of body 1

y_2 = measured position of body 3

z_1 = performance variable, position of body 1

z_2 = performance variable, position of body 3

v = measurement noise

This problem is taken from [1].

Now for simplicity in handling the problem let

$$m_1 = m_2 = m_3 = m = 1$$

$$b_1 = b_2 = b_3 = b_4 = b = 0.002.$$

Let the nominal value of the spring constants be

$$k_1 = \ldots = k_6 = 1$$

with the parametric uncertainty manifested as a *simultaneous* variation in the all of the spring constants such that

$$k_1 = \ldots = k_6 = k$$

and

$$0.5 \leq k \leq 2.0.$$

Obviously, uncertainty in the value of the spring constants could result in a large number of plant variations. This simultaneous variation is intended for simplicity in handling the problem. No effort has been made to check whether this represents a worst or best case in terms of plant variation and uncertainty.

The design specifications may be considered essentially the same as those in Chapter 3.

4.3 Analysis of the Plant

The nominal plant has the singular value plot shown in Figure 4.3 and clearly reveals the system has three pairs of lightly damped poles. The system has no transmission zeros. As k varies the singular value plots at the extreme variations, $k = 0.5$ and $k = 2.0$, are shown in Figures 4.2 and 4.4. A comparison of the maximum singular values as k varies is shown in Figure 4.5. The changing value of k affects both DC gain and pole location of the plant. The gain varies about 10 dB and the poles move about 1.5 rads/sec in frequency.

The nominal poles, natural frequencies, and damping ratios are tabulated below.

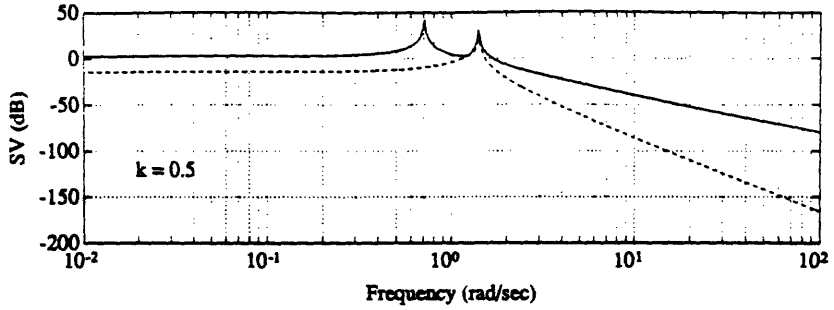

Figure 4.2: Singular Value Plot of G for $k = 0.5$

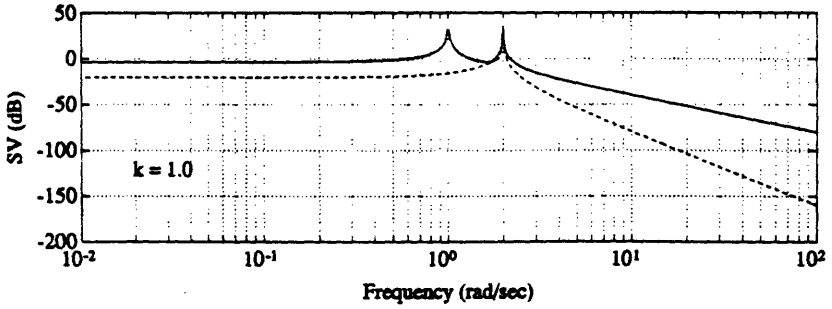

Figure 4.3: Singular Value Plot of G for $k = 1.0$

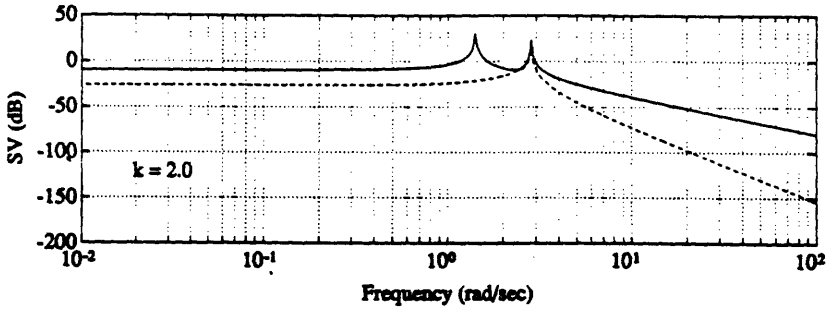

Figure 4.4: Singular Value Plot of G for $k = 2.0$

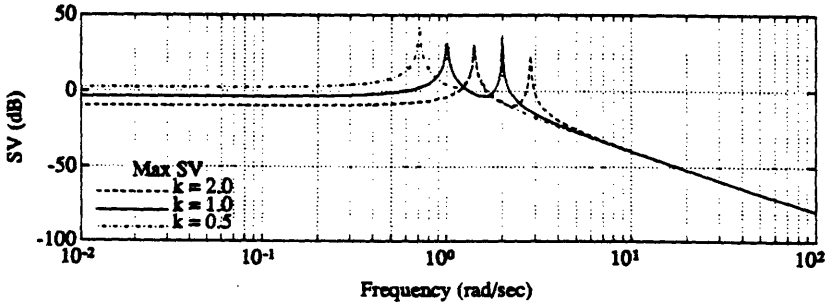

Figure 4.5: Maximum Singular Value Plot of G for $k = 0.5,\ 1.0,\ 2.0$

Pole	ζ	ω
-0.001+1.000j	0.0010	1.000
-0.001-1.000j	0.0010	1.000
-0.001+2.000j	0.0010	2.000
-0.001-2.000j	0.0010	2.000
-0.003+2.000j	0.0015	2.000
-0.003-2.000j	0.0015	2.000

Table 4.1: Poles of the Nominal MIMO MSD System

The locations of the poles are shown as a function of the spring constant, k, in Figure 4.6 below. Note that varying k only changes the real part of each pole, the imaginary part remains fixed.

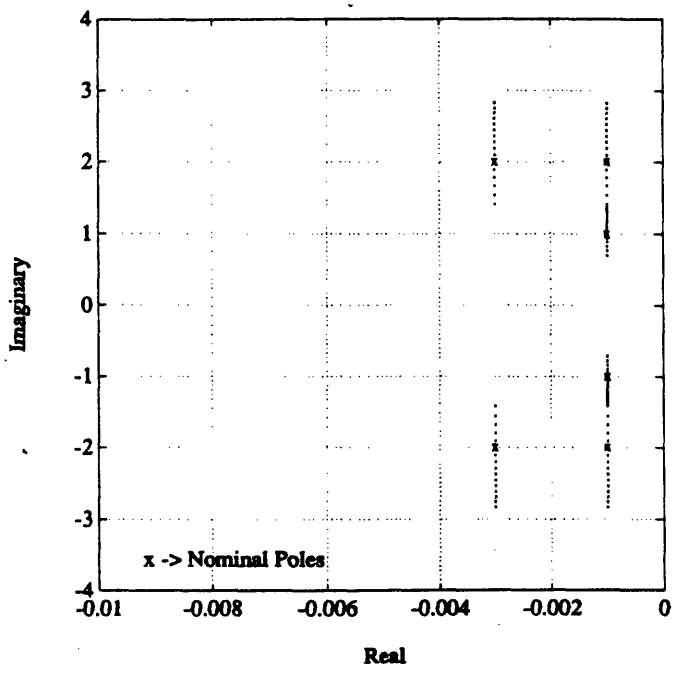

Figure 4.6: Plant Pole Location for $0.5 \leq k \leq 2.0$

With this in mind an attempt will be made to design the inner loop compensator.

4.4 Design of the Model-Matching Inner Loop Compensator

The first step in designing the inner loop compensator is choosing a desired plant, H_d. To assist in doing this it will be necessary to obtain bode plots of the individual plant input/ouput channels. These are shown in Figure 4.7 for the nominal plant. Interestingly, channels G_{12}, G_{21}, and G_{22} are identical while G_{11} has a higher DC gain and rolls off more slowly. Notice each transfer function contains two pairs of lightly-damped poles and no zeros, except for G_{11} which has a pair of lightly-damped zeros.

After several iterations a desired plant is chosen such that it mimics the actual plant but has all of its poles on the real axis. The transfer function elements of the desired plant were picked by moving the undamped poles of the nominal plant to the real axis (at the same natural frequency) and choosing the DC gain so the desired plant element's magnitude is less than the actual plant element's magnitude over all frequencies, as per the SISO inner loop designs. Except for the 11 channel where the plant has lightly damped zeros and the desired transfer function omits both those zeros and a lightly damped pair of poles. The desired plant, H_d, which meets the conditions above has individual channel transfer functions of

$$H_d^{11} = \frac{(0.5)(1.4142)^2}{(s+1.4142)(s+1.4142)}$$

$$H_d^{12} = \frac{(0.2)(2)^2}{(s+1)^2(s+2)^2}$$

$$H_d^{21} = \frac{(0.2)(2)^2}{(s+1)^2(s+2)^2}$$

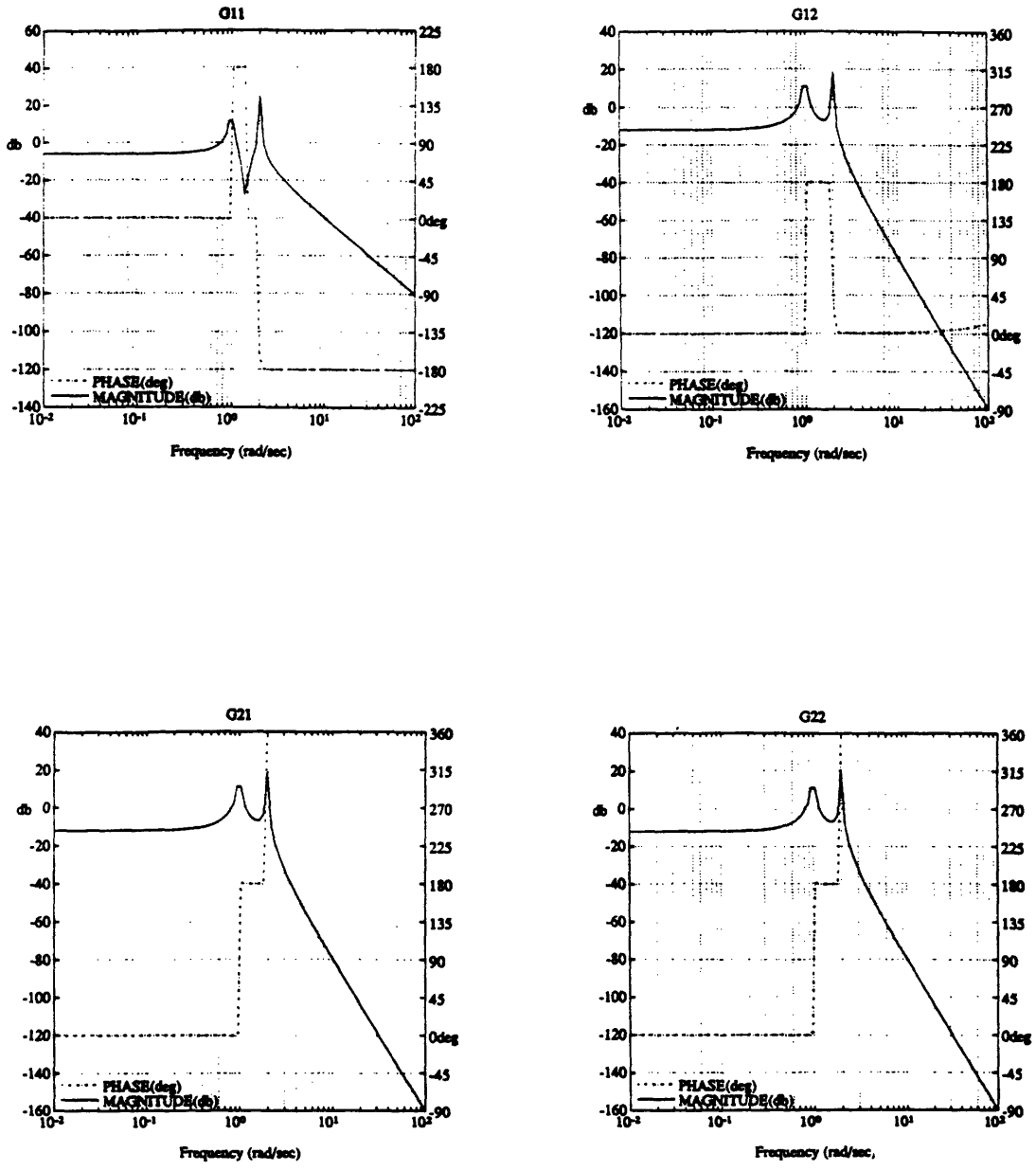

Figure 4.7: Bode Plots of the Channels of the Nominal Plant

$$H_d^{22} = \frac{(0.2)(2)^2}{(s+1)^2(s+2)^2}.$$

These transfer functions are shown in Figure 4.8, which compares the magnitude plot of each channel of the desired plant with the respective magnitude plot of each channel of the nominal plant. This illustrates the points discussed above.

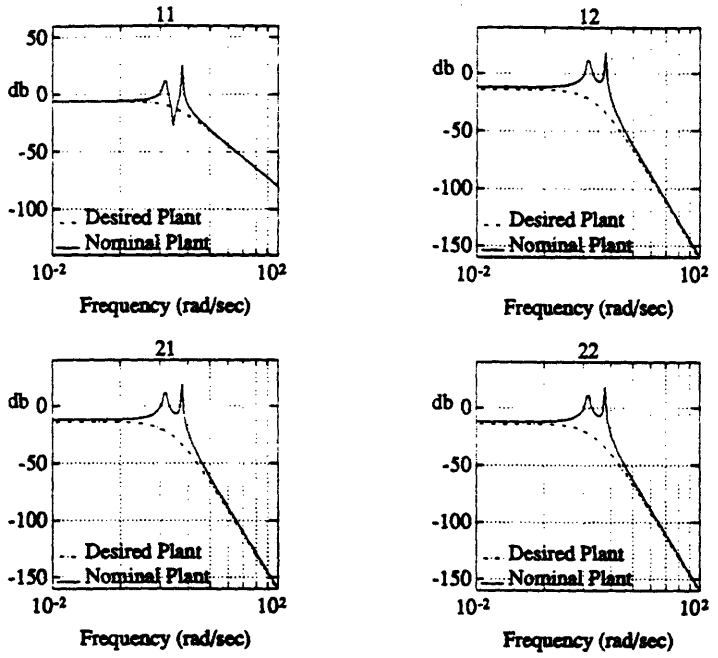

Figure 4.8: Bode Plots Comparing the Channels of the Desired Plant, H_d, to the Nominal Plant, G

Computing the frequency plots of the ideal compensator, K_{ideal}, (again, channel by channel) from equation 2.29 yields the results shown in Figure 4.9. The ideal compensator is similar to the SISO problem in being essentially a lead network, or here, a set of lead networks. Obviously, this may cause measurement noise problems. In any case it is desirable to have the compensator design of the lowest order which effectively removes most of the parameter uncertainty. After several iterations on compensator order and pole location

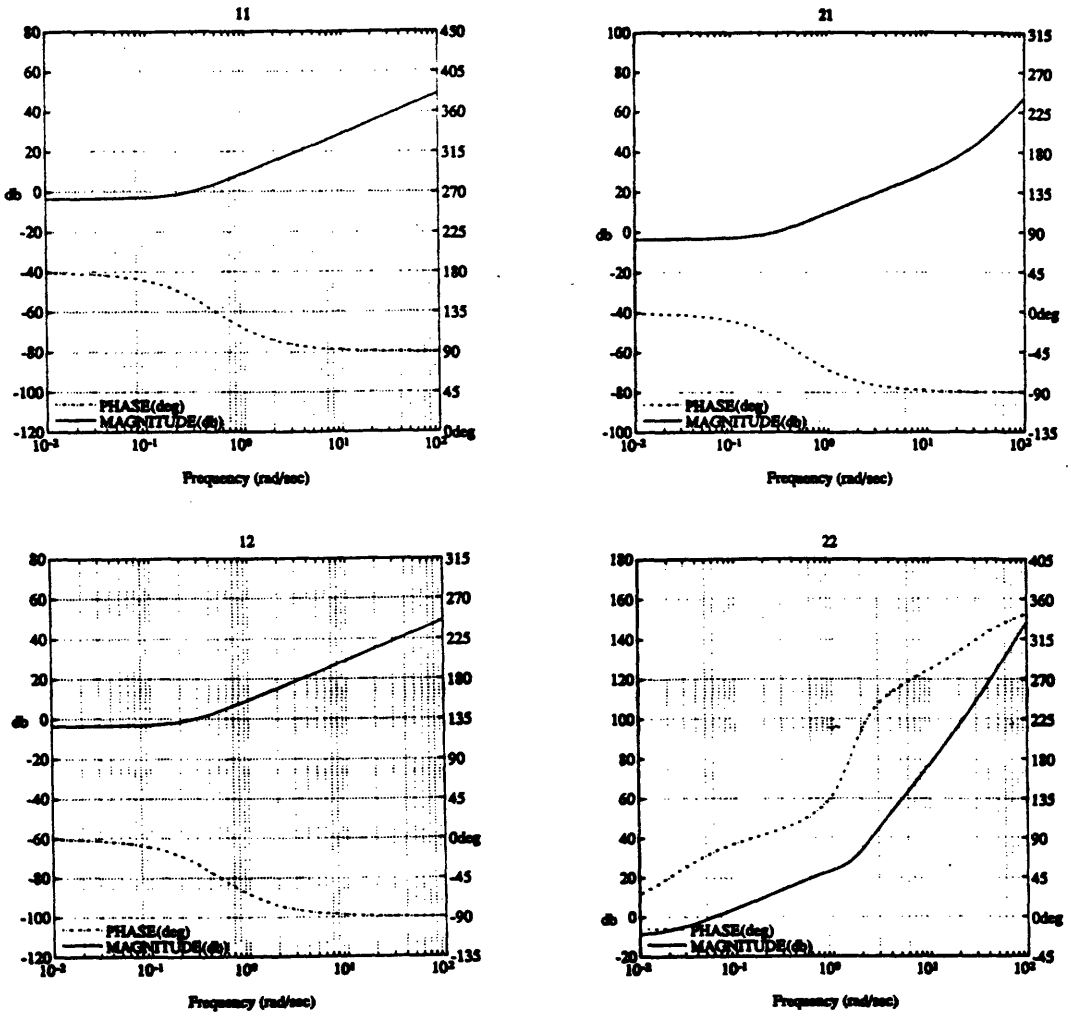

Figure 4.9: Bode Plots of the Channels of the Ideal Compensator, K_{ideal}

the model matching design method produced the following compensator:

$$K_{inner}^{11} = \frac{0.976(2.755s+1)}{0.01s+1}$$

$$K_{inner}^{12} = \frac{-1.193(2.769s-1)}{0.01s+1}$$

$$K_{inner}^{21} = \frac{-1.178(2.819s-1)}{0.01s+1}$$

$$K_{inner}^{22} = \frac{-0.580(-33.49s+1)(0.439s^2+0.6598s+1)}{(0.01s+1)(0.01s+1)(0.02s+1)}$$

The actual compensator has less lead than the ideal compensator. Channels 11, 12, and 21 each contain a lead-lag, while channel 22 has three lead-lags. The design process showed that it is channel 22 which is crucial to the design. The compensator poles were chosen to give causal compensator realizations which would allow the desired transfer function H_d be attained, yet reduce the effects of the large lead networks necessary at high frequencies. As can be seen from the transfer functions, the poles had to remain at high frequency and the channel 22 lead network is of large magnitude at frequencies above crossover. The bode plot of each channel of the actual compensator, K_{inner} is shown in Figure 4.10 and the compensator singular value plot is hsown in Figure 4.11.

When this inner loop compensator is combined with the plant, it yields the closed loop poles, with respective frequencies ω and damping ratios ζ, as compiled in Table 4.2 for the standard values of k.

The inner loop compensator provides a closed loop transfer function, T_{inner}, which is stable over the entire range of parameter variation. The damping ratios of the closed loop poles are also substantially improved over those of the base plant for the full range of parameter variation. The movement of the closed loop poles as the spring constant varies, is shown in the root locus in

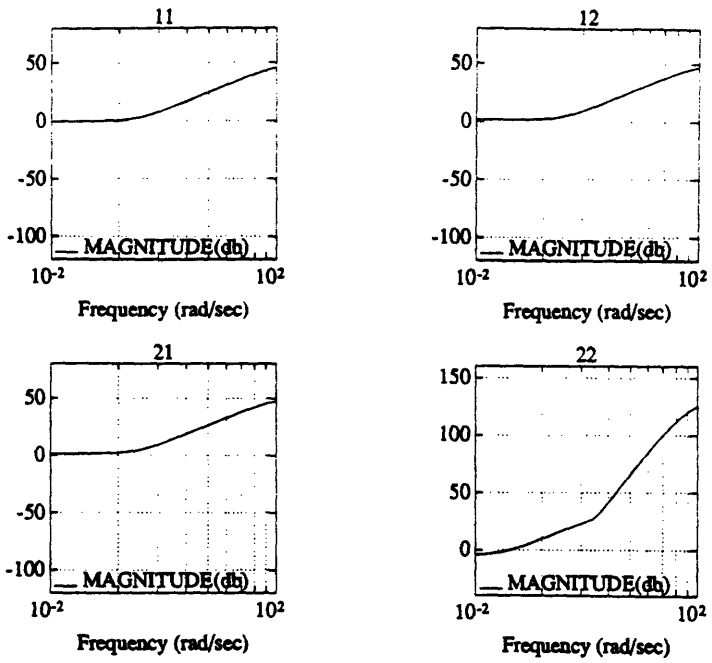

Figure 4.10: Bode Plots of the Inner Loop Compensator, K_{inner}, Channels

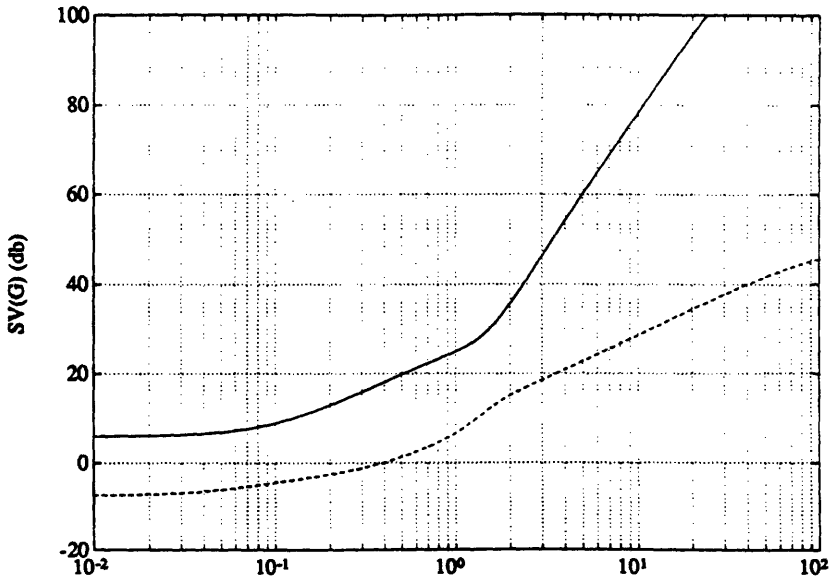

Figure 4.11: Singular Value Bode Plot of the Inner Loop Compensator, K_{inner}

$k = 0.5$			$k = 1.0$			$k = 2.0$		
Poles	ω	ζ	Poles	ω	ζ	Poles	ω	ζ
-0.2168	.2168	1	-0.5862	.5862	1	-.4083-.8373j	.9316	.4382
-0.5658	.5658	1	-.8103-.7179j	1.083	0.7485	-.4083+.8373j	.9316	.4382
-1.321	1.321	1	-.8103+.7179j	1.083	0.7485	-1.315	1.315	1
-1.528-1.438j	2.098	0.7282	-1.47-1.089j	1.829	0.8036	-1.397-2.299j	2.69	.5194
-1.528+1.438j	2.098	0.7282	-1.47+1.089j	1.829	0.8036	-1.397+2.299j	2.69	.5194
-2.518	2.518	1	-15.37	15.37	1	-12.41-20.56j	24.01	.5168
-36.12	36.12	1	-17.47	17.47	1	-12.41+20.56j	24.01	.5168
-97.22	97.22	1	-97.22	97.22	1	-97.23	97.23	1
-104.5-18.04j	106	0.9854	-107.4-23.69j	110	0.9765	-111.5-30.47j	115.6	.9646
-104.5+18.04j	106	0.9854	-107.4+23.69j	110	0.9765	-111.5+30.47j	115.6	.9646

Table 4.2: Poles of the Closed Loop System, T_{inner}, $k = 0.5,\ 1.0,\ 2.0$

Figure 4.12. This is the root locus of the poles of T_{inner}, obtained by varying the spring constant, k, in the closed loop A matrix, as were those shown for the benchmark problem.

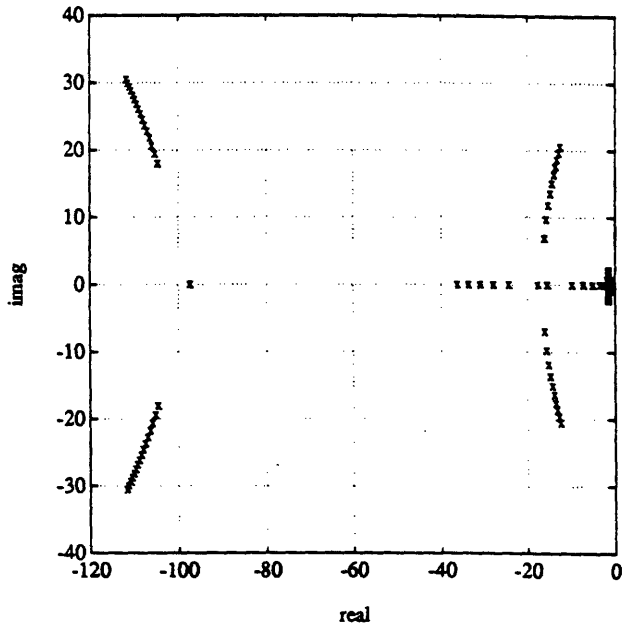

Figure 4.12: Root Locus of the Closed Loop System, T_{inner}, for $0.5 \leq k \leq 2.0$

The next three figures show the open loop singular value plots of the system, with the loop broken at the plant output GK_{inner}, for the standard values of k. Figure 4.13 shows $k = 0.5$, Figure 4.14 shows $k = 1.0$ and Figure 4.15 shows $k = 2.0$. Figure 4.16 compares the maximum singular values of each.

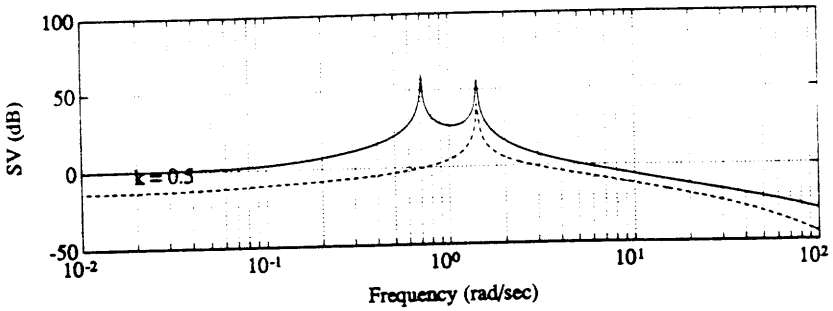

Figure 4.13: Open Loop Singular Value Plot of GK_{inner} for $k = 0.5$

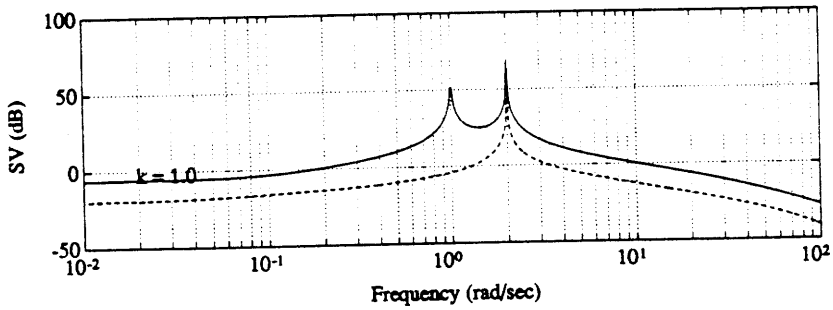

Figure 4.14: Open Loop Singular Value Plot of GK_{inner} for $k = 1.0$

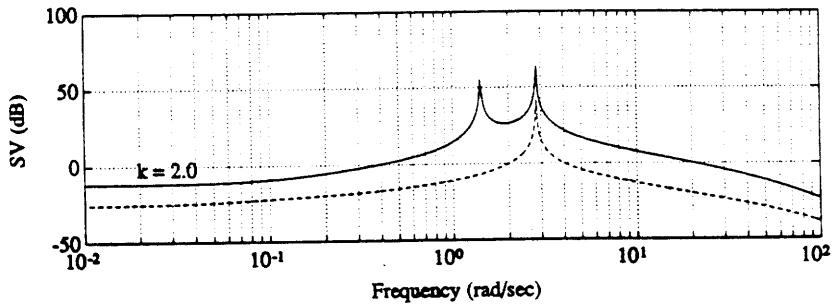

Figure 4.15: Open Loop Singular Value Plot of GK_{inner} for $k = 2.0$

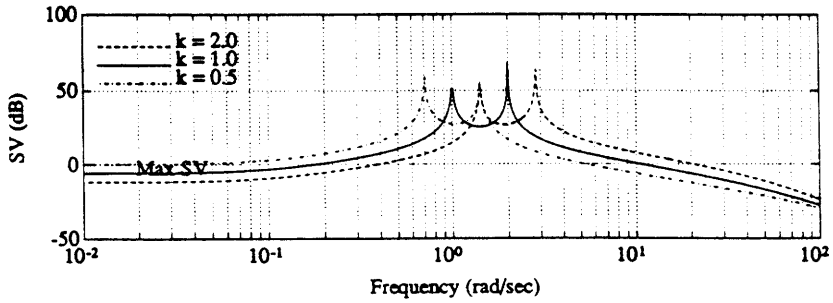

Figure 4.16: Open Loop Maximum Singular Value Plot for $k = 0.5,\ 1.0,\ 2.0$

Similarly, the closed loop, T_{inner}, singular value plots are contained in Figure 4.17, Figure 4.18, Figure 4.19 and Figure 4.20. The inner loop compensator has successfully removed a large amount of the plant variation generated by the parametric uncertainty, the poles are well damped and the remaining uncertainty consists of varying DC gain and system bandwidth. Since the DC gain of T_{inner} still varies with k, the H_∞ compensator will be augmented with an integrator to eliminate this in the final closed loop transfer function, T. The system is amenable to stable H_∞ designs over the range of parametric uncertainty.

4.5 Design of the H_∞ Compensator

The design of the H_∞ compensator begins with the selection of weights. In this problem, as before, $W_1(s)$ will be used to provide not only disturbance rejection but integrators to provide a DC gain of one in the closed loop system regardless of the value of k. The integrator, again approximated as a very slow pole, will also provide zero steady state error to any commanded reference input. Since the closed loop sensitivity of the entire system will differ from that as constrained by $W_1(s)$, as explained in Section 2.5, it must be chosen carefully. $W_3(s)$ will provide a limit on the closed loop bandwidth of the system, it is chosen to provide reasonable time response without unduly extending the closed loop bandwidth. If the closed loop bandwidth were overextended, it could have negative implications for both performance and stability robustness. Finally, W_2 will be used to guarantee that the augmented plant, P', meets the requirements of the H_∞ methodology.

The weights chosen after some iteration were

$$W_1(s) = \frac{1}{\gamma}\begin{bmatrix} \frac{0.2\rho}{s+0.000001} & 0 \\ 0 & \frac{0.2\rho}{s+0.000001} \end{bmatrix}$$

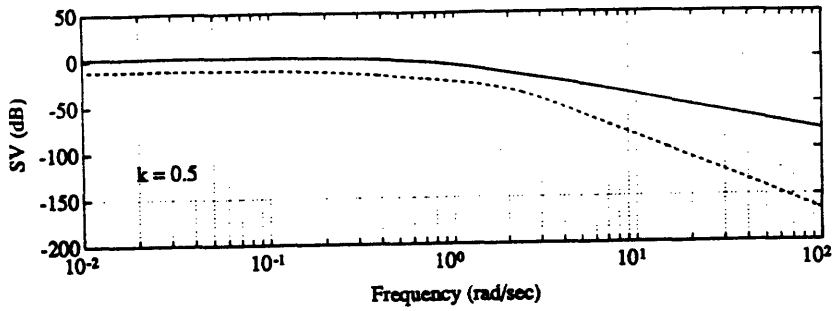

Figure 4.17: Closed Loop Singular Value Plot of T_{inner} for $k = 0.5$

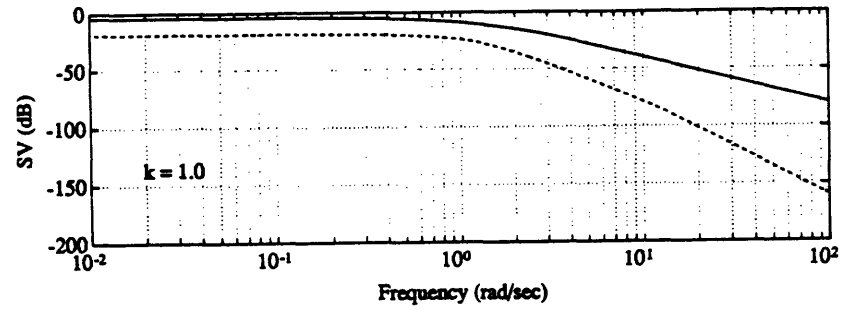

Figure 4.18: Closed Loop Singular Value Plot of T_{inner} for $k = 1.0$

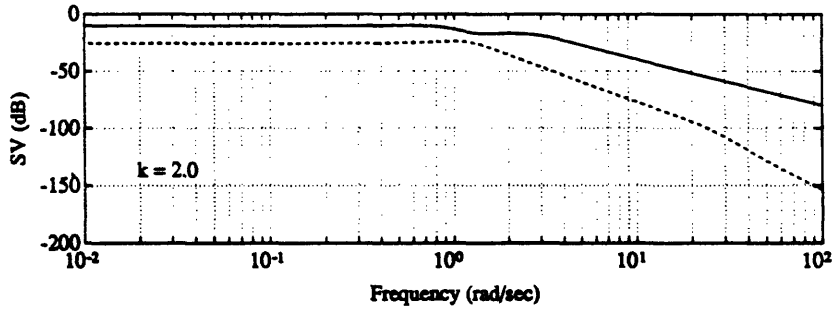

Figure 4.19: Closed Loop Singular Value Plot of T_{inner} for $k = 2.0$

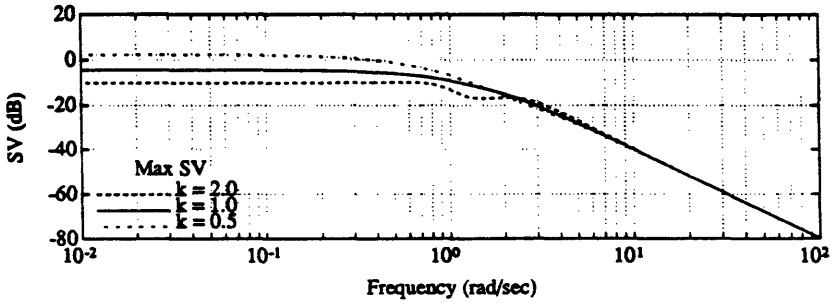

Figure 4.20: Closed Loop Maximum Singular Value Plot for $k = 0.5,\ 1.0,\ 2.0$

$$W_2 = \frac{1}{\gamma}\begin{bmatrix} 0.02 & 0 \\ 0 & 0.02 \end{bmatrix}$$

$$W_3(s) = \frac{1}{\gamma}\begin{bmatrix} 0.5s^2 & 0 \\ 0 & 0.5s^2 \end{bmatrix}$$

Where, in the compensator chosen,

$$\rho = 3.8$$

$$\gamma = 1.$$

These parameters were chosen by fixing γ, and, thusly, the closed loop bandwidth of the system, and then varying ρ until the sensitivity function is nearly minimized in the frequency range below crossover. The bode magnitude plots of the diagonal elements of the weights are shown in Figure 4.21 along with the constraint implied on the actual sensitivity function, $W_1'(s)$.

The singular value plot of the compensator obtained from these weights is shown in Figure 4.22. The integrators are apparent in the plot of the compensator. The compensator has a large magnitude across the frequency range of interest (the frequencies around the open loop crossover frequency). The state-space realization of the compensator is given in Appendix B.3.1.

4.6 Analysis of the Closed Loop System

The closed loop system, $T(s)$ is stable over the entire range of parameter variation, $0.5 \leq k \leq 2.0$ and is stable over a range of

$$0.21 < k < 7.89.$$

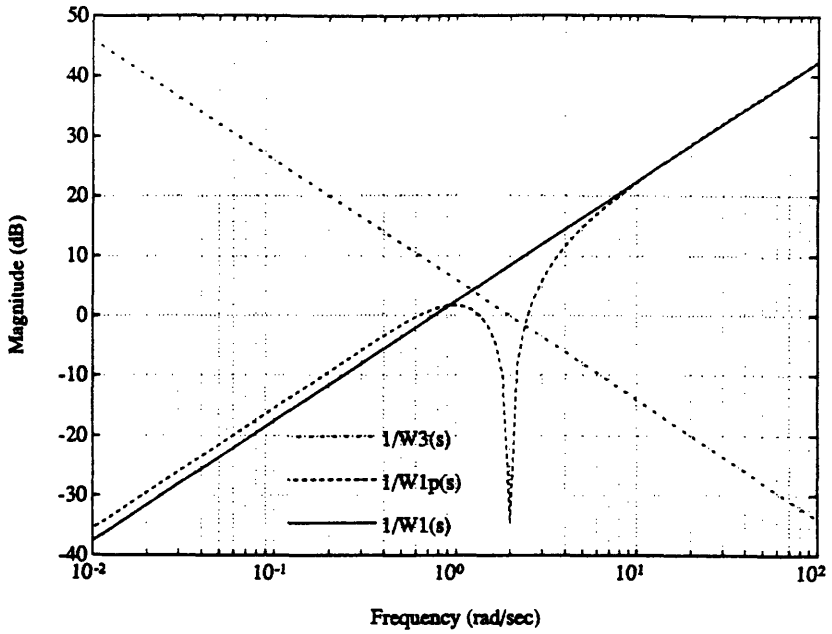

Figure 4.21: Bode Plots of the H_∞ Weighting Functions, $W_1(s)$ and $W_3(s)$, and the Implied Constraint $W_1'(s)$

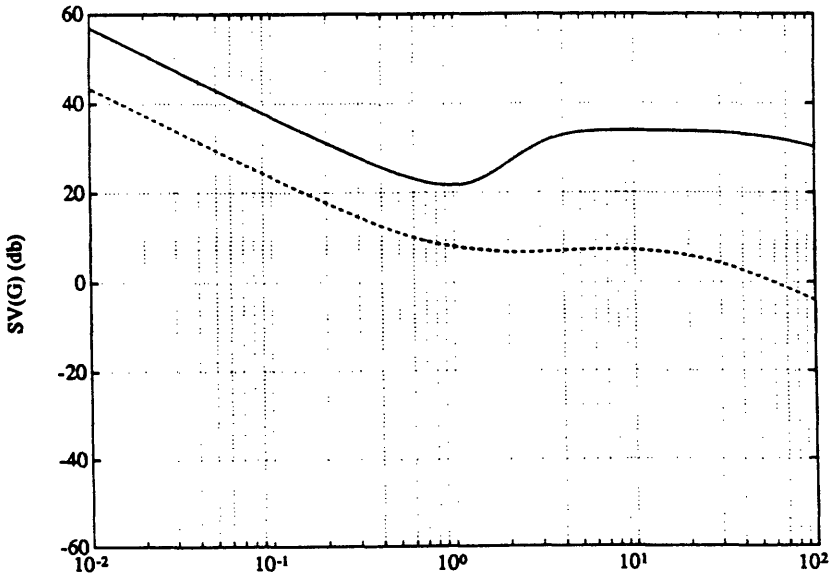

Figure 4.22: Singular Value Plot of the H_∞ Compensator

The movement of the poles with k is illustrated by the root locus in Figure 4.23. Closed loop damping decreases as k varies from its nominal value. A survey of the minimum damping ratios and their associated natural frequencies among the closed loop poles for the three standard values highlights this fact. The data is presented in the table below, Table 4.3.

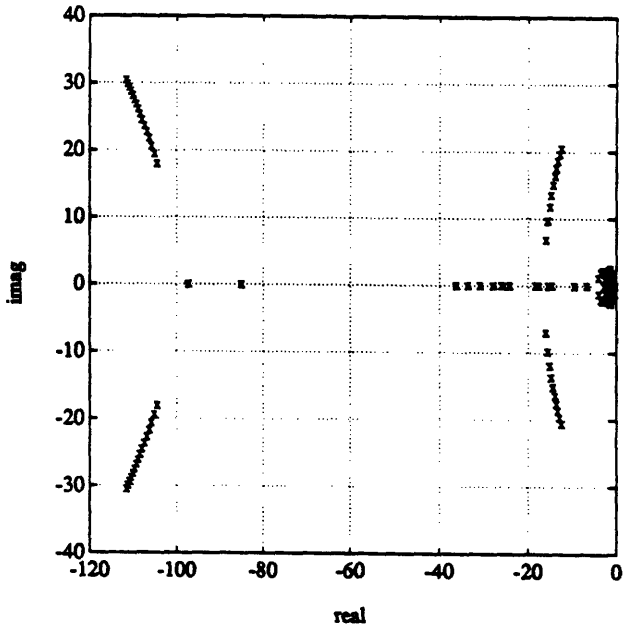

Figure 4.23: Root Locus of the Poles of the Closed Loop System for $0.5 \geq k \geq 2.0$

	$k = 0.5$	$k = 1.0$	$k = 2.0$
Minimum ζ	0.2712	0.6356	0.3839
ω	1.086	2.165	1.232

Table 4.3: Table of the Minimum Damping Ratio of the Closed Loop Poles

Figure 4.24 shows the effect on the minimum damping ratio of the low frequency poles of k varying from 0.5 to 2.0. The performance degradation as k varies will be more pronounced than in the SISO case due to these under-damped poles at low frequencies.

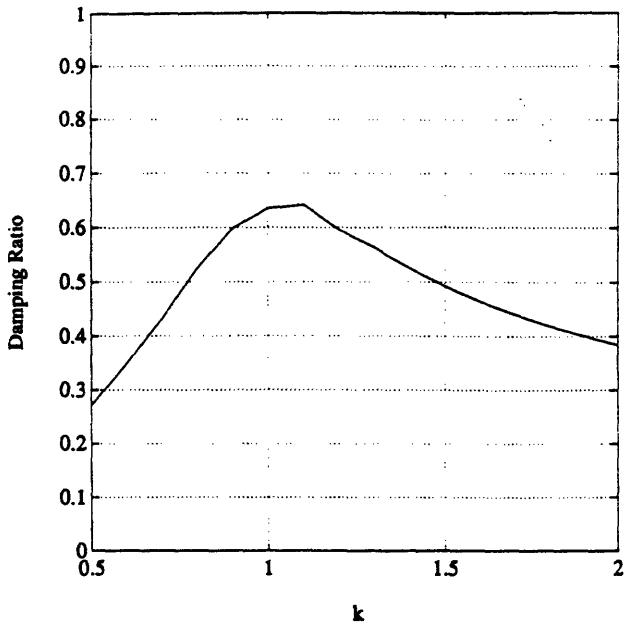

Figure 4.24: Minimum Zeta of the Closed Loop System as a Function of k

The gain and phase margins of the closed loop system are presented in Table 4.4. The system demonstrates good stability margins *for the entire range of parameter uncertainty.* Furthermore, it must be remembered that:

- This is a *conservative* measure of stability (See Section 2.2).
- The optimal values are obtained by taking the ∞-norm of the sensitivity function equal to one and substituting it into the definitions for the gain/phase margins, equations 2.7, 2.8, 2.9.

  $\downarrow$Gain Margin $= \frac{1}{2}$

  $\uparrow$Gain Margin $= \infty$

  Phase Margin $= 60$ degrees

	$k = 0.5$	$k = 1.0$	$k = 2.0$
$\uparrow GM$	5.408	3.204	2.024
$\downarrow GM$	0.550	0.592	0.664
PM (deg)	48.10	40.23	29.31

Table 4.4: Multivariable Gain and Phase Margins of the Closed Loop System

4.7 Frequency Response of the Compensated System

The open loop singular value plots of the system with the loop broken at the plant output are shown in Figures 4.25 to 4.28. The figures show the open loop singular values for (in descending order) $k = 0.5$, $k = 1.0$, $k = 2.0$ and the maximum singular values of each superimposed. The regulator open loop singular value plots are identical to the servo plots presented here and are shown in Figures 4.29 to 4.32. This implies that stability margins at the plant input are identical to those at the plant output.

The closed loop singular values are generally shaped well with minimal peaking for the cases $k = 1.0$, 2.0. There is more peaking at $k = 0.5$ which is not surprising given the low damping ratio of the closed loop poles. The plots, presented in the same format as the open loop singular values, are shown in Figures 4.33 to 4.36.

The capability of the compensated system to reject disturbances at the loop output, as measured by the sensitivity function, is presented in Figures 4.37 to 4.40. The best disturbance rejection occurs when $k = 0.5$. Though the disturbance is fairly consistent over the range of k, there is additional peaking at 20 - 30 rad/sec when $k = 2.0$. The plant will reject most disturbances over the range of parametric uncertainty. The disturbance rejection performance could have been predicted from the stability margins, see Section 2.2.

The transfer function from the specific disturbance specified in the problem

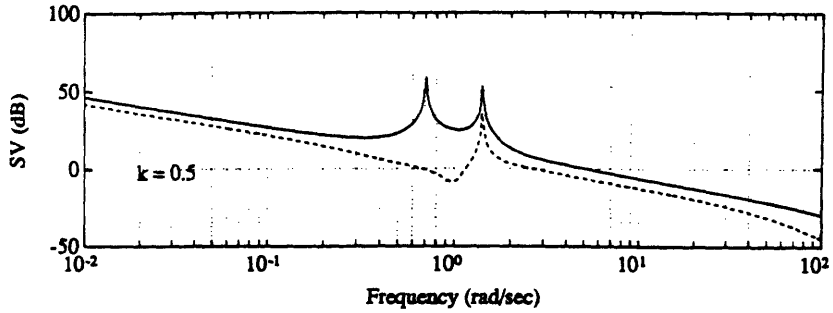

Figure 4.25: Singular Value Plot of the Open Loop Servo Transfer Function for $k = 0.5$

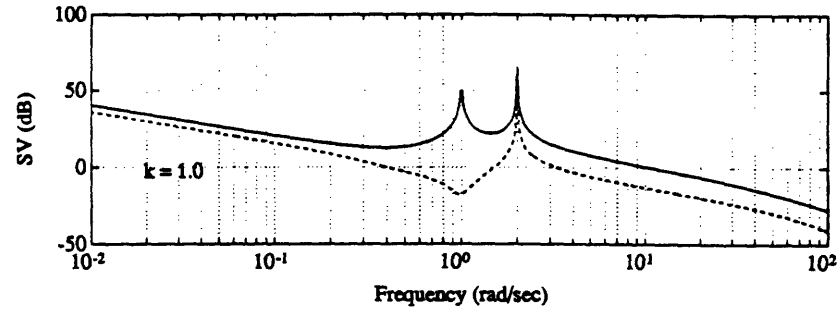

Figure 4.26: Singular Value Plot of the Open Loop Servo Transfer Function for $k = 1.0$

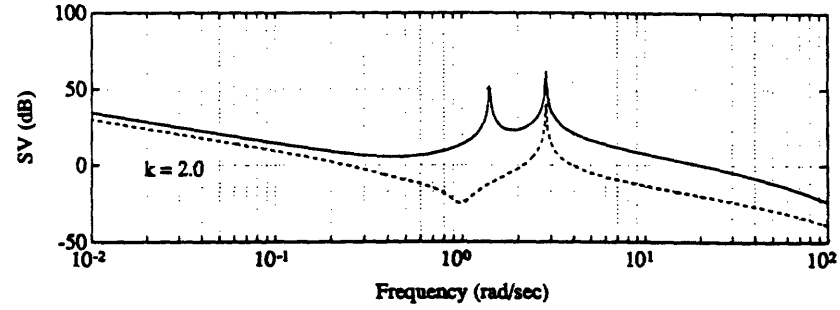

Figure 4.27: Singular Value Plot of the Open Loop Servo Transfer Function for $k = 2.0$

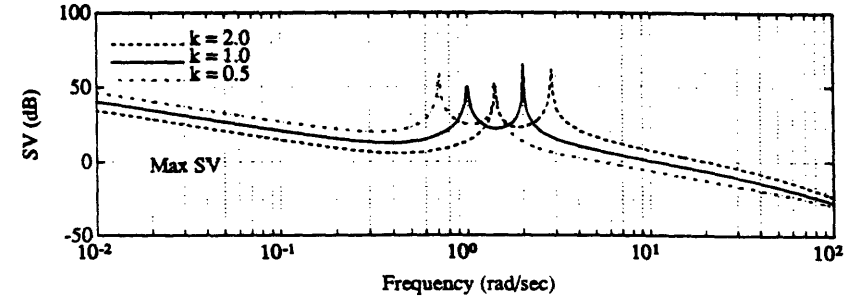

Figure 4.28: Maximum Singular Values of the Open Loop Servo Transfer Functions

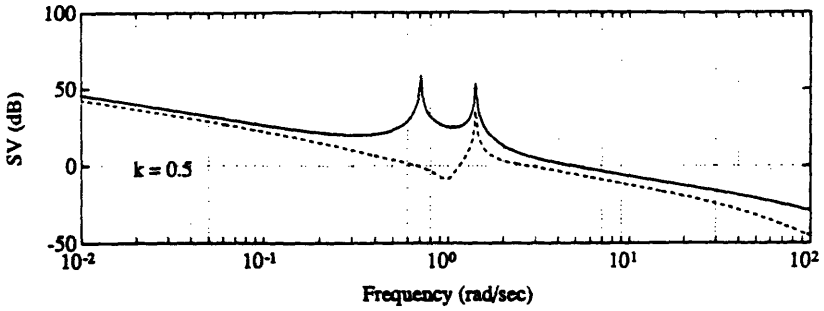

Figure 4.29: Singular Value Plot of the Open Loop Regulator Transfer Function for $k = 0.5$

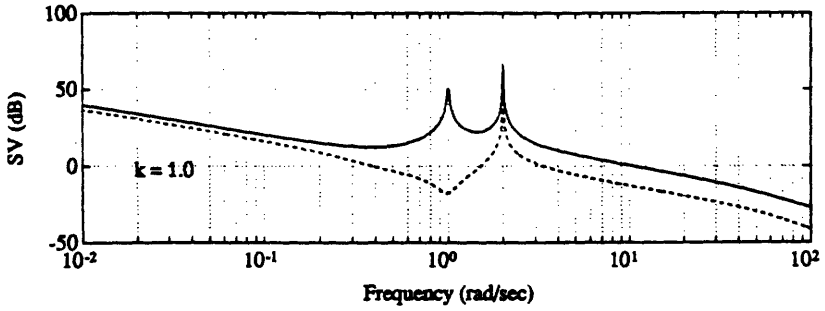

Figure 4.30: Singular Value Plot of the Open Loop Regulator Transfer Function for $k = 1.0$

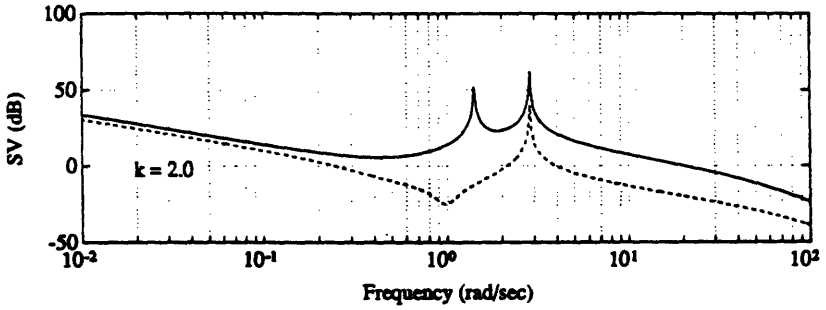

Figure 4.31: Singular Value Plot of the Open Loop Regulator Transfer Function for $k = 2.0$

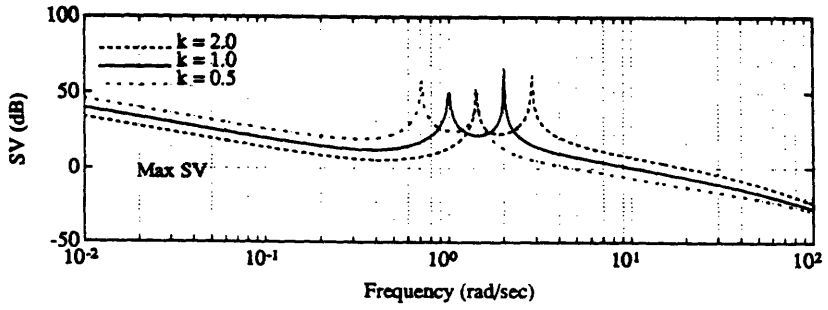

Figure 4.32: Maximum Singular Values of the Open Loop Regulator Transfer Functions

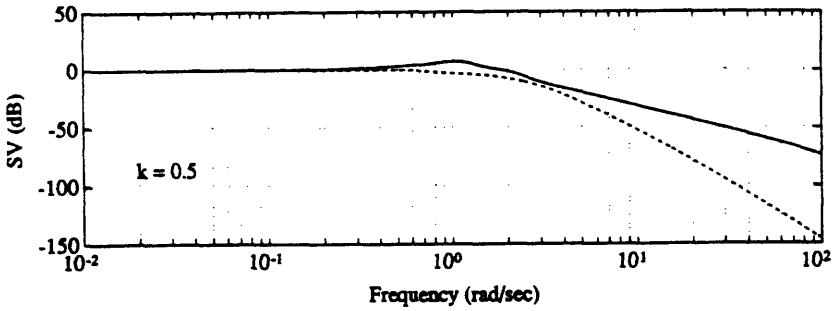

Figure 4.33: Singular Value Plot of the Closed Loop Transfer Function for $k = 0.5$

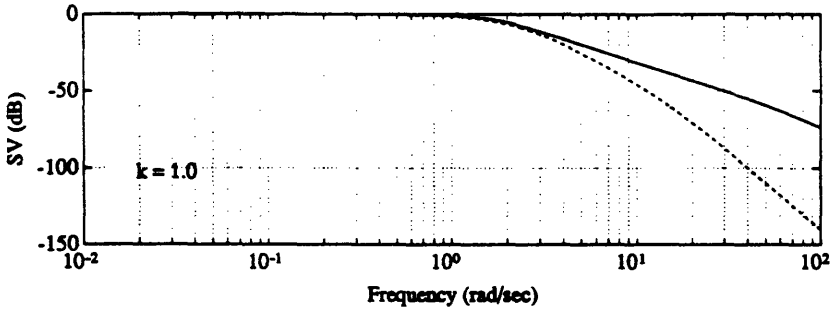

Figure 4.34: Singular Value Plot of the Closed Loop Transfer Function for $k = 1.0$

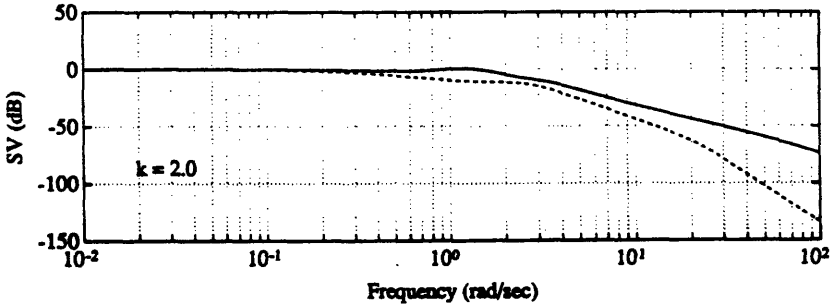

Figure 4.35: Singular Value Plot of the Closed Loop Transfer Function for $k = 2.0$

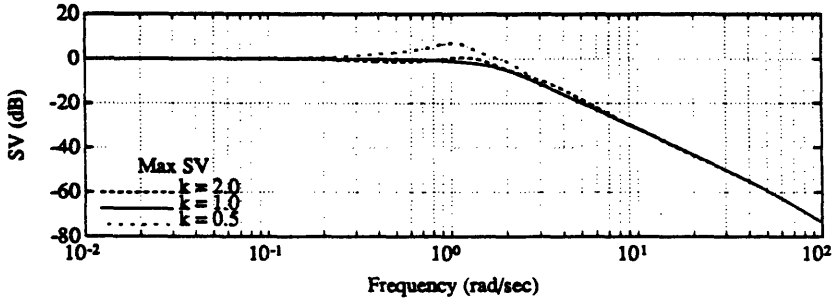

Figure 4.36: Maximum Singular Values of the Closed Loop Transfer Functions

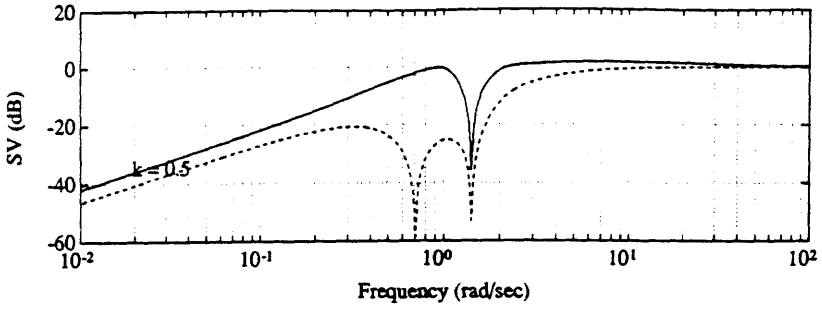

Figure 4.37: Singular Value Plot of the Sensitivity Transfer Function for $k = 0.5$

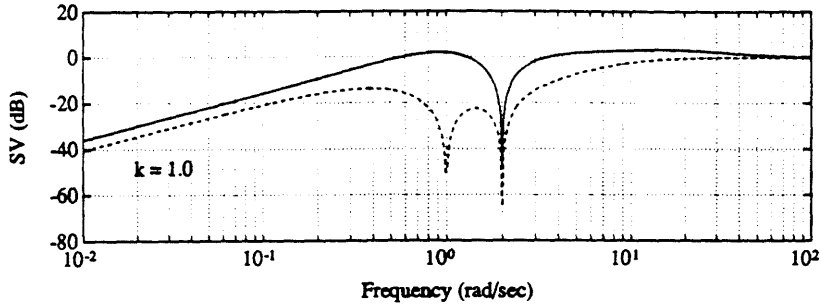

Figure 4.38: Singular Value Plot of the Sensitivity Transfer Function for $k = 1.0$

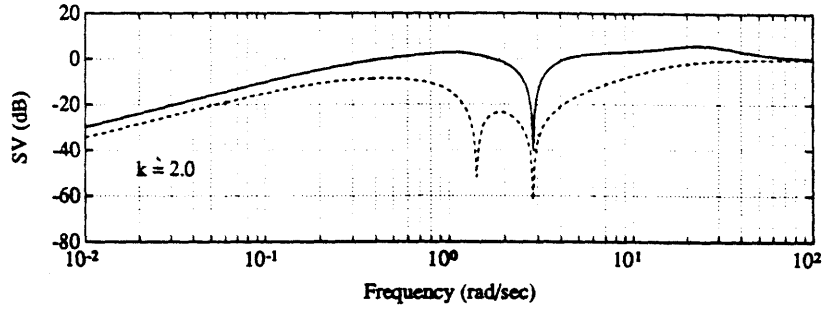

Figure 4.39: Singular Value Plot of the Sensitivity Transfer Function for $k = 2.0$

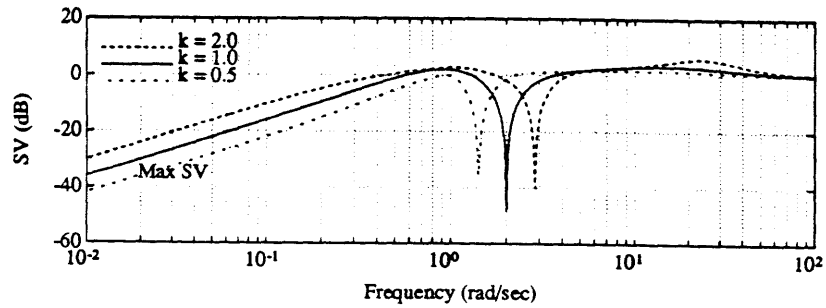

Figure 4.40: Maximum Singular Values of the Sensitivity Transfer Functions

statement to the performance variable z is considered. Since there is only a single disturbance input there is only one singular value. This is presented as a function of frequency in Figure 4.41 which contains the singular values of the transfer function for the three standard cases of k. The response is attenuated well, peaking at 0 dB for the case when k is 0.5, otherwise it is always less than 0 dB.

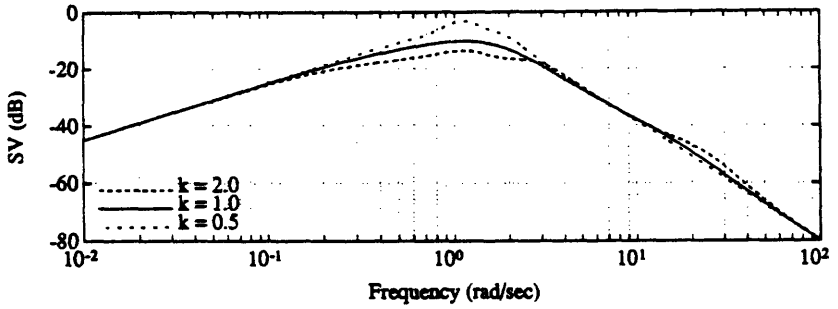

Figure 4.41: Singular Values of the Transfer Function from Disturbance to Output for $k = 0.5,\ 1.0,\ 2.0$

Finally, the transfer function from measurement noise to the performance variable is considered, $N(s)$, the singular value plots are shown in Figures 4.42 to 4.45. They indicate that measurement noise is amplified in the output, primarily due to the inner loop compensator channel 22. This effect is worst for k equal to 1.0, where it extends out to 30 rad/sec.

4.8 Time Response of the Compensated System

The time response of the compensated system is considered for a variety of disturbances and commands, both with and without noise. Specifically, the time responses are:

- A unit impulse disturbance at time zero.

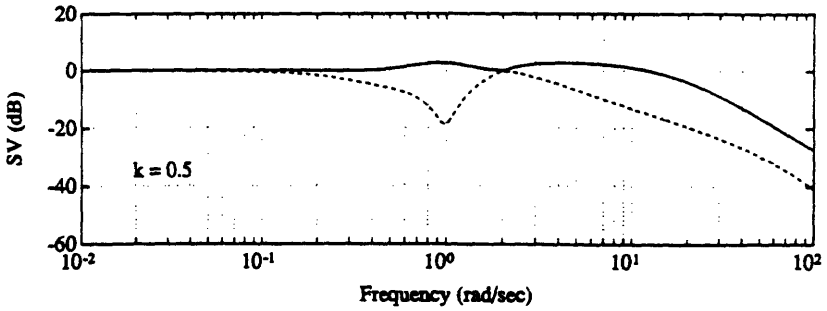

Figure 4.42: Singular Value Plot of the Transfer Function, $N(s)$ for $k = 0.5$

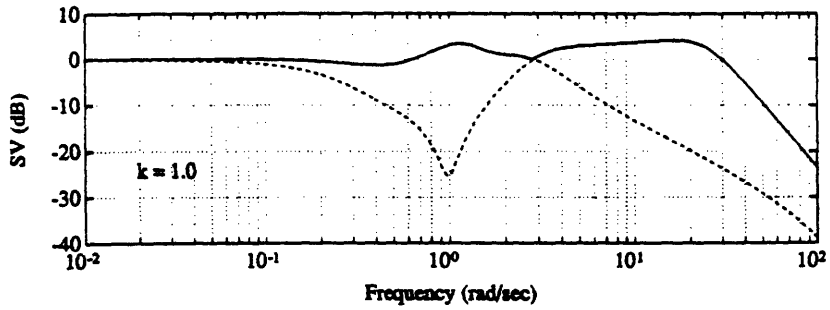

Figure 4.43: Singular Value Plot of the Transfer Function, $N(s)$ for $k = 1.0$

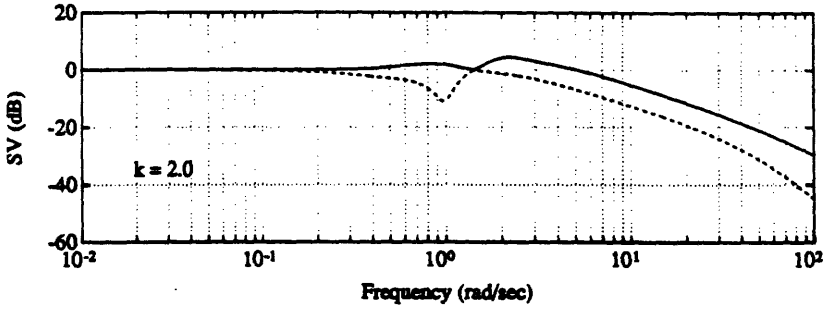

Figure 4.44: Singular Value Plot of the Transfer Function, $N(s)$ for $k = 2.0$

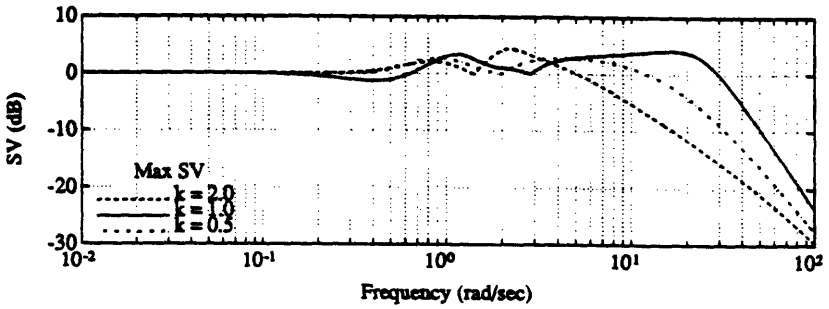

Figure 4.45: Maximum Singular Values of the Transfer Functions, $N(s)$

- A unit impulse disturbance at time zero with measurement noise.
- A constant sinusoidal disturbance.
- Step commands in the references at time zero.

For a unit impulse at time zero the system behaves as shown in the following several plots. For the cases $k = 0.5,\ 1.0,\ 2.0$ the following plots are given for each:

1. The performance variable z.
2. The inner loop compensator control signals.
3. The H_∞ compensator control signals.

The plots for k equal to 0.5 are contained in Figure 4.46, for k equal to 1.0 in Figure 4.47, and for k equal to 2.0 in Figure 4.48. For $k = 1.0,\ 2.0$ z settles within 10 seconds. The lower damping when $k = 0.5$ degrades that response considerably, but it still settles within 15 seconds. As could be expected from the previous chapter the initial inner loop control effort is quite large in the second control output. This is due to the large lead network in the 22 channel of the inner loop compensator. The first inner loop output and the H_∞ control effort are of reasonable magnitude.

The response to the impulse disturbance with measurement noise present in is presented in Figures 4.49 to 4.51 for k equal to 0.5, 1.0, and 2.0. The noise is considerably amplified by K_{inner}^{22}. This effect can be seen in the output regardless of the value of k and is not surprising if one considers Figures 4.42 to 4.45.

The response to a sinusoidal input disturbance at a frequency of 0.5 rad/sec is shown in Figures 4.52 to 4.54 in the standard format. The disturbance is well attenuated (as expected from Figure 4.41) and asymptotically rejected in 15 seconds or less over the full range of parametric uncertainty.

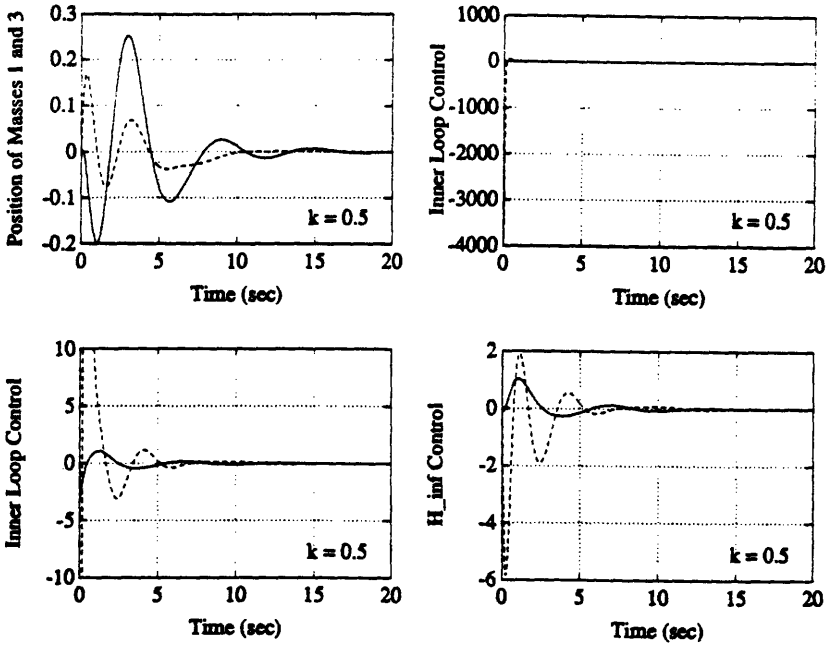

Figure 4.46: Closed Loop System Response to an Impulse Disturbance for $k = 0.5$

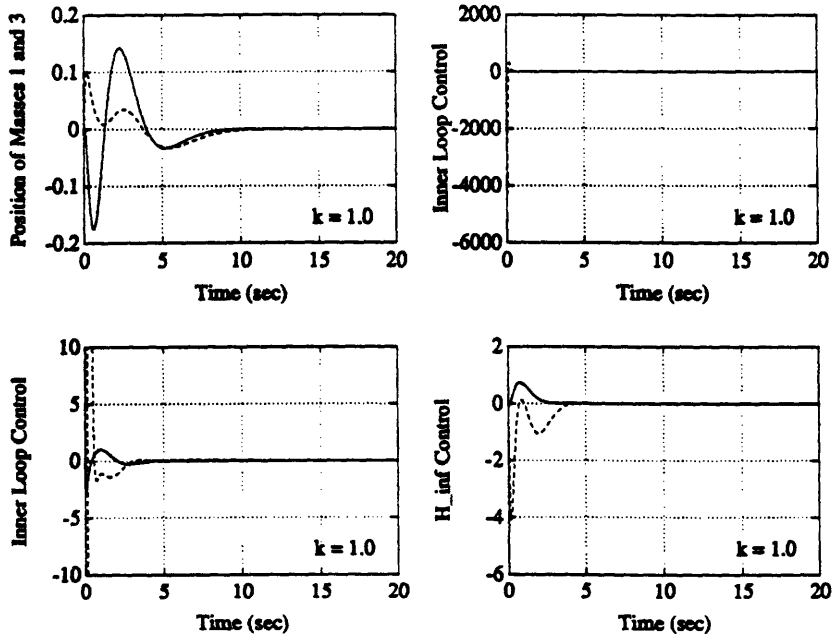

Figure 4.47: Closed Loop System Response to an Impulse Disturbance for $k = 1.0$

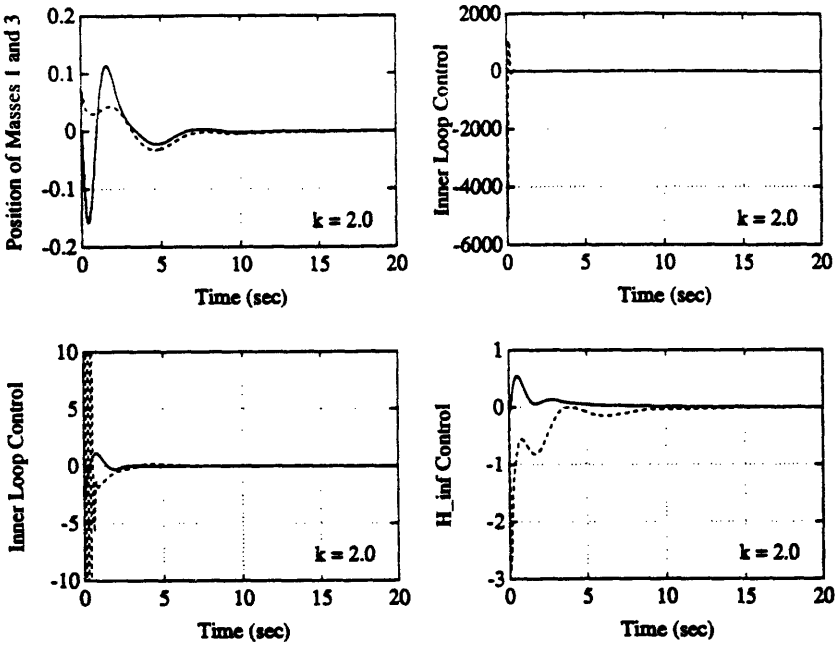

Figure 4.48: Closed Loop System Response to an Impulse Disturbance for $k = 2.0$

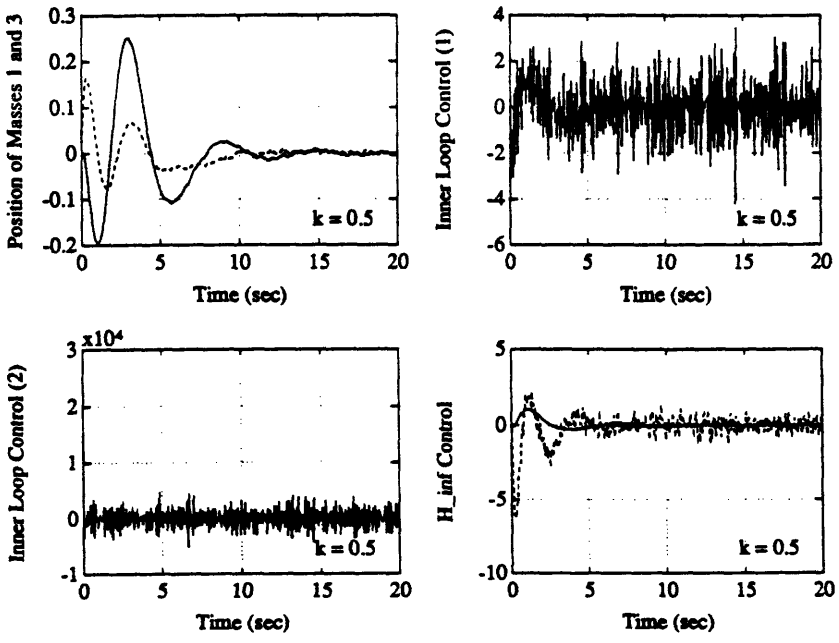

Figure 4.49: Closed Loop System Response to an Impulse Disturbance with Measurement Noise for $k = 0.5$

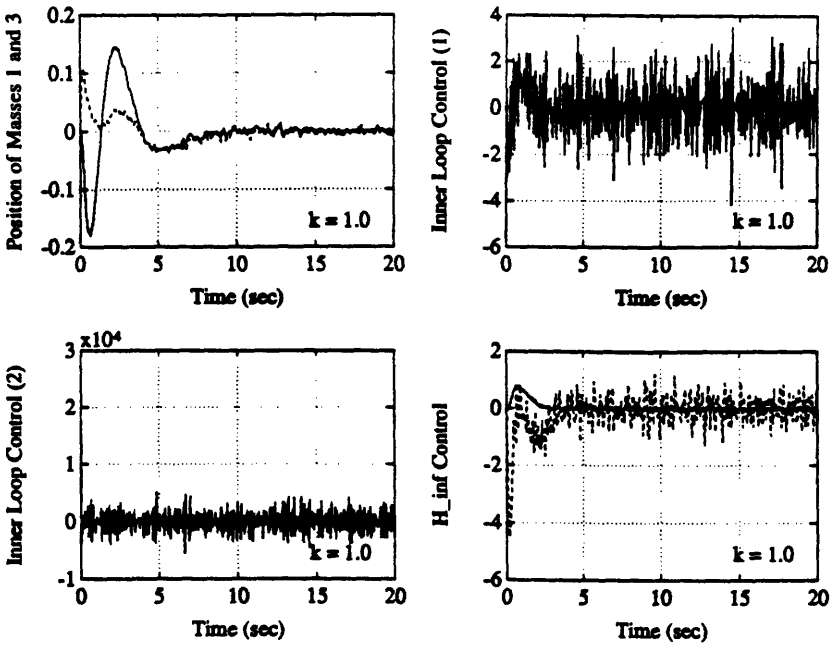

Figure 4.50: Closed Loop System Response to an Impulse Disturbance with Measurement Noise for $k = 1.0$

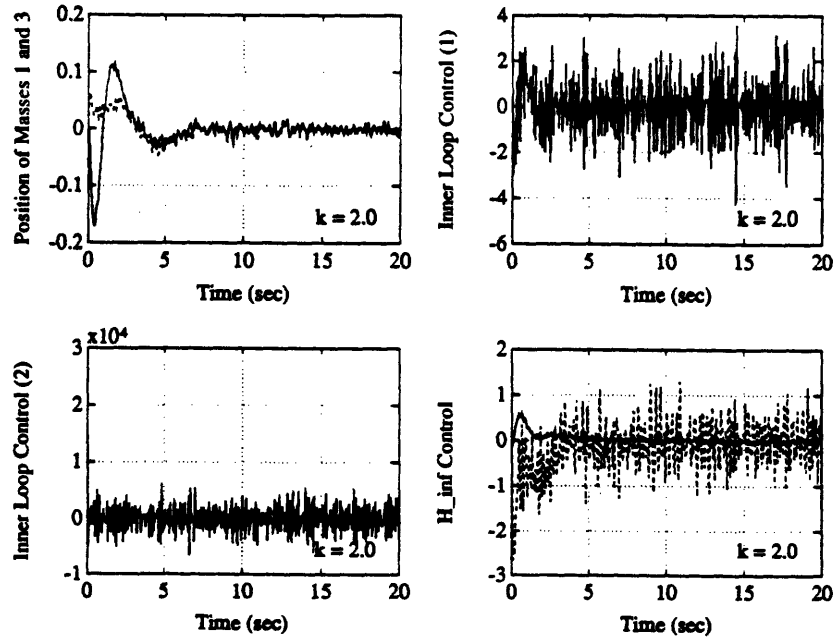

Figure 4.51: Closed Loop System Response to an Impulse Disturbance with Measurement Noise for $k = 2.0$

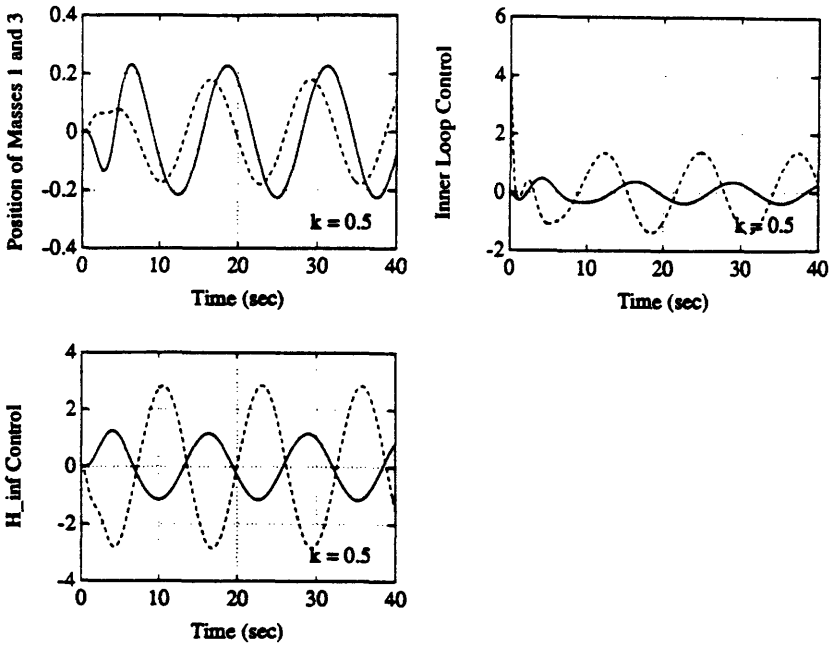

Figure 4.52: Closed Loop System Response to a Sinusoidal Disturbance for $k = 0.5$

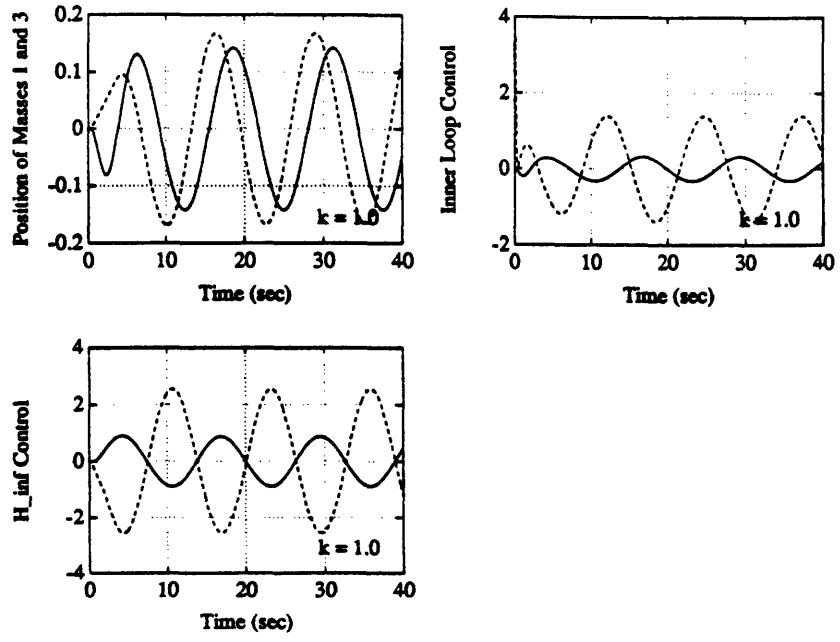

Figure 4.53: Closed Loop System Response to a Sinusoidal Disturbance for $k = 1.0$

Finally, to understand the command following capabilities of the system, equal and opposite step changes to the references were injected. The results are presented in Figures 4.55 to 4.57. For the nominal case response is excellent with a rise time of less than 3 seconds and no overshoot in either output. The off nominal designs don't fare as well; for k equal to 0.5 there is an overshoot of about 70% and a settling time greater than 10 seconds for the position of mass 1. Mass 3 is better with less than 20% overshoot and a rise time less than 3 seconds. For k equal to 2.0 there is no overshoot but rise times are at about 10 seconds for both masses.

4.9 H_∞ Compensator Order Reduction

The H_∞ compensator constructed has 12 states. To reduce the number of states a square root balanced-truncation algorithm was applied and a 7 state compensator resulted. The infinity norm of the difference between the compensators is equal to 1.1207. However, the difference in the singular values of the full and reduced order compensator is shown in Figure 4.58. This difference is very small over the entire frequency range shown. The full state-space realization is found in Appendix B.3.2.

The closed loop root locus, obtained by varying k from 0.5 to 2.0, is shown in Figure 4.59 and Figure 4.60. No loss in stability or performance robustness occurs with the reduced order compensator. The remainder of the frequency and time response plots are very similar to those found above for the full order H_∞ compensator. They may be found in Appendix E.

4.10 Design Summary

The design methodology was used to design two compensators for a MIMO mass-spring-damper system with three lightly-damped pole pairs and with

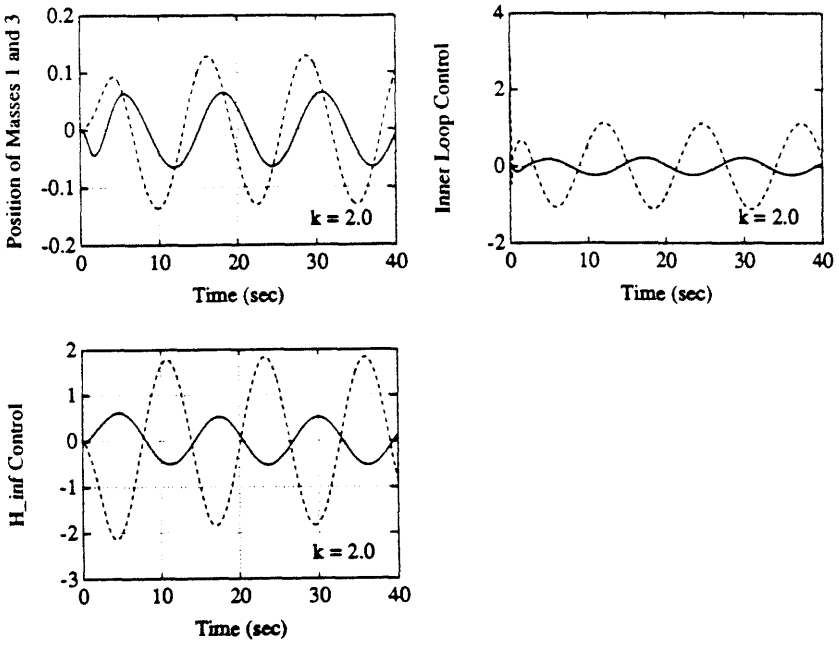

Figure 4.54: Closed Loop System Response to a Sinusoidal Disturbance for $k = 2.0$

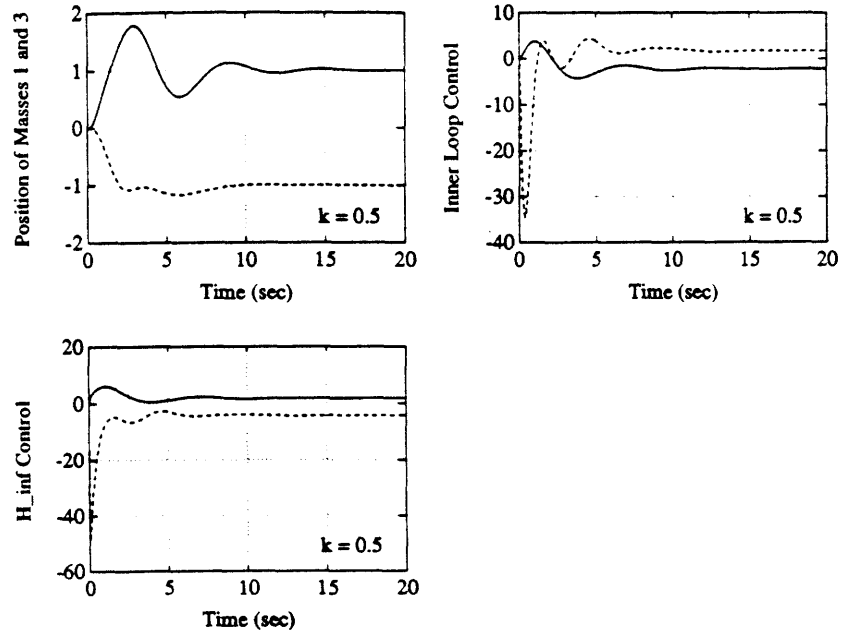

Figure 4.55: Closed Loop System Response to a Reference Step Change for $k = 0.5$

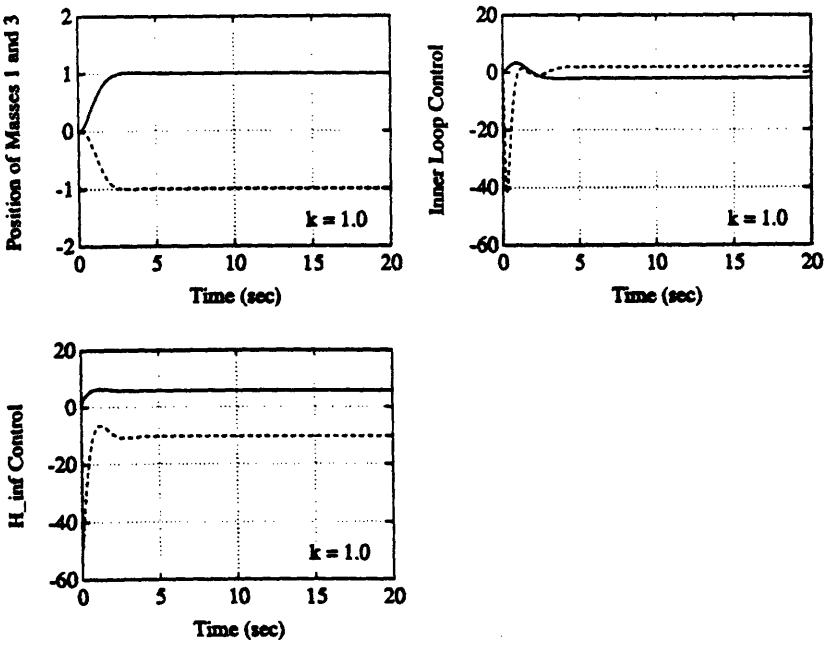

Figure 4.56: Closed Loop System Response to a Reference Step Change for $k = 1.0$

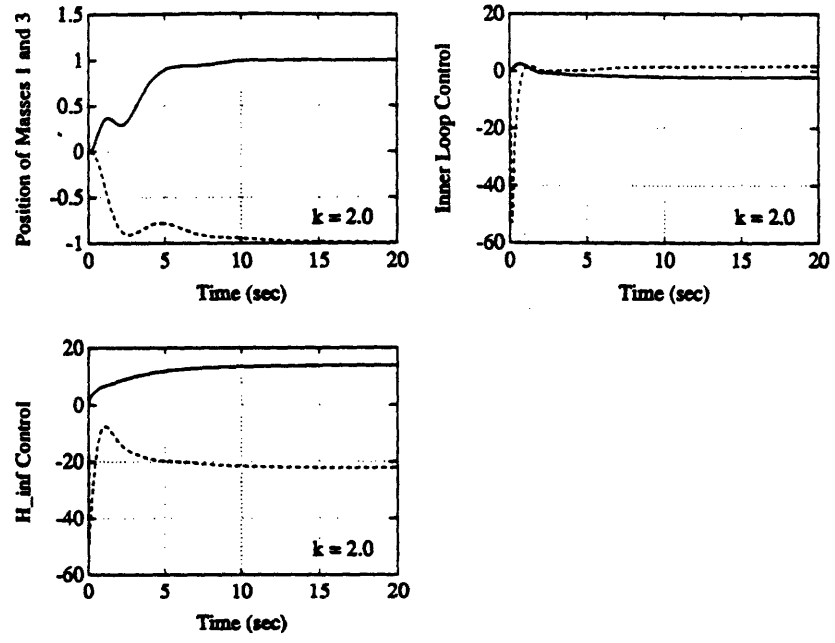

Figure 4.57: Closed Loop System Response to a Reference Step Change for $k = 2.0$

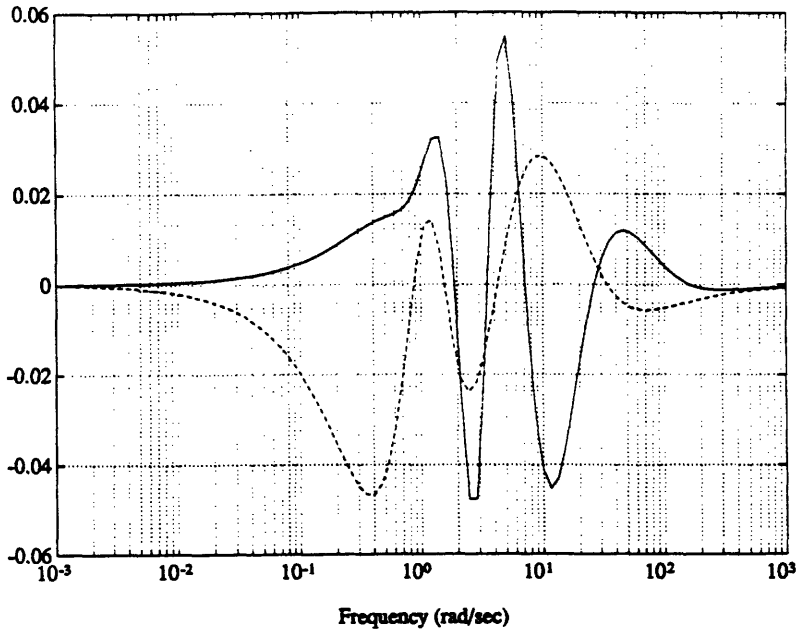

Figure 4.58: Difference in the Maximum/Minimum Singular Values of the Full and Reduced Order H_∞ Compensators

simultaneous uncertainty in the value of the spring constants, k. The resultant compensator consists of a four state inner loop compensator and a seven state reduced order H_∞compensator, so the compensator system has twelve states.The compensated system accomplished the following:

- The closed loop system was stable over the entire range of parameter variation, $0.5 \leq k \leq 2.0$ and extended the range of stability to

$$0.21 < k < 7.89.$$

- The multivariable stability margins were for the range of parametric variation:

$$29.31 \leq PM \leq 48.13$$

$$2.02 \leq \uparrow GM \leq 5.42$$

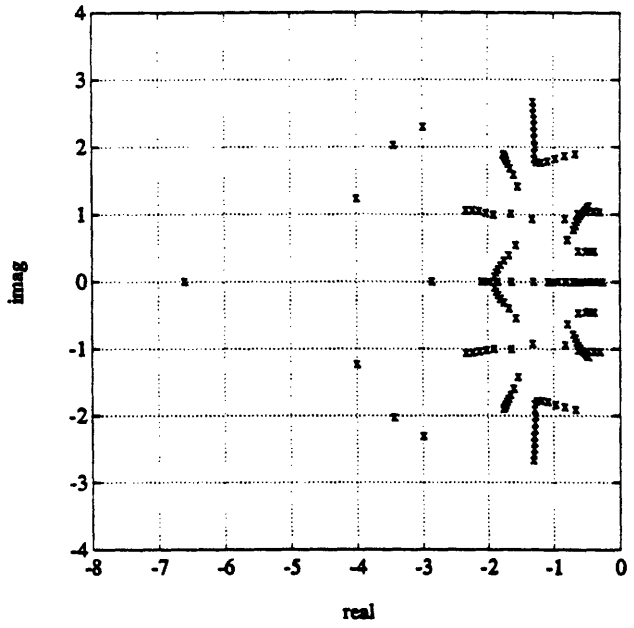

Figure 4.59: Root Locus of the Closed Loop System with the Reduced Order H_∞ Compensator for $0.5 \leq k \leq 2.0$ – Poles Near the Origin

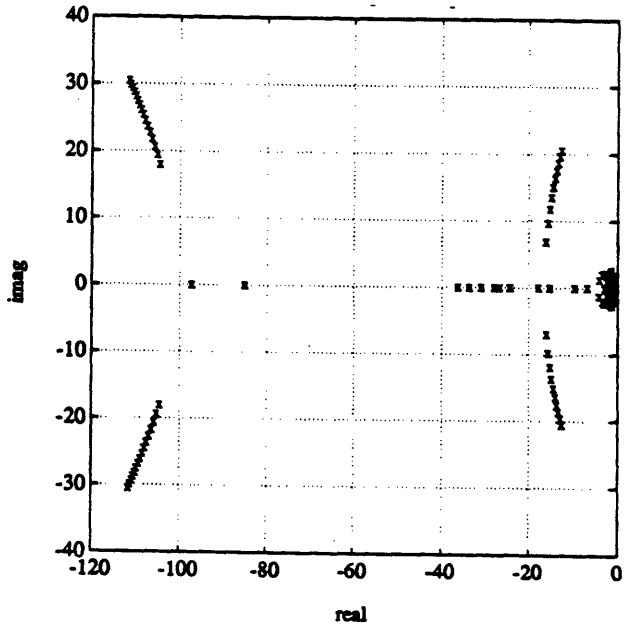

Figure 4.60: Root Locus of the Closed Loop System with the Reduced Order H_∞ Compensator for $0.5 \leq k \leq 2.0$

$$0.66 \geq \downarrow GM \geq 0.55$$

- Good disturbance rejection characteristics were obtained for the entire range of parameter variation. The benchmark design problem specifications (Section 3.2) were met over the entire range of variation.
- Good command following characteristics were obtained for the nominal case.

The design had the following drawbacks:

- Total compensator order was twice that of the plant (12 states).
- The inner loop compensator had a channel with large amounts of lead, resulting in noise amplification and large impulse response compensator effort.
- Command following performance was not robust to parameter variation.

The design methodology was sucessful in creating a design which met most of the system requirements. The drawbacks involving compensator complexity and large controller effort have been addressed previously in Section 3.4.7. The lack of robustness in command following performance is more difficult to address. It might possibly be improved by a new H_∞ or inner loop design, though this was not attempted.

Chapter 5

Conclusions and Directions for Further Research

5.1 Conclusions

The methodology was shown to be effective in providing compensator designs which demonstrated performance and stability robustness to parametric uncertainty. This was shown to be true for both the SISO and MIMO examples. The methodology was shown to be flexible and relatively easy to use with all specifications being presented in the frequency domain.

The advantage of the compensator design is an ability to desensitze the H_∞ methodology to parametric uncertainty, at least for the case of lightly damped poles. This is achieved by an inner loop compensator whose advantages are based on its flexibility.

First, one can minimize the order of the inner loop compensator to that necessary to achieve the desired performance level. Given, that H_∞ compensators produce designs with order equal to that of the augmented plant this may be quite important for implementation. Notice also, a similar model-matching conpensator could be designed in place of the H_∞ compensator [18, 20] to fur-

ther reduce the system complexity. Though there might not be any advantage versus the reduced order H_∞ compensator.

Another advantage is the ability to constrain elements of the compensator to account for physical or designer prescribed constraints in the problem. This was demonsatrated in the first thesis example. For certain types of problems this could allow inner feedback compensators in which only some of the output variables are used by the inner loop compensator, resulting in a simpler system.

While not used in these problems, the inner loop compensator can be designed to weigh certain channels of the desired plant over others. For example, if the plant had only one set of lightly damped poles, which only appeared in certain channels of that plant, the methodology could be used to damp only those channels. Then the resulting compensator might not need all of the output variables, as described above.

The inner loop design method allows designers the ability to easily specify the desired performance of the closed loop system through the desired plant. For plants with lightly-damped poles this method was shown to work quite well. Notice the method was equally straightforward for both SISO and MIMO systems.

Drawbacks of the compensator designs were their high order, typically twice that of the plants used in the examples. This seems to be unavoidable and is a tradeoff for the performance attained. However, given plants in which not all of the poles are lightly damped or near the real axis, the compensator order should not continue to increase. For example, given a plant with two sets of lightly damped poles, plus other plant dynamics, actuator dynamics, etc., it is not expected that the inner loop compensator order would increase to almost the plant order.

Another drawback was that for plants with lightly-damped poles and accompanying large phase loss the inner loop designs tended to be large lead

networks. As was shown, such designs are sensitive to measurement noise causing large control effort. The closed loop system was shown to have the frequency at which the noise rolled off extended by the inner loop compensator.

Also for the inner loop compensator, the quality of the methodology that allows its flexibility with regards to compensator order, constraints, weights, etc., its implementation as point-by-point calculations of frequency responses, prevents it from achieving any guaranteed stability or performance. However, the calculation of the ideal compensator frequency response provides clues as to whether a realizable compensator can be achieved which will stabilize the system. If the ideal compensator does not have a "smooth" shape, it indicates that a stabilizing compensator will be harder to achieve. Similarly, the same holds true for the desired plant. A well chosen desired plant which is achievable should yield a well behaved ideal compensator. Notice that for all of the examples shown here this was true. A method is suggested in [18] in which the least-squares problem is modified to find the numerator transfer function matrix of the Youla parameter. Given a stable denominator transfer function matrix the resulting compensator would have guaranteed nominal stability. However, it would be impossible to fix any elements of the structure of this compensator.

Finally, while there is no guarantee of convergence in the inner loop least-squares minimization algorithm, for well chosen desired plants the algorithm tends to converge quickly. If it does not, it is best to try a different desired plant. Again, some possible improvements are given in [18].

Overall, the methodology was effective and staightforward enough that a controls engineer with a basic knowledge of MIMO control design could use it quite easily. While commercialized computer tools that perform the inner loop design are not currently available, they may be in the future and could be relatively easily constructed given a basic controls package such as PRO-

MATLAB. H_∞ computer design tools are readily available and can also be relatively easily constructed given a Riccati equation solver.

5.2 Directions for Further Research

While the methodology fared well in the examples presented here, a wider range of plants with parametric uncertainty need to be considered. For example, plants with multiple uncertain parameters. In the MIMO example presented in Chapter 4 the spring constants could be permitted to vary independently of each other or the masses could also be permitted to vary. Given this multiple parameter uncertainty, one must still determine its effect on the individual transfer function elements of the plant in order to choose a desired plant.

The use of robustness measures such as the SSV, MSM, etc., which can measure the effects of real parametric uncertainty need to be considered alongside the methodology. For example, given a design which has a plant with multiple uncertain parameters, what is the robustness of a compensator design to the uncertainty. Since the design methodology presented here does not explicitly account for the parametric uncertainty, a method is needed to check the robustness of the closed loop system for plants with multiple varying parameters. The examples presented in this thesis avoided this problem by dealing with a single parameter variation. Notice that as an example, both of these concerns could be addressed through Design 3 of the benchmark problem.

As mentioned above certain improvements to the model-matching method are possible and should be explored. Also, it would be desirable to apply the methodology to a realistic plant rather than the academic plants considered here.

It should be remembered that while direct measurements of parametric

uncertainty are desirable because they reduce the conservativeness of a design, unstructured uncertainty is always present due to nonlinear dynamics, high frequency dynamics, etc.

Also design techniques which directly account for parametric uncertainty, for example [19], need to be evaluated.

Bibliography

[1] Michael Athans. Multivariable control systems I – problem set 3. MIT, 1988.

[2] Michael Athans. Viewgraphs for multivariable control systems I. MIT, 1988.

[3] Michael Athans. Viewgraphs for multivariable control systems II. MIT, 1989.

[4] Edward V. Byrns, Jr. and Anthony J. Calise. Fixed order dynamic compensation for the H_2/H_∞ benchmark problem. In *Proceedings of the American Control Conference*, 1990.

[5] Richard Y. Chiang and Michael G. Safonov. *Robust-Control Toolbox User's Guide.* South Natick, MA, 1988.

[6] R.Y. Chiang and M.G. Safonov. H_∞ robust control synthesis for an undamped, non-colocated spring-mass system. In *Proceedings of the American Control Conference*, 1990.

[7] E.G. Collins, Jr. and D.S. Bernstein. Robust control design for a benchmark problem using a structured covariance approach. In *Proceedings of the American Control Conference*, 1990.

[8] Ian Keith Craig. Sensitivity of H_∞ controller designs to structured uncertainty. Master's thesis, Massachusetts Institute of Technology, 1989.

[9] R. Lane Dailey. Lecture notes for the workshop on H-infinity and mu methods for robust control. American Control Conference, 1990.

[10] John C. Doyle. Structured uncertainty in control system design. In *Proceedings of the 24th IEEE Conference on Decision and Control*, pages 260–265, 1985.

[11] John C. Doyle. A review of μ for case studies in robust control. In *Proceedings of the IFAC World Congress*, 1987.

[12] John C. Doyle, Keith Glover, Pramod P. Khargonekar, and Bruce A. Francis. State-space solutions to standard H_2 and H_∞ control problems. *IEEE Transactions of Automatic Control*, 34(8), August 1989.

[13] Bruce A. Francis. *A Course in H_∞ Control Theory.* Springer-Verlag, 1987.

[14] A. Inoue. Structural properties of optimality base controller parametrizations. Master's thesis, Massachusetts Institute of Technology, 1990.

[15] Hiroaki Kuraoka, Naoto Ohka, Masahiro Ohba, Shigeyuki Hosoe, and Feifei Zhang. Application of h-infinity design to automotive fuel control. *IEEE Control Systems Magazine*, pages 102–105, April 1990.

[16] Norman A. Lehtomaki, Nils R. Sandell, Jr., and Michael Athans. Robustness results in linear-quadratic gaussian based multivariable control designs. *IEEE Transactions on Automatic Control*, 26(1), February 1981.

[17] Uy-Loi Ly. Robust control design using nonlinear constrained optimization. In *Proceedings of the American Control Conference*, 1990.

[18] J.M. Maciejowski. *Multivariable Feedback Design.* Addison-Wesley, 1989.

[19] Appasaheb N. Madiwale, Wassim M. Haddad, and Dennis S. Bernstein. Robust H_∞ control designs for systems with structured parametric uncertainty. *Systems and Control Letters*, 2(5):393–407, June 1989.

[20] K. D. Minto and J. H. Chow. *ISICLE Users Guide.* GE - CRD, 1988.

[21] K. Dean Minto, Joe H. Chow, and Jan Beseler. Lateral axis autopilot design for large transport aircraft: An explicit model matching approach. In *Proceedings of the American Control Conference*, 1989.

[22] Ihnseok Rhee and Jason L. Speyer. Application of a game theoretic controller to a benchmark problem. In *Proceedings of the American Control Conference*, 1990.

[23] Michael G. Safonov. Tight bounds on the response of multivariable systems with component uncertainty. In *Proceedings of the Sixteenth Allerton Conference*, 1978.

[24] Athanasios Sideris and Ricardo S. Sànchez Peña. Robustness margin calculation with dynamic and real parametric uncertainty. In *Proceedings of the American Control Conference*, pages 1201 – 1206, 1988.

[25] Bong Wie and Dennis S. Bernstein. A benchmark problem for robust control design. In *Proceedings of the American Control Conference*, 1990.

Appendix A

Derivation of Model-Matching Design Equations

The folowing is a derivation of the result given in 2.4.5 which sets up the model-matching least squares minimization. Since all of the transfer function matrices described in this appendix are expressed point-by-point in the frequency domain, over an approriate frequency range of $\omega_{min} \leq \omega \leq \omega_{max}$ where the transfer function matrices are non-singular, the inverses of any of the transfer function matrices are always available.

Given a plant, G, and a desired plant, H_d, it is desired to find the feedback path compensator, K, which minimizes the least squares error, ϵ, between the closed loop system, H, and H_d. H may be expressed as

$$H = (I + GK)^{-1}G \tag{A.1}$$

and ϵ is defined as

$$\epsilon \triangleq H_d - H. \tag{A.2}$$

This least squares minimization problem may be expressed as

$$\min_K \|H_d - H\|_2. \tag{A.3}$$

To accomplish the minimization it is desired to place equation A.3 in the form

$$\min_K \|Y - AKB\|_2. \tag{A.4}$$

To do so it is wished to convert equation A.2 to a form which can be placed in the minimization problem in equation A.4.

Then starting with equation A.2 the derivation proceeds as follows:

$$\begin{aligned}
\epsilon &= H_d - H && \text{(A.5)}\\
&= H_d - (I + GK)^{-1}G && \text{(A.6)}\\
&= (I + GK)^{-1}[(I + GK)H_d - G] && \text{(A.7)}\\
&= (I + GK)^{-1}[GK + (I - GH_d{}^{-1})]H_d && \text{(A.8)}\\
&= (I + GK)^{-1}GKH_d + (I + GK)^{-1}(I - GH_d{}^{-1})H_d && \text{(A.9)}\\
&= HKH_d + (I + GK)^{-1}(H_d - G) && \text{(A.10)}\\
&= HKH_d - H + (I + GK)^{-1}H_d && \text{(A.11)}\\
&= HKH_d - H + HG^{-1}H_d && \text{(A.12)}\\
&= HKH_d - H(I - G^{-1}H_d) && \text{(A.13)}\\
&= H(G^{-1}H_d - I) + HKH_d && \text{(A.14)}
\end{aligned}$$

This is now in the form of equation A.4 with

$$\begin{aligned}
Y &= H(G^{-1}H_d - I) && \text{(A.15)}\\
A &= -H && \text{(A.16)}\\
B &= H_d && \text{(A.17)}
\end{aligned}$$

This completes the derivation.

Appendix B

H_∞ Compensator State-Space Realizations

B.1 H_∞ Compensator State-Space Realizations for the Benchmark Problem: Design A

B.1.1 State-Space Realization of the H_∞ Compensator

$$
A_{K_\infty} = \begin{bmatrix}
-1.31 & 84.82 & -10.66 & -1.165 & 0 & 0 & 469.2 & 0 & 0 & 0 & 0 \\
-84.82 & -116.5 & 60.63 & 13.63 & 0 & 0 & 3827 & 0 & 0 & 0 & 0 \\
10.66 & 60.63 & -39.66 & -13.91 & 0 & 0 & -1371 & 0 & 0 & 0 & 0 \\
-1.165 & -13.63 & 13.91 & -9.153 & 0 & 0 & 214.8 & 0 & 0 & 0 & 0 \\
0 & 0 & 0 & 0 & 0 & 1 & 0 & 0 & 0 & 0 & 0 \\
-153 & -3964 & 801.6 & 385.8 & -88.1 & -19.05 & -6.935 & -209.9 & 1442 & 663.8 & 149.8 \\
0 & 0 & 0 & 0 & 0 & 0 & 0 & 1 & 0 & 0 & 0 \\
0 & 0 & 0 & 0 & 1 & 0 & -1 & 0 & 0 & 0 & 0 \\
0 & 0 & 0 & 0 & 0 & 0 & 0 & 0 & -0.01 & 0 & 0 \\
0 & 0 & 0 & 0 & 0 & 0 & 0 & 0 & 1 & 0 & 0 \\
0 & 0 & 0 & 0 & 0 & 0 & 0 & 0 & 0 & 1 & 0
\end{bmatrix}
$$

$$
B_{K_\infty} = \begin{bmatrix}
0 \\ 0 \\ 0 \\ 0 \\ 0 \\ 0 \\ 0 \\ 0 \\ 1 \\ 0 \\ 0
\end{bmatrix}
$$

$$
C_{K_\infty} = \begin{bmatrix} -622.2 & -137 & -569.2 & 171 & -87.1 & -19.05 & -7.935 & -209.9 & 1442 & 663.8 & 149.8 \end{bmatrix}
$$

$$
D_{K_\infty} = [0]
$$

B.1.2 State-Space Realization of the Reduced Order H_∞ Compensator

$$
\begin{aligned}
A_{K_\infty^{ro}} &= \begin{bmatrix} 0.1659 & -1.367 & 0.1354 & -1.196 \\ -0.1279 & 1.527 & -1.283 & 3.36 \\ -0.2791 & 5.559 & -26.21 & 9.089 \\ 0.4196 & 0.3891 & -28.05 & 4.699 \end{bmatrix} \\
B_{K_\infty^{ro}} &= \begin{bmatrix} -0.1579 \\ .02501 \\ -2.012 \\ 4.679 \end{bmatrix} \\
C_{K_\infty^{ro}} &= \begin{bmatrix} -2.21 & 69.78 & -404 & 133.9 \end{bmatrix} \\
D_{K_\infty^{ro}} &= [0]
\end{aligned}
$$

B.2 H_∞ Compensator State-Space Realizations for the Benchmark Problem: Design B

B.2.1 State-Space Realization of the H_∞ Compensator

$$A_{K_\infty} = \begin{bmatrix} -1.272 & 84.7 & -10.3 & -1.138 & 0 & 0 & 473.5 & 0 & 0 \\ -84.7 & -117 & 60.06 & 13.48 & 0 & 0 & 3935 & 0 & 0 \\ 10.3 & 60.06 & -39.04 & -13.71 & 0 & 0 & -1384 & 0 & 0 \\ -1.138 & -13.48 & 13.71 & -9.334 & 0 & 0 & 217.9 & 0 & 0 \\ 0 & 0 & 0 & 0 & 0 & 1 & 0 & 0 & 0 \\ -204.9 & -4053 & 839.2 & 337.8 & -125.8 & -19.56 & 2415 & -223.1 & 576.3 \\ 0 & 0 & 0 & 0 & 0 & 0 & 0 & 1 & 0 \\ 0 & 0 & 0 & 0 & 1 & 0 & -1 & 0 & 0 \\ 0 & 0 & 0 & 0 & 0 & 0 & 0 & 0 & -1.0 \times 10^{-06} \end{bmatrix}$$

$$B_{K_\infty} = \begin{bmatrix} 0 \\ 0 \\ 0 \\ 0 \\ 0 \\ 0 \\ 0 \\ 0 \\ 1 \end{bmatrix}$$

$$C_{K_\infty} = \begin{bmatrix} -678.4 & -117.5 & -545.1 & 119.9 & -124.8 & -19.56 & 2414 & -223.1 & 576.3 \end{bmatrix}$$

$$D_{K_\infty} = [0]$$

B.2.2 State-Space Realization of the Reduced Order H_∞ Compensator

$$A_{K_\infty^{ro}} = \begin{bmatrix} -11.52 & 7.671 & 0.7173 & -1.495 & -3.391 & -6.23 \\ -4.302 & 1.999 & 2.105 & 0.2834 & 1.079 & 1.83 \\ 10.06 & -3.887 & -12.11 & -3.346 & -14.03 & -24.89 \\ 10.93 & 9.338 & 0.116 & -2.4 & 15.25 & 29.69 \\ 7.699 & -18.07 & 7.619 & 11.23 & -12.08 & -8.995 \\ -2.919 & 13.93 & -5.523 & -8.321 & 11.29 & 1.981 \end{bmatrix}$$

$$B_{K_\infty^{ro}} = \begin{bmatrix} 0.2078 \\ -0.966 \\ -0.1515 \\ -0.02466 \\ 0.05578 \\ -0.05424 \end{bmatrix}$$

$$C_{K_\infty^{ro}} = \begin{bmatrix} 939.2 & -334.5 & -376.7 & -51.17 & -79.67 & -75.3 \end{bmatrix}$$

$$D_{K_\infty^{ro}} = [0]$$

B.3 H_∞ Compensator State-Space Realizations for the MIMO MSD Problem

B.3.1 State-Space Realization of the H_∞ Compensator

$$A_{K_\infty} =$$

$$\begin{bmatrix}
-196.8 & 94.8 & 21.02 & -.00039124 & -1.224 & 0 & \cdots \\
-94.8 & -25.28 & -16.69 & 3.967\times10^{-6} & -1.4 & 0 & \cdots \\
21.02 & 16.69 & -27.92 & -.0007111 & 0.6826 & 0 & \cdots \\
-.0003935 & -3.985\times10^{-6} & -.0007151 & -100 & 164.3 & 0 & \cdots \\
0 & 0 & 0 & 0 & 0 & 0 & \cdots \\
0 & 0 & 0 & 0 & 0 & 0 & \cdots \\
0 & 0 & 0 & 0 & 0 & 0 & \cdots \\
-574.4 & -632.1 & 277.6 & 130.4 & -292.5 & -10.55 & \cdots \\
23941 & -16040 & 2638 & -6.96 & 183.6 & -167.9 & \cdots \\
0 & 0 & 0 & 0 & 1 & 1 & \cdots \\
0 & 0 & 0 & 0 & 0 & 0 & \cdots \\
0 & 0 & 0 & 0 & 0 & 0 & \cdots
\end{bmatrix}$$

$$\begin{bmatrix}
\cdots & 33049 & 0 & 0 & 0 & 0 & 0 \\
\cdots & 5951 & 0 & 0 & 0 & 0 & 0 \\
\cdots & -1802 & 0 & 0 & 0 & 0 & 0 \\
\cdots & 0.03912 & 0 & 0 & 0 & 0 & 0 \\
\cdots & 0 & 1 & 0 & 0 & 0 & 0 \\
\cdots & 0 & 0 & 1 & 0 & 0 & 0 \\
\cdots & 0 & 0 & 0 & 1 & 0 & 0 \\
\cdots & 344.6 & -25.81 & -5.442 & -23.47 & 45.05 & 269.5 \\
\cdots & -4265700 & -5.442 & -86.53 & -391.2 & -306.3 & 4228 \\
\cdots & -3 & 0 & 0 & -0.002 & 0 & 0 \\
\cdots & 0 & 0 & 0 & 0 & -1.0\times10^{-6} & 0 \\
\cdots & 0 & 0 & 0 & 0 & 0 & -1.0\times10^{-6}
\end{bmatrix}$$

$$B_{K_\infty} = \begin{bmatrix}
0 & 0 \\ 0 & 0 \\ 0 & 0 \\ 0 & 0 \\ 0 & 0 \\ 0 & 0 \\ 0 & 0 \\ 0 & 0 \\ 0 & 0 \\ 0 & 0 \\ 0 & 0 \\ 1 & 0 \\ 0 & 1
\end{bmatrix}$$

$$C_{K_\infty} = \begin{bmatrix}
-573.2 & -633.5 & 276.9 & -33.85 & -20.56 & -11.55 & 13.32 & -25.81 & -5.444 & \cdots \\
-9108 & -10089 & 4439 & -6.999 & -149.5 & -164.9 & -279 & -5.444 & -86.52 & \cdots
\end{bmatrix}$$

$$\begin{bmatrix}
\cdots & -23.47 & 45.05 & 269.5 \\
\cdots & -391.2 & -306.3 & 4228
\end{bmatrix}$$

$$D_{K_\infty} = \begin{bmatrix}
0 & 0 \\ 0 & 0
\end{bmatrix}$$

B.3.2 State-Space Realization of the Reduced Order H_∞ Compensator

$$A_{K_\infty^{ro}} =$$

$$\begin{bmatrix}
-1.0\times10^{-6} & 4.128\times10^{-12} & 4.161\times10^{-5} & 2.377\times10^{-7} & 2.970\times10^{-6} & 3.376\times10^{-6} & -4.919\times10^{-7} \\
5.852\times10^{-12} & -1.0000\times10^{-6} & -5.744\times10^{-5} & 7.807\times10^{-7} & -6.957\times10^{-6} & 1.232\times10^{-5} & -7.726\times10^{-7} \\
4.315\times10^{-5} & -4.966\times10^{-5} & -85.76 & -14.21 & -12.31 & -0.7097 & 0.7907 \\
-6.446\times10^{-7} & 3.033\times10^{-7} & 15.47 & -0.01706 & 0.03305 & -0.3324 & 0.02863 \\
3.805\times10^{-6} & -4.1178\times10^{-6} & -12.83 & 0.2044 & -3.824 & 0.7621 & 0.05705 \\
-8.869\times10^{-7} & 1.4234\times10^{-5} & 13.56 & -0.09500 & 6.429 & -27.83 & 6.836 \\
-4.023\times10^{-7} & 1.019\times10^{-6} & 2.002 & -0.02563 & 1.017 & -6.504 & -0.7726
\end{bmatrix}$$

$$B_{K_\infty^{ro}} = \begin{bmatrix}
-1.408 & 2.254 \\
-1.038 & -0.6481 \\
4.608 & -64.72 \\
-0.2963 & 0.8256 \\
0.5415 & -5.622 \\
6.762 & 5.609 \\
0.2454 & 0.7823
\end{bmatrix}$$

$$C_{K_\infty^{ro}} = \begin{bmatrix}
-1.245 & -1.081 & -3.288 & 0.8826 & -1.639 & 8.775 & -0.7411 \\
2.348 & -0.573 & -64.81 & 0.02983 & -5.406 & -0.4239 & 0.3506
\end{bmatrix}$$

$$D_{K_\infty^{ro}} = \begin{bmatrix}
0 & 0 \\
0 & 0
\end{bmatrix}$$

Appendix C

Benchmark Example: Design A Reduced Order System Time and Frequency Response

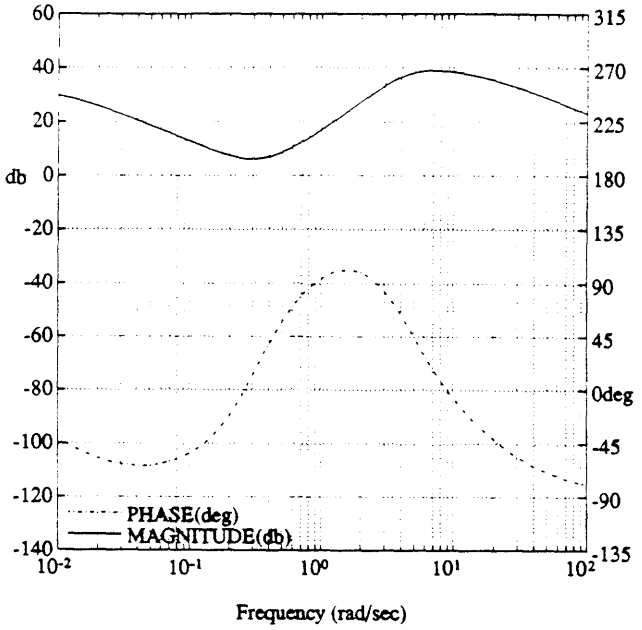

Figure C.1: Bode Plot of the H_∞ Compensator

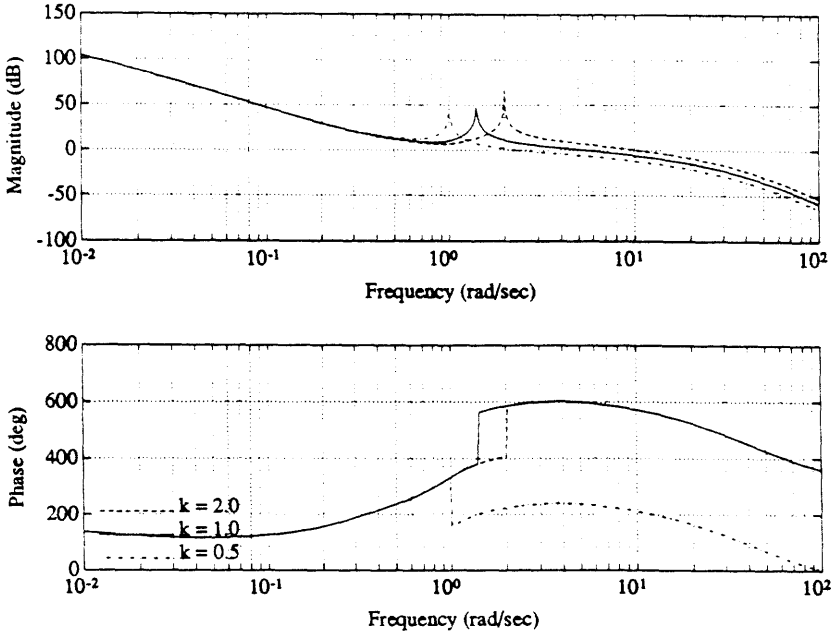

Figure C.2: Bode Plot of the Open Loop System $G(K_{inner} + K_\infty)$ for $k = 0.5, 1.0, 2.0$

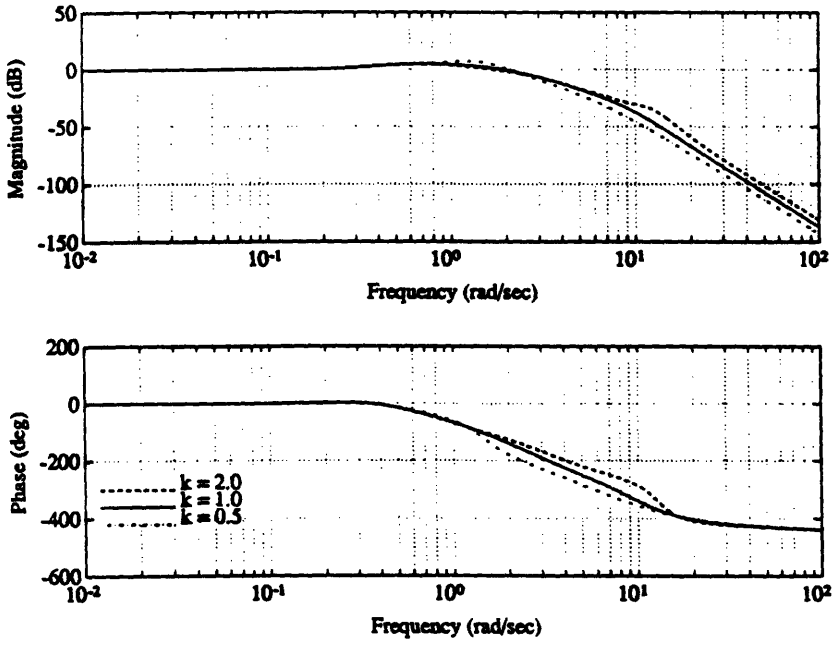

Figure C.3: Bode Plot of the Closed Loop System $T(s)$ for $k = 0.5,\ 1.0,\ 2.0$

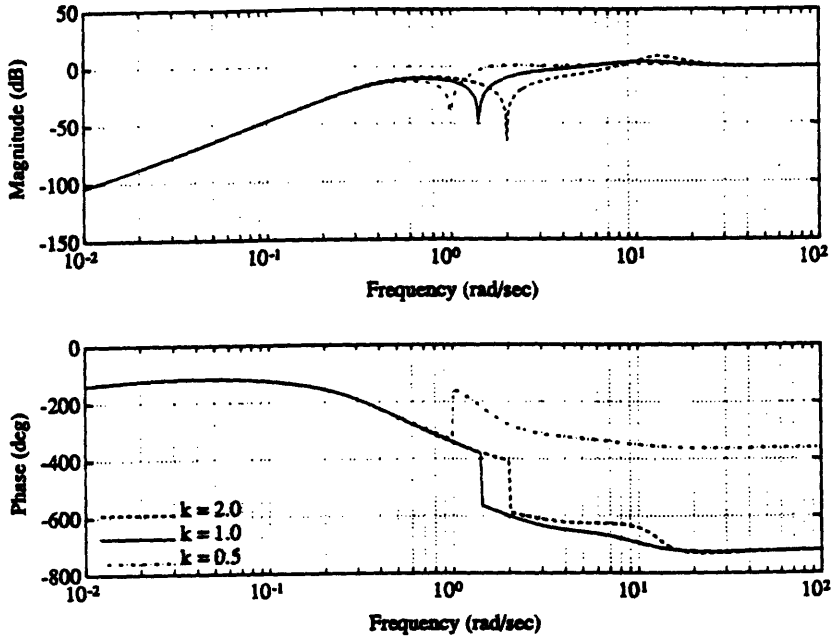

Figure C.4: Bode Plot of the Sensitivity Transfer Function $S(s)$ for $k = 0.5,\ 1.0,\ 2.0$

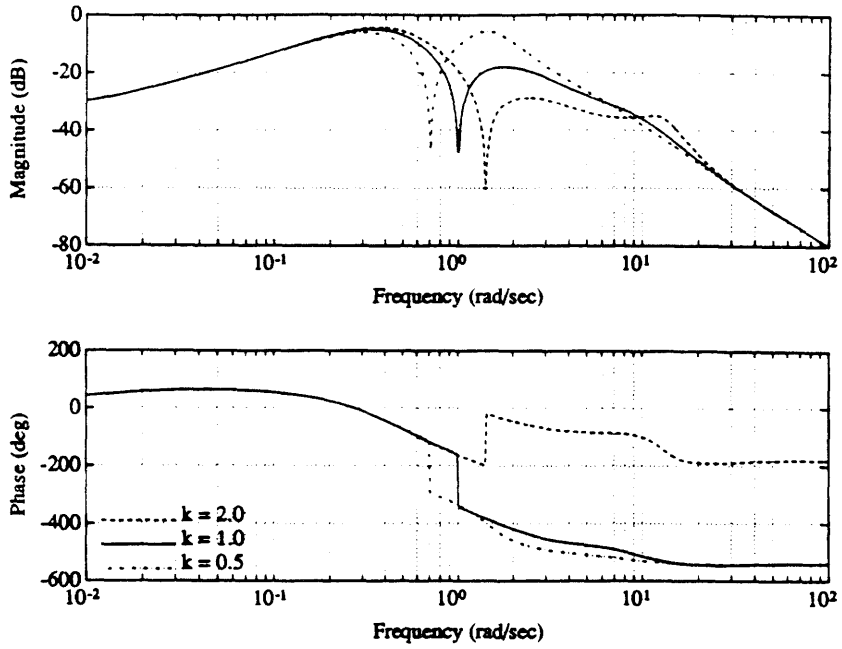

Figure C.5: Bode Plot of the Transfer Function from w to z for k = 0.5, 1.0, 2.0

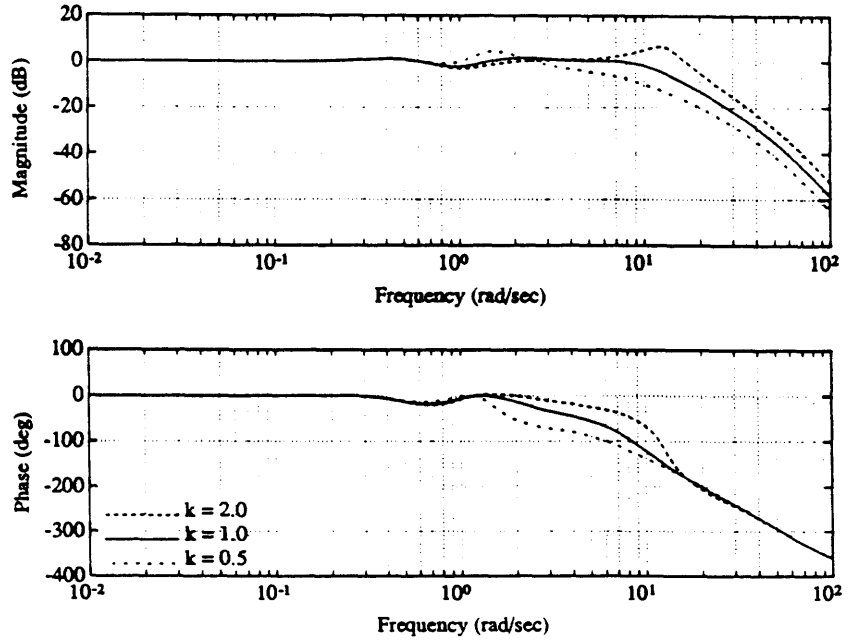

Figure C.6: Bode Plot of the Transfer Function, $N(s)$, for k = 0.5, 1.0, 2.0

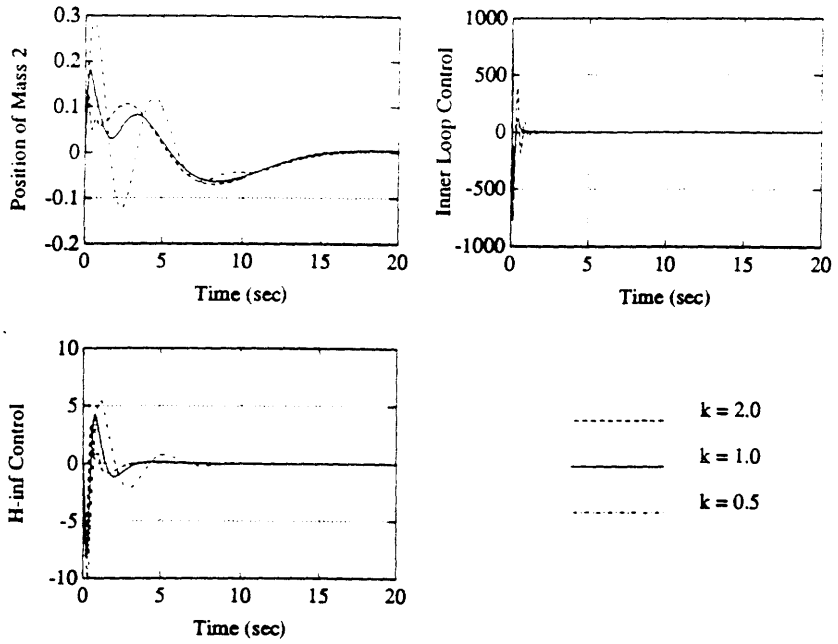

Figure C.7: Closed Loop System Response to a Unit Impulse Disturbance

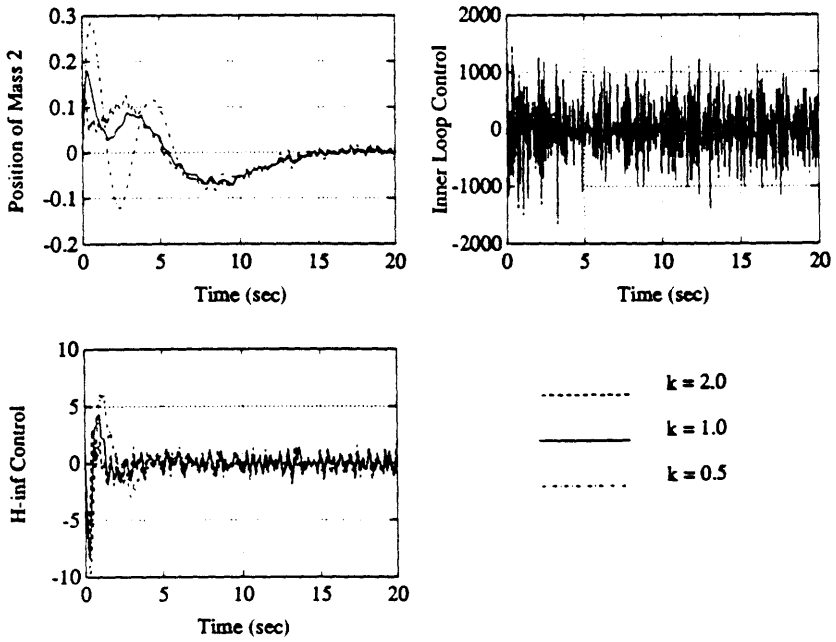

Figure C.8: Closed Loop System Response with Measurement Noise to a Unit Impulse Disturbance

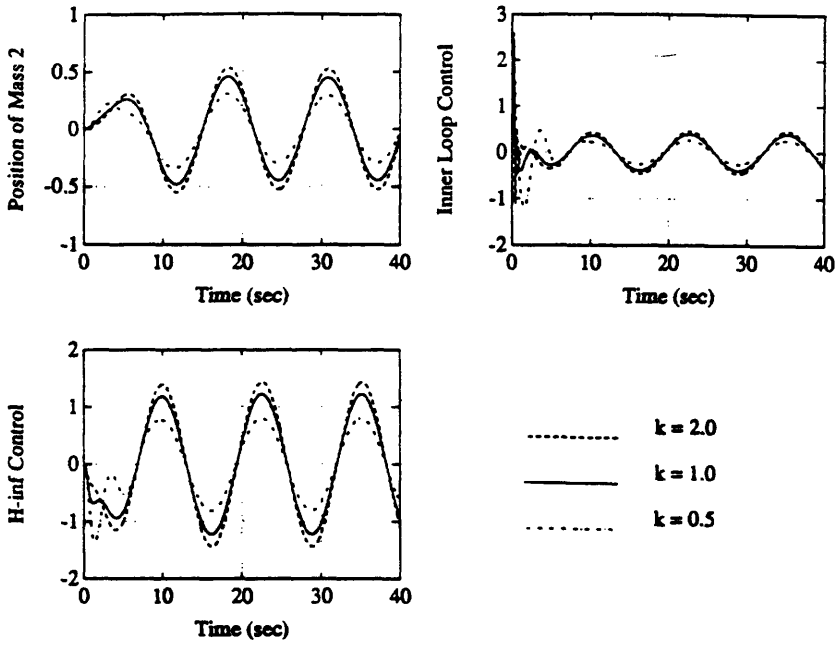

Figure C.9: Closed Loop System Response to a Sinusoidal Disturbance

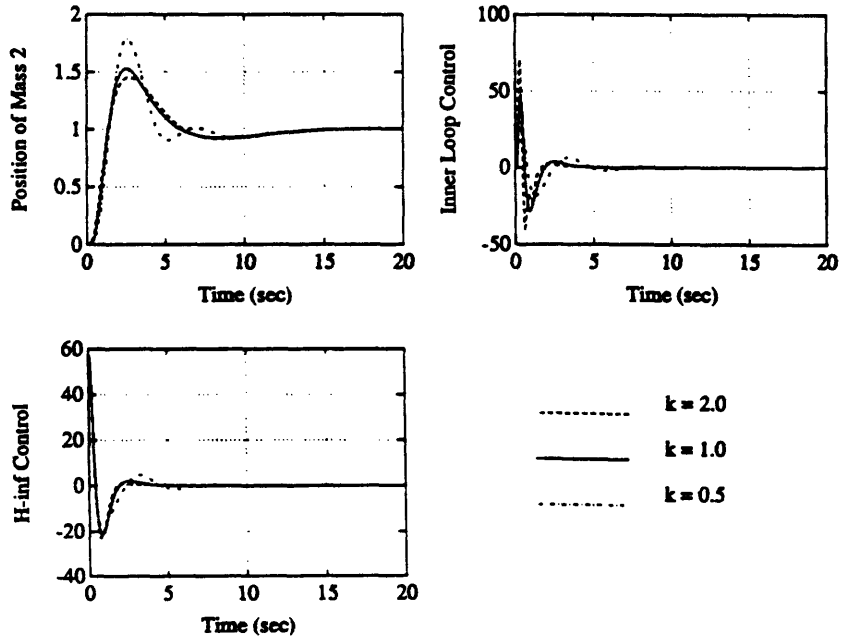

Figure C.10: Closed Loop System Response to a Unit Step in the Reference

Appendix D

Benchmark Example: Design B Reduced Order System Time and Frequency Response

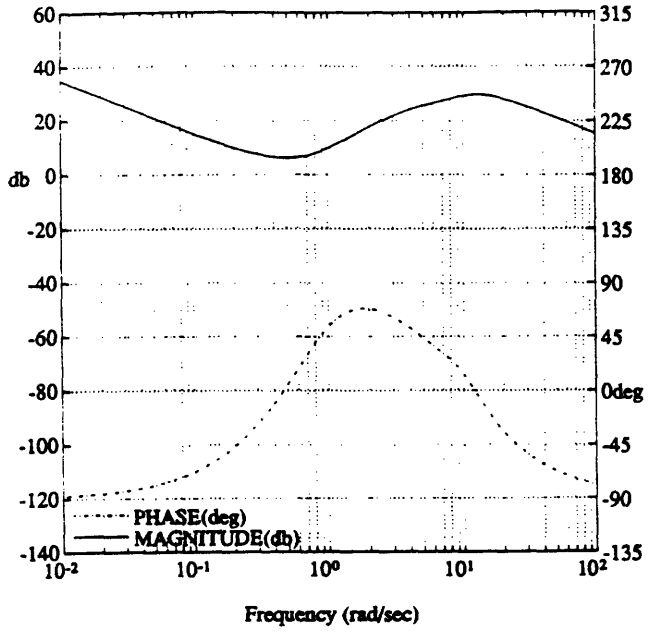

Figure D.1: Bode Plot of the H_∞ Compensator

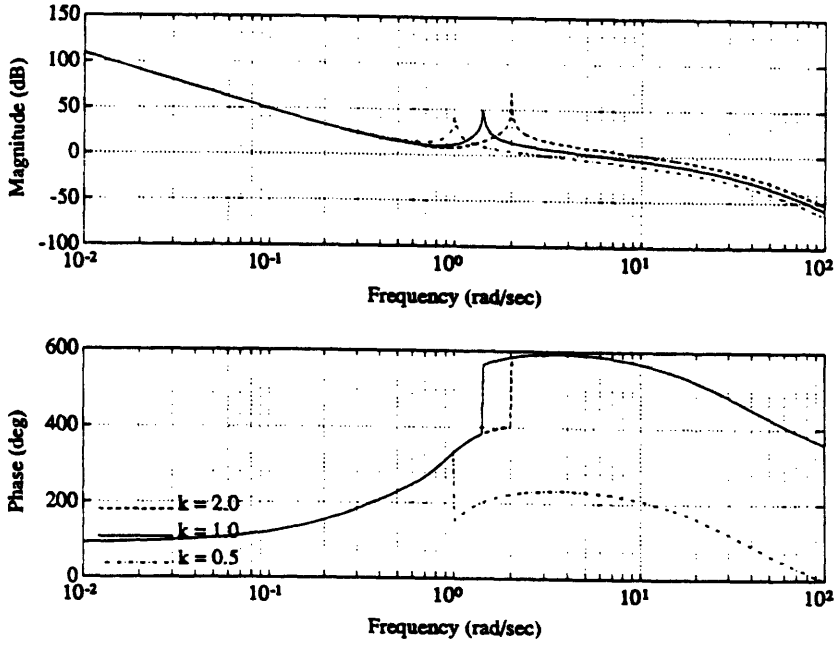

Figure D.2: Bode Plot of the Open Loop System $G(K_{inner} + K_\infty)$ for $k = 0.5, 1.0, 2.0$

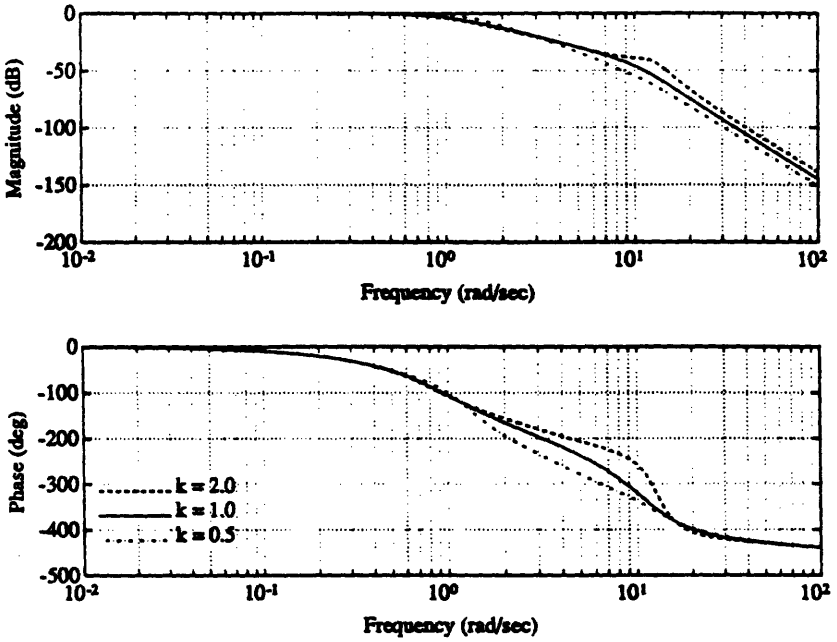

Figure D.3: Bode Plot of the Closed Loop System $T(s)$ for $k = 0.5,\ 1.0,\ 2.0$

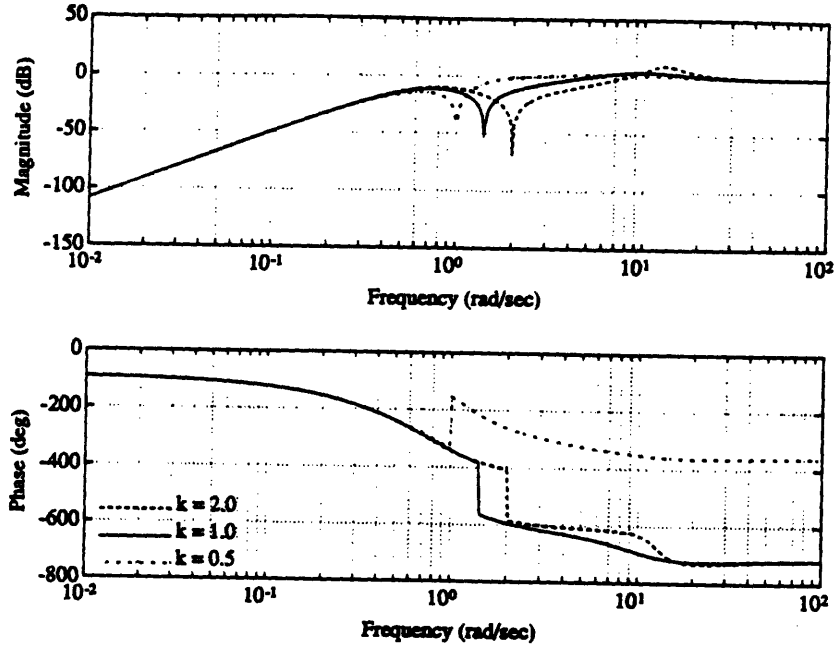

Figure D.4: Bode Plot of the Sensitivity Transfer Function $S(s)$ for $k = 0.5,\ 1.0,\ 2.0$

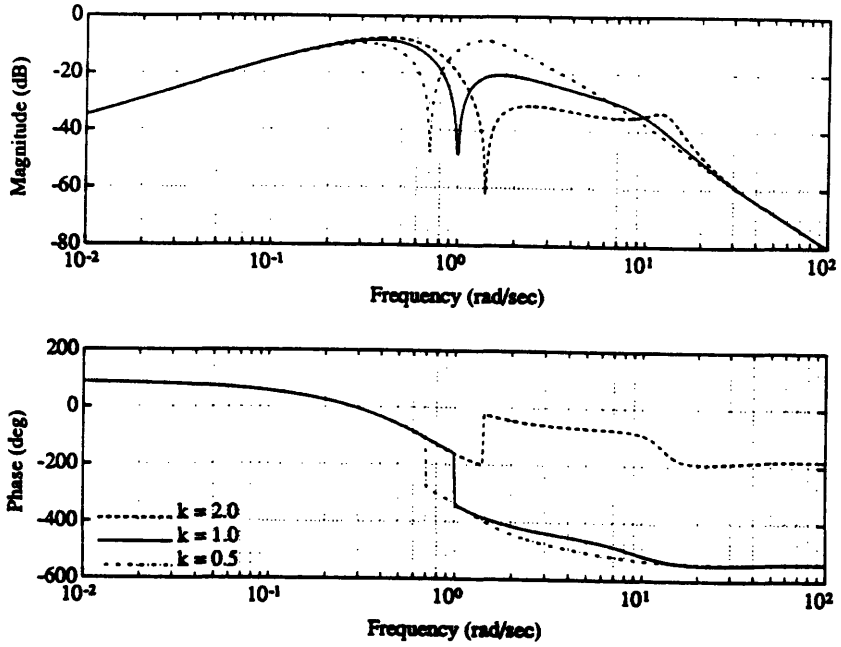

Figure D.5: Bode Plot of the Transfer Function from w to z for k = 0.5, 1.0, 2.0

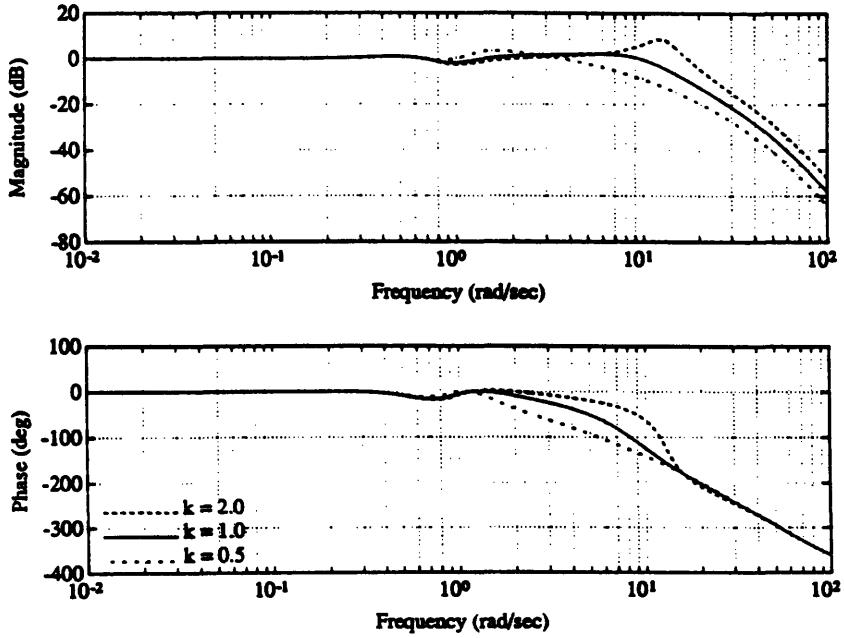

Figure D.6: Bode Plot of the Transfer Function, $N(s)$, for $k = 0.5,\ 1.0,\ 2.0$

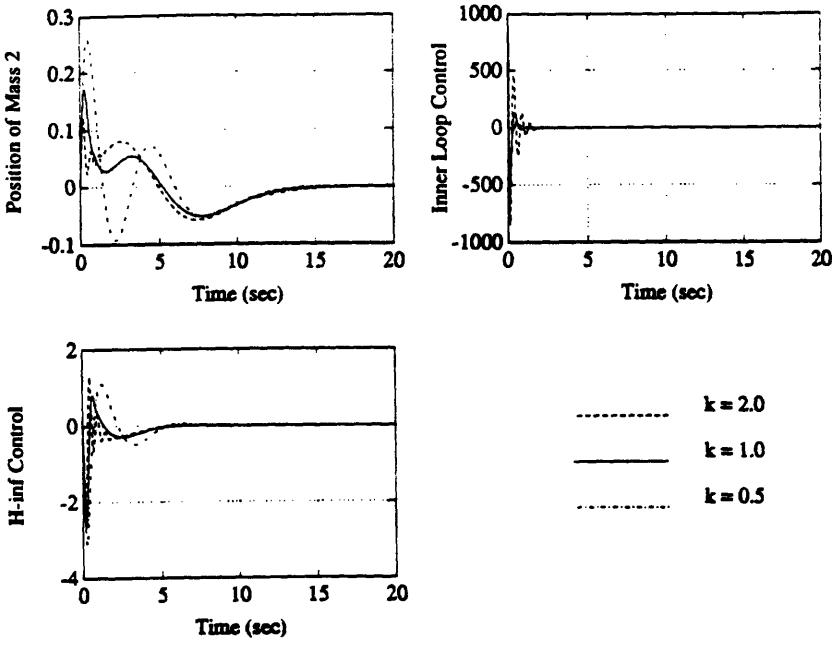

Figure D.7: Closed Loop System Response to a Unit Impulse Disturbance

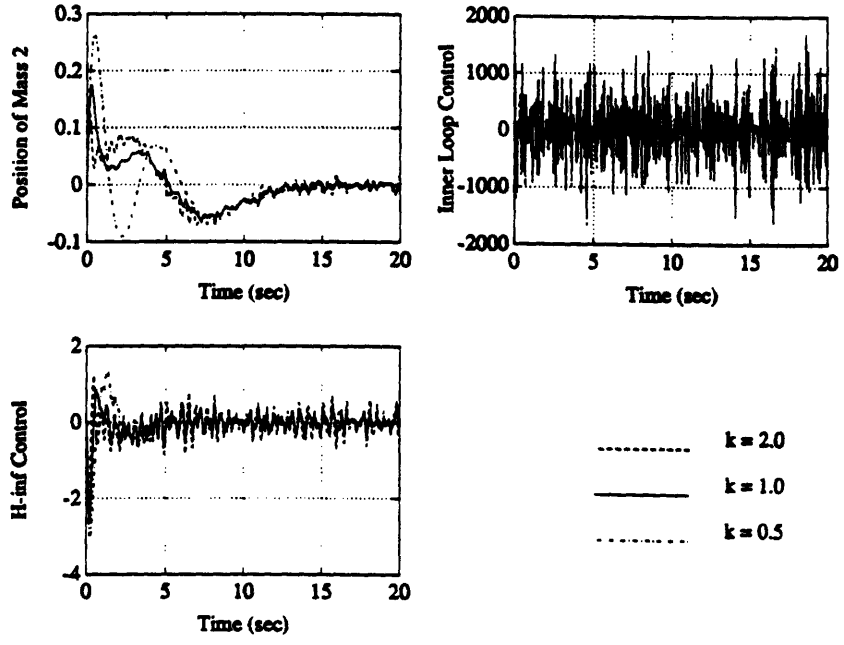

Figure D.8: Closed Loop System Response with Measurement Noise to a Unit Impulse Disturbance

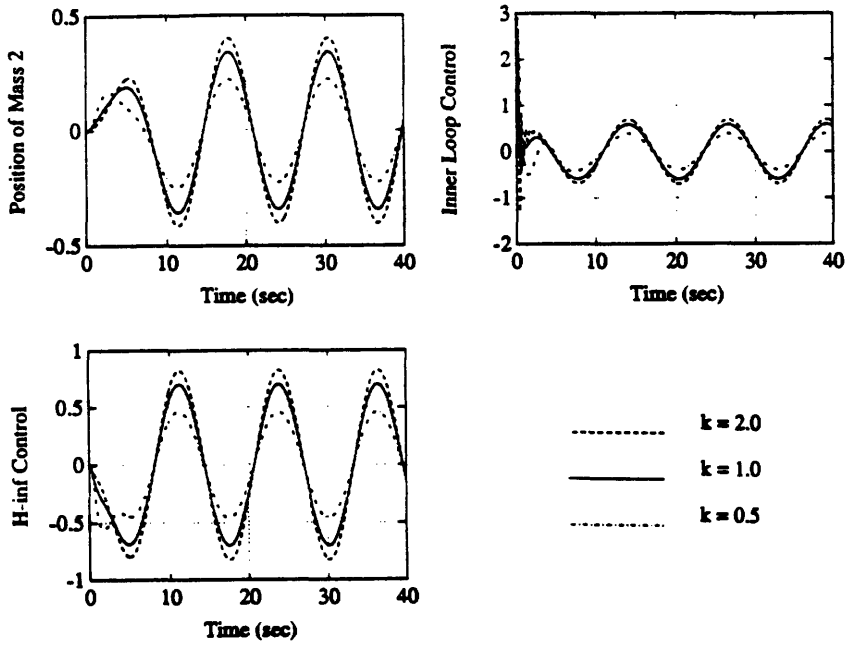

Figure D.9: Closed Loop System Response to a Sinusoidal Disturbance

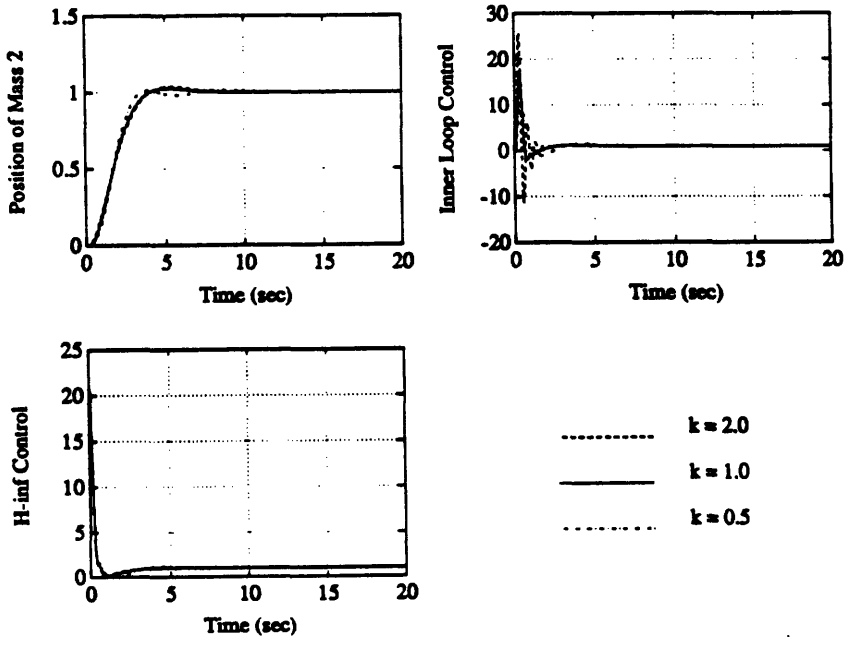

Figure D.10: Closed Loop System Response to a Unit Step in the Reference

Appendix E

MIMO Example Reduced Order System Time and Frequency Response

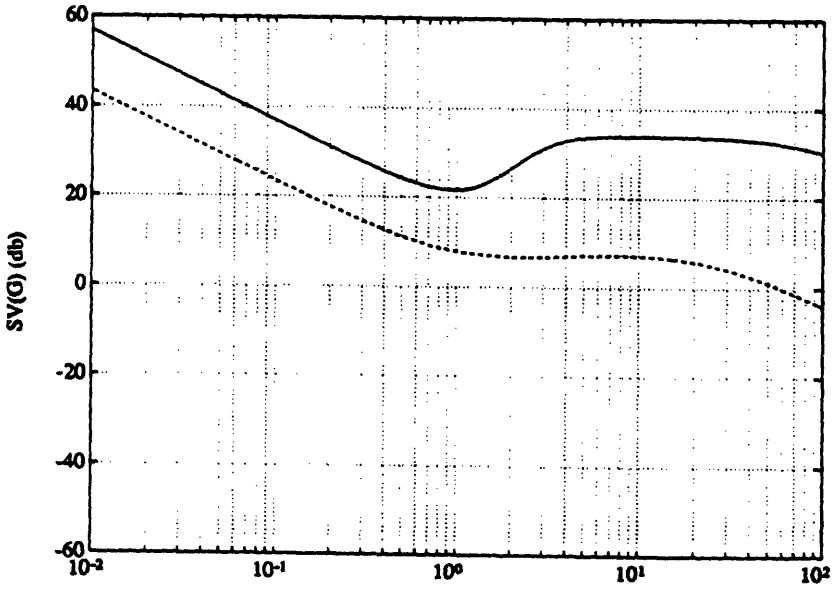

Figure E.1: Singular Value Plot of the H_∞ Compensator

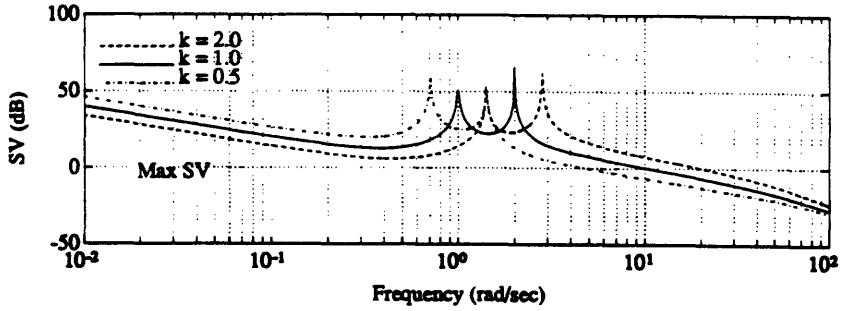

Figure E.2: Singular Value Plot of the Open Loop Servo Transfer Function for $k = 0.5$

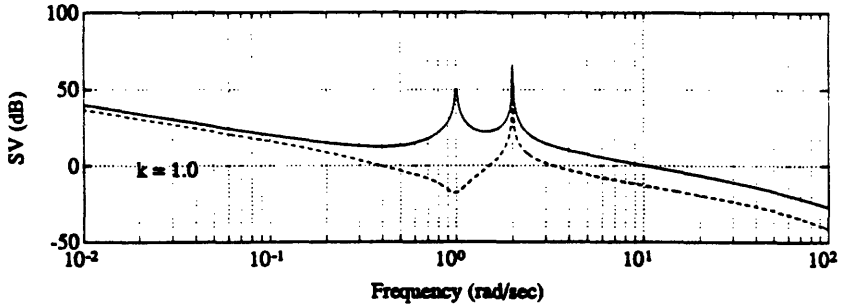

Figure E.3: Singular Value Plot of the Open Loop Servo Transfer Function for $k = 1.0$

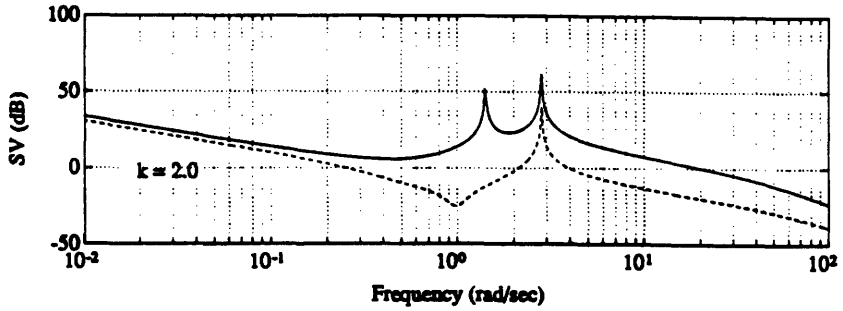

Figure E.4: Singular Value Plot of the Open Loop Servo Transfer Function for $k = 2.0$

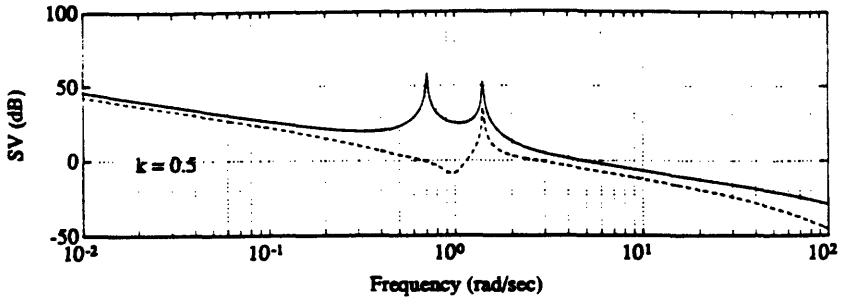

Figure E.5: Maximum Singular Values of the Open Loop Servo Transfer Functions

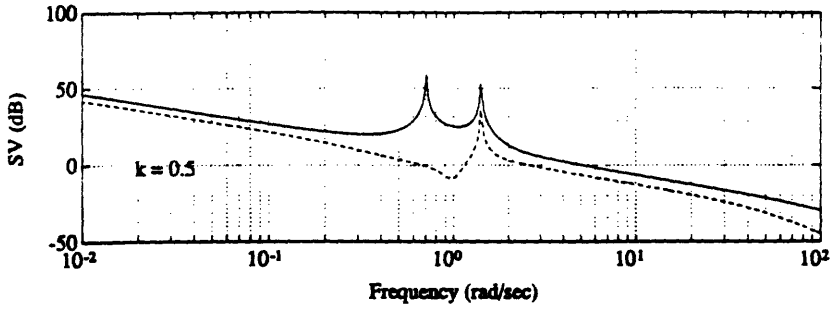

Figure E.6: Singular Value Plot of the Open Loop Regulator Transfer Function for $k = 0.5$

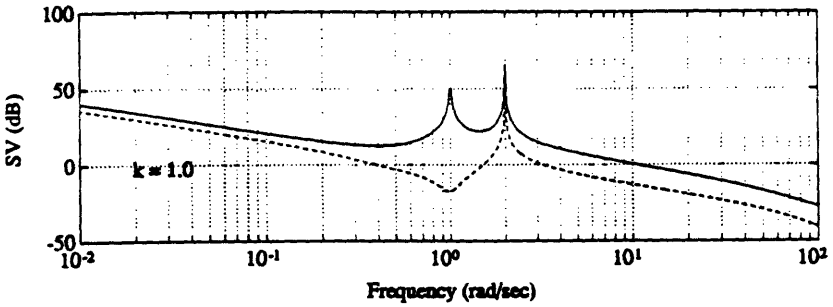

Figure E.7: Singular Value Plot of the Open Loop Regulator Transfer Function for $k = 1.0$

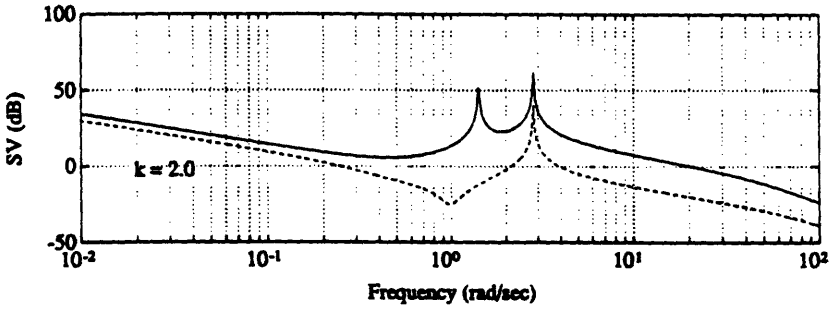

Figure E.8: Singular Value Plot of the Open Loop Regulator Transfer Function for $k = 2.0$

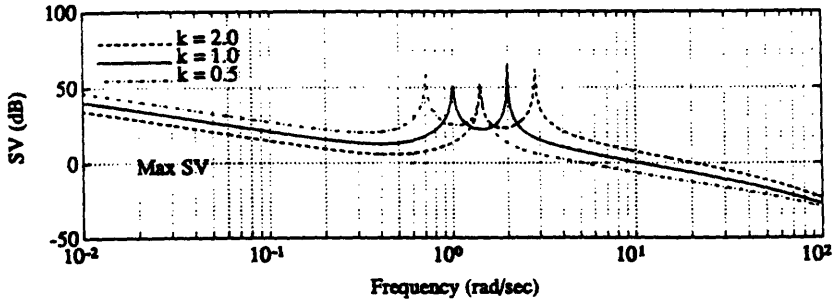

Figure E.9: Maximum Singular Values of the Open Loop Regulator Transfer Functions

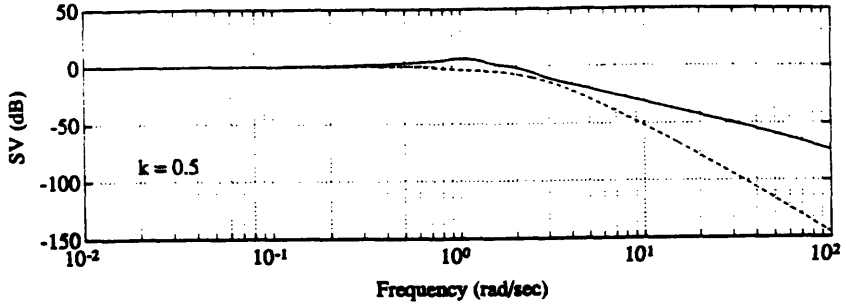

Figure E.10: Singular Value Plot of the Closed Loop Transfer Function for $k = 0.5$

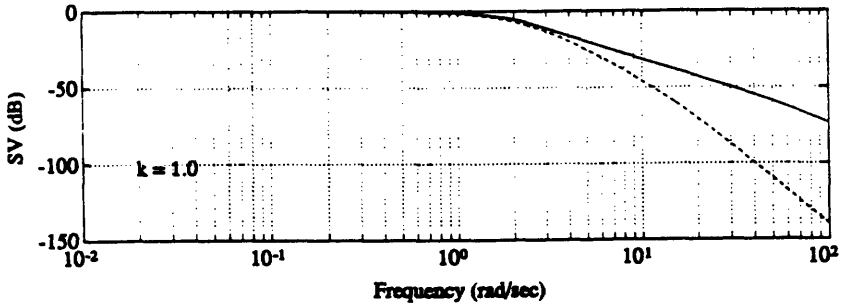

Figure E.11: Singular Value Plot of the Closed Loop Transfer Function for $k = 1.0$

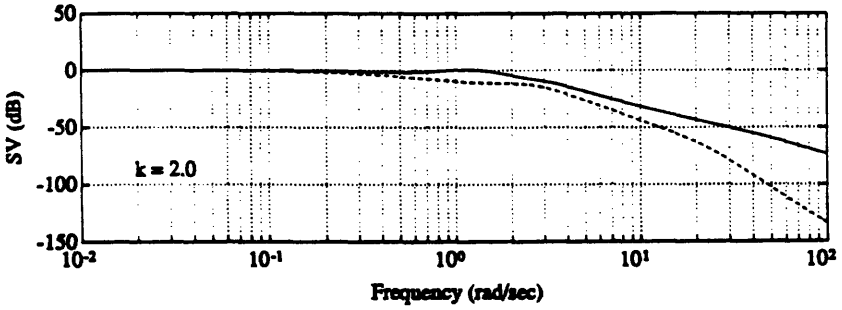

Figure E.12: Singular Value Plot of the Closed Loop Transfer Function for $k = 2.0$

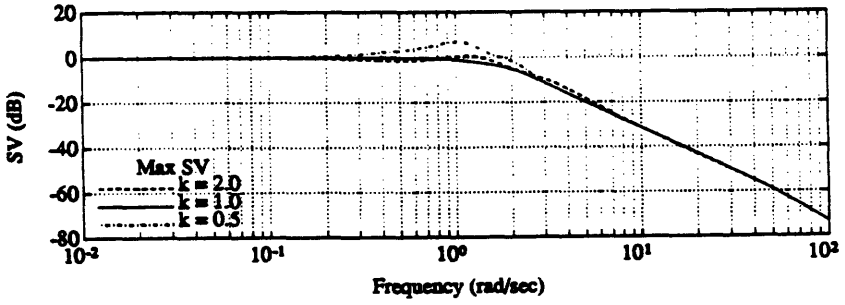

Figure E.13: Maximum Singular Values of the Closed Loop Transfer Function

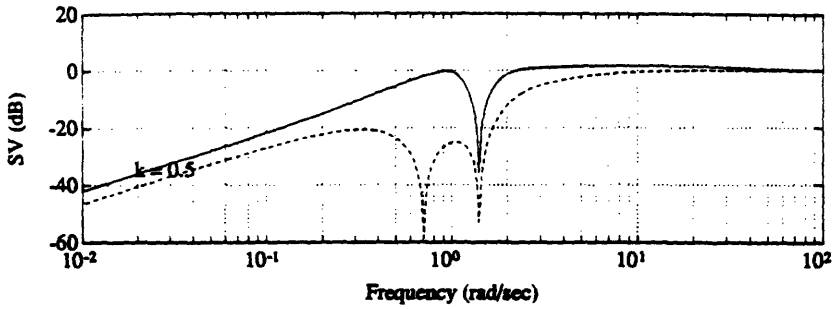

Figure E.14: Singular Value Plot of the Sensitivity Transfer Function for $k = 0.5$

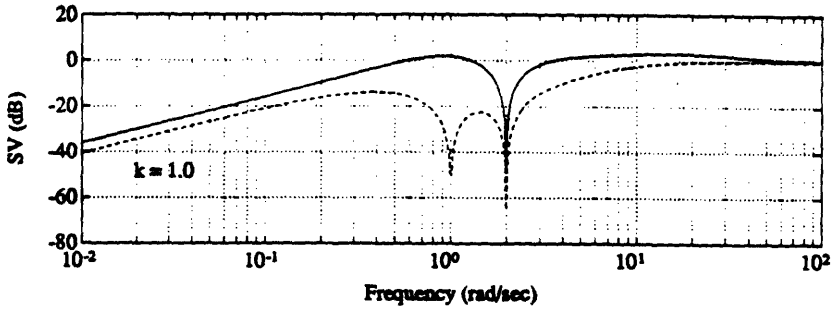

Figure E.15: Singular Value Plot of the Sensitivity Transfer Function for $k = 1.0$

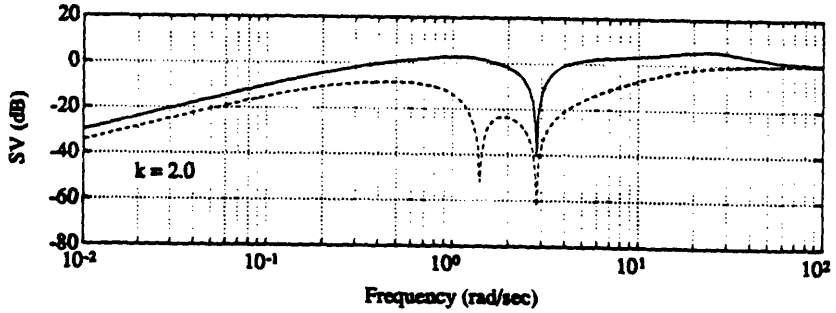

Figure E.16: Singular Value Plot of the Sensitivity Transfer Function for $k = 2.0$

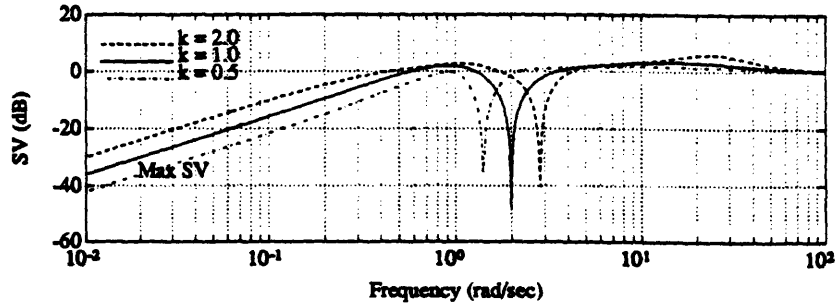

Figure E.17: Maximum Singular Values of the Sensitivity Transfer Functions

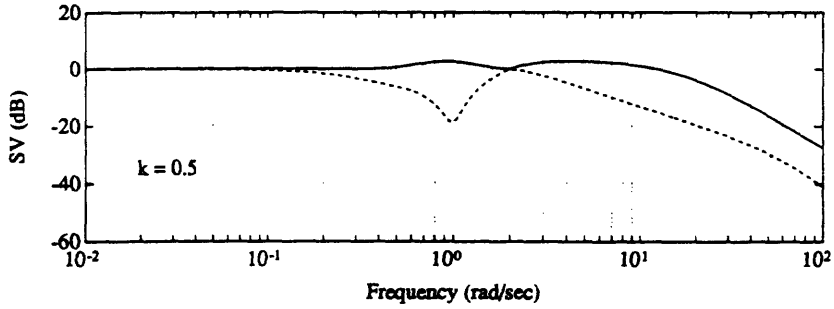

Figure E.18: Singular Value Plot of the Transfer Function, $N(s)$ for $k = 0.5$

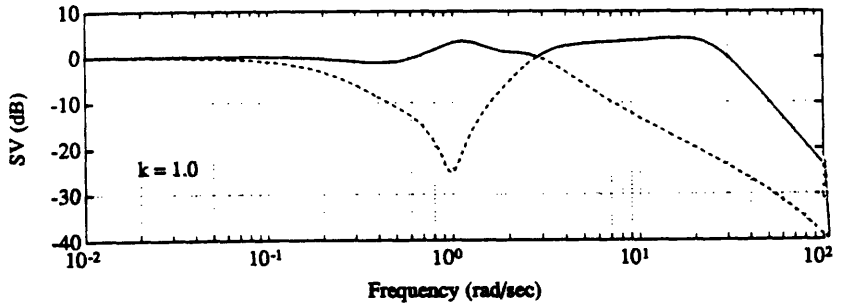

Figure E.19: Singular Value Plot of the Transfer Function, $N(s)$ for $k = 1.0$

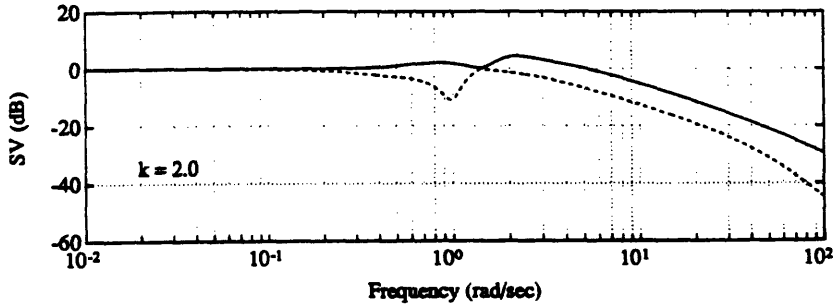

Figure E.20: Singular Value Plot of the Transfer Function, $N(s)$ for $k = 2.0$

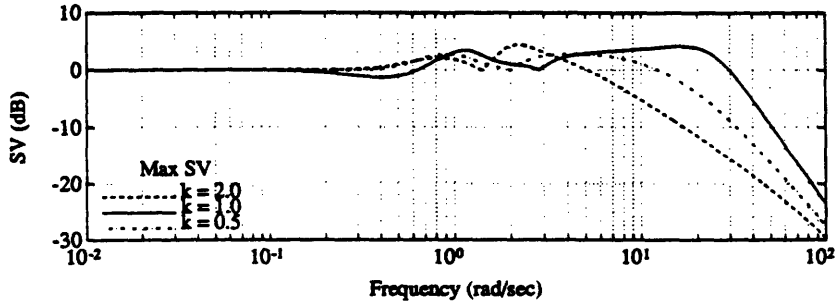

Figure E.21: Maximum Singular Values of the Transfer Functions, $N(s)$

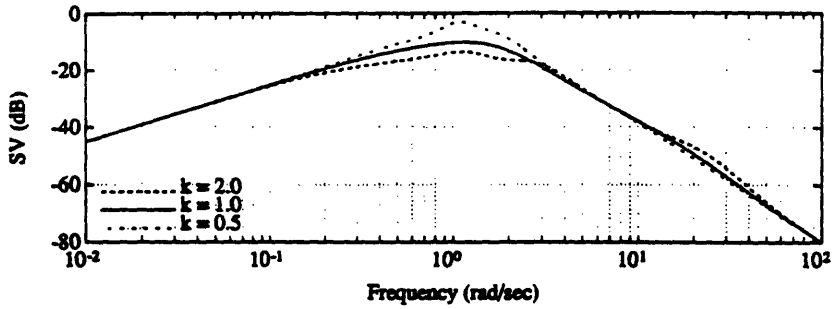

Figure E.22: Singular Values of the Transfer Function from Disturbance to Output for $k = 0.5$, 1.0, 2.0

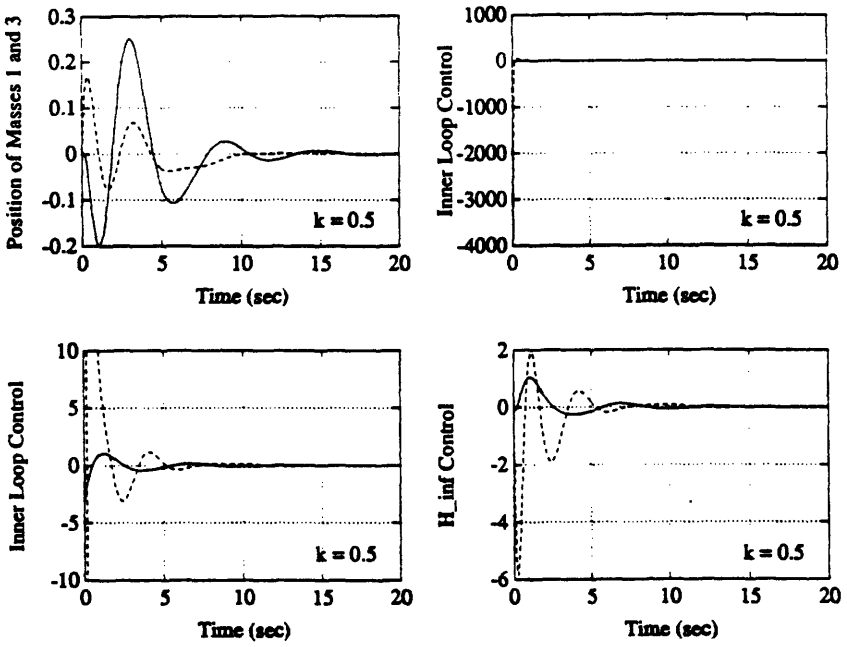

Figure E.23: Closed Loop System Response to an Impulse Disturbance for $k = 0.5$

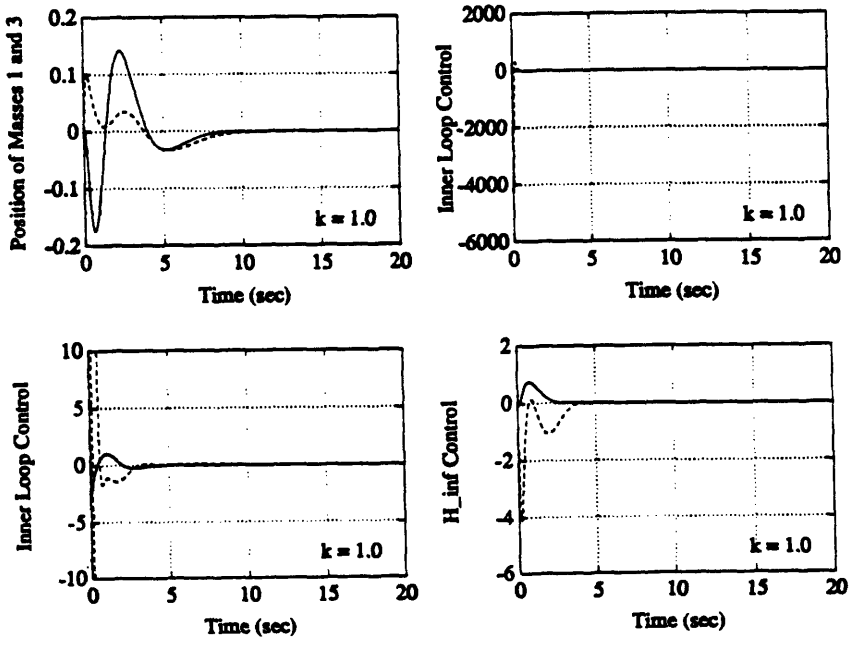

Figure E.24: Closed Loop System Response to an Impulse Disturbance for $k = 1.0$

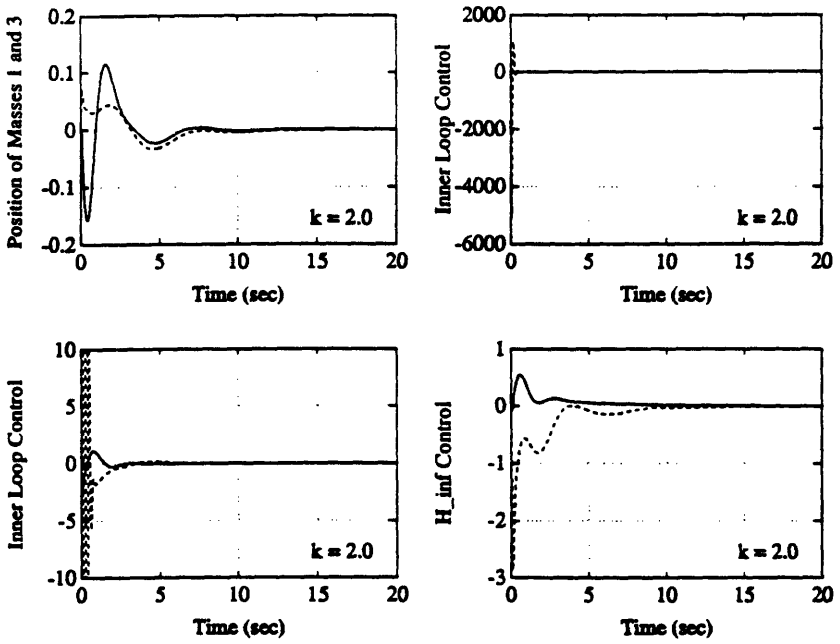

Figure E.25: Closed Loop System Response to an Impulse Disturbance for $k = 2.0$

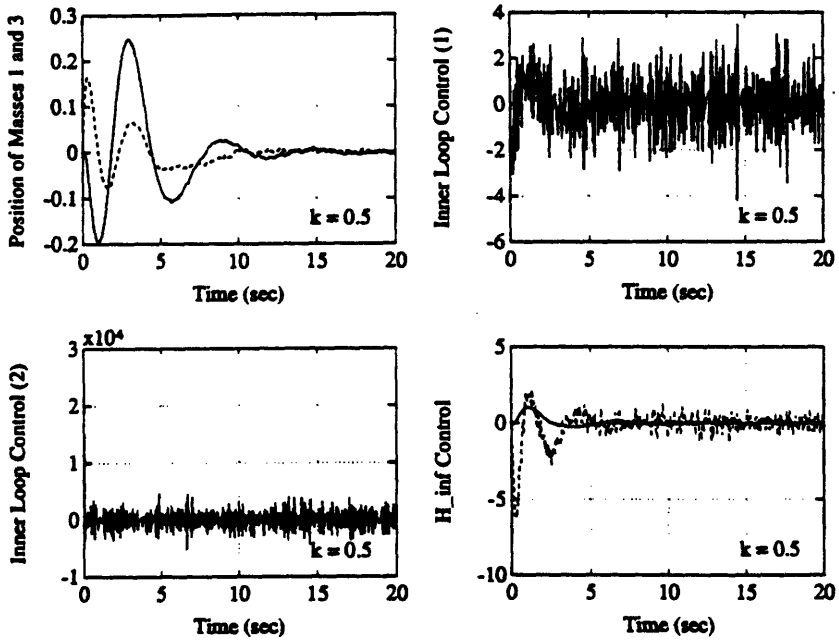

Figure E.26: Closed Loop System Response to an Impulse Disturbance with Measurement Noise for $k = 0.5$

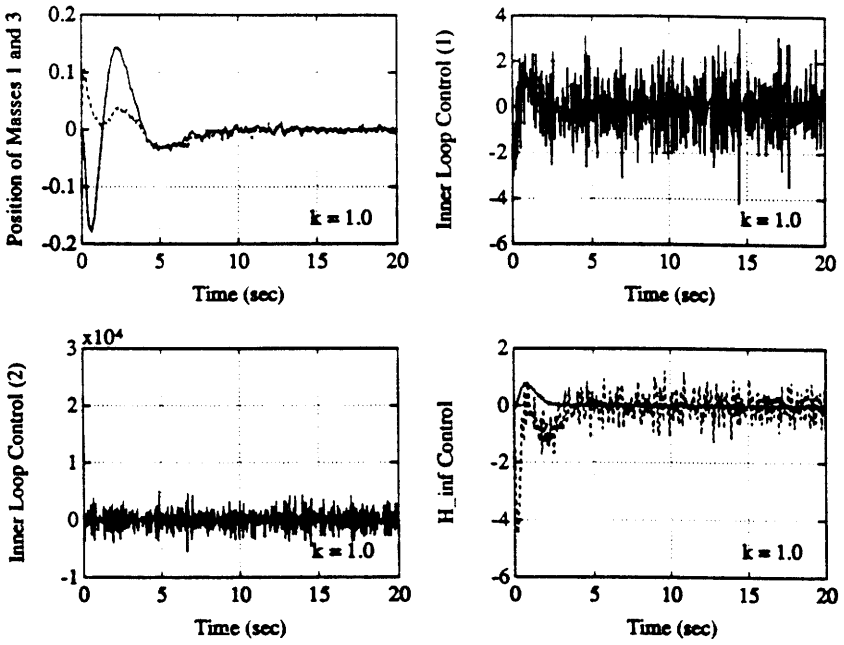

Figure E.27: Closed Loop System Response to an Impulse Disturbance with Measurement Noise for $k = 1.0$

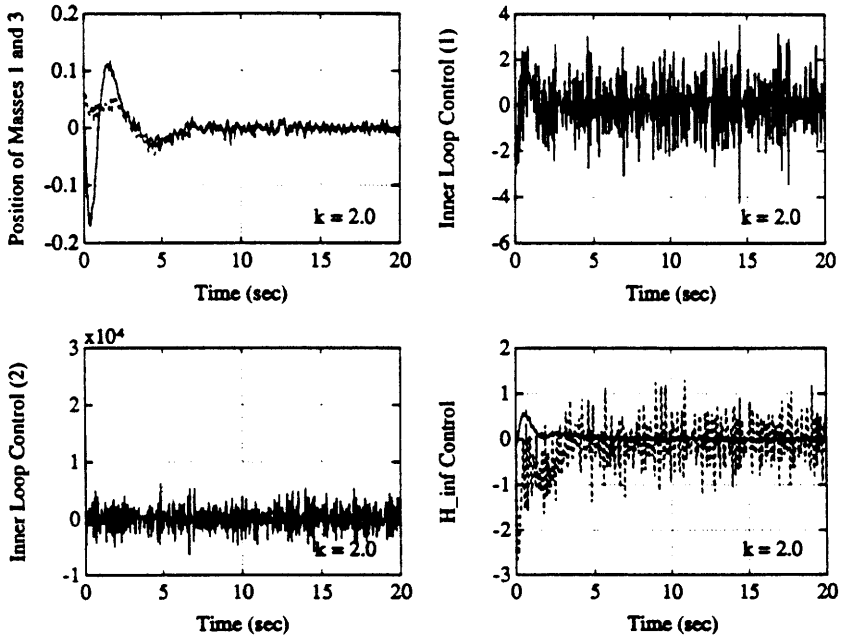

Figure E.28: Closed Loop System Response to an Impulse Disturbance with Measurement Noise for $k = 2.0$

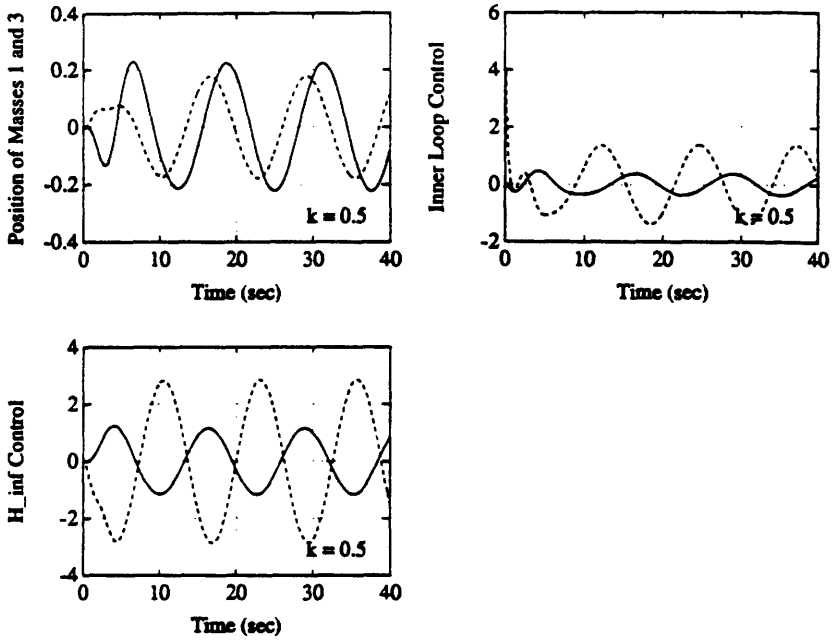

Figure E.29: Closed Loop System Response to a Sinusoidal Disturbance for $k = 0.5$

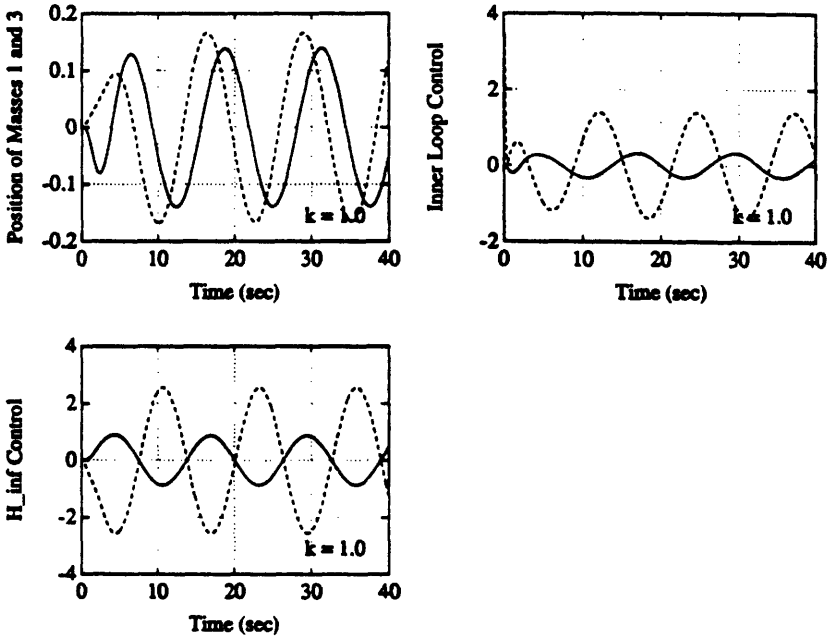

Figure E.30: Closed Loop System Response to a Sinusoidal Disturbance for $k = 1.0$

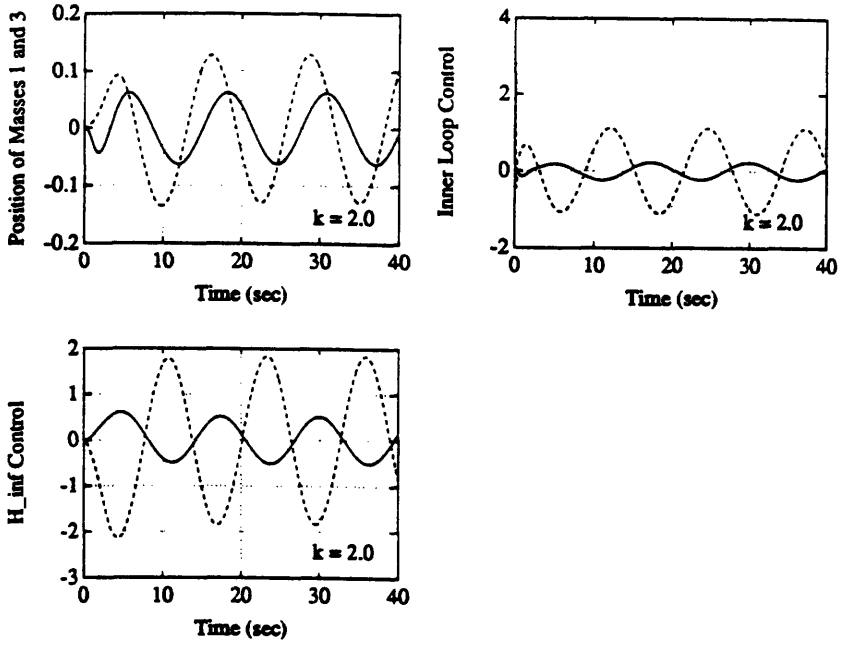

Figure E.31: Closed Loop System Response to a Sinusoidal Disturbance for $k = 2.0$

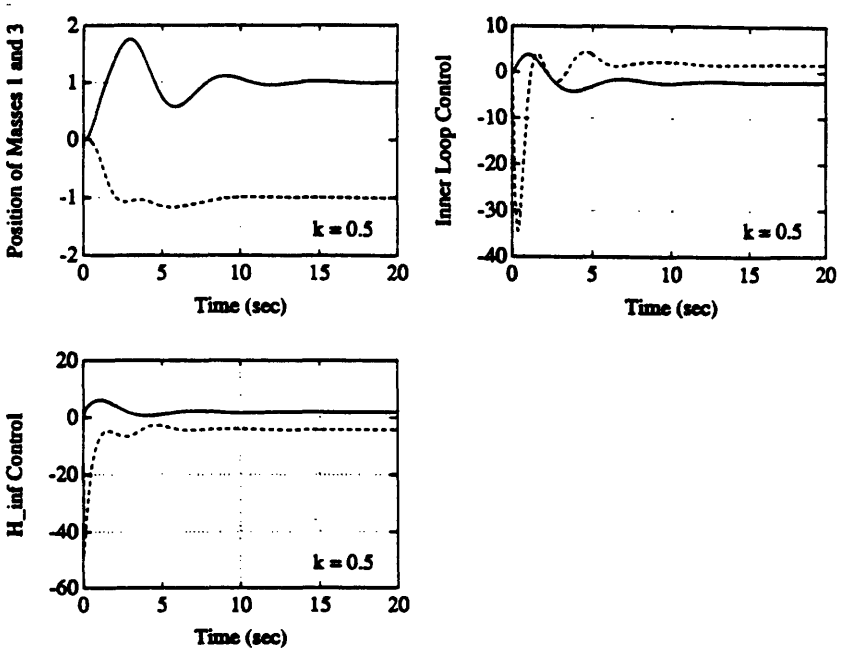

Figure E.32: Closed Loop System Response to a Reference Step Change for $k = 0.5$

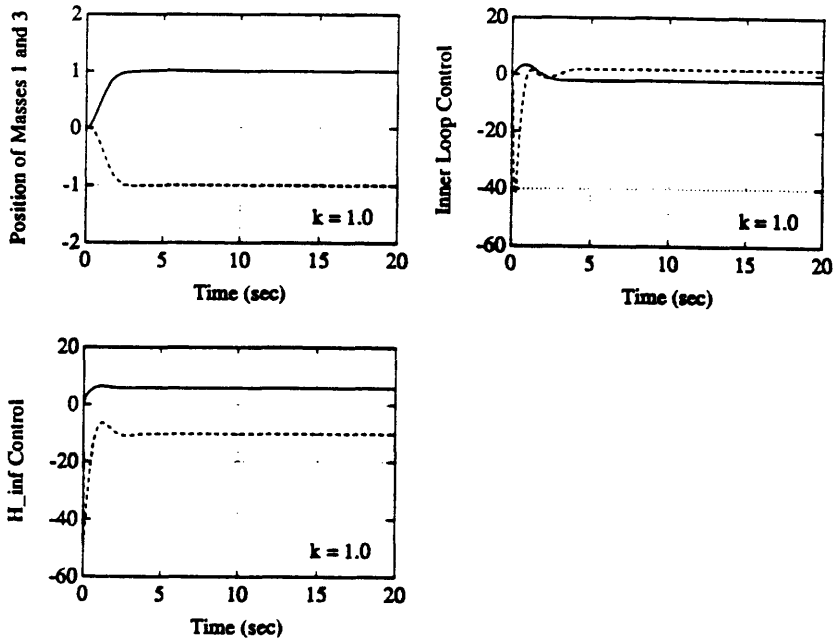

Figure E.33: Closed Loop System Response to a Reference Step Change for $k = 1.0$

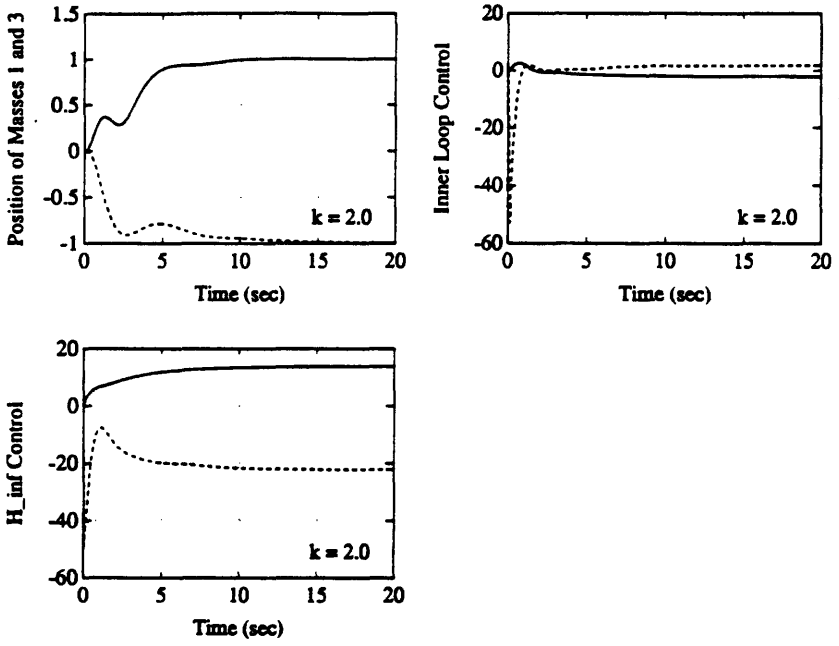

Figure E.34: Closed Loop System Response to a Reference Step Change for $k = 2.0$